




Advanced Engineering Research

Theoretical and scientific-practical journal

Vol. **21**

ISSN 2687-1653 

no. **3**
2021

1

Mechanics

2

Machine Building and Machine Science

3

Information Technology, Computer Science, and Management

DOI 10.23947/2687-1653

vestnik-donstu.ru

Advanced Engineering Research

Vol. 21, no. 3

**Theoretical
and scientific-practical journal**

Published since 1999

Quarterly
July-September 2021

ISSN 2687-1653
DOI: 10.23947/2687-1653

**Founder and publisher — Federal State Budgetary Educational Institution of Higher Education
Don State Technical University (DSTU)**

The journal was known as Vestnik of Don State Technical University (until August 2020)

Included in the list of peer-reviewed scientific editions where the basic research results of doctoral, candidate's theses should be published (State Commission for Academic Degrees and Titles List) in the following research areas:

01.02.01 – Analytical Mechanics (Engineering Sciences)
01.02.04 – Deformable Solid Mechanics (Engineering Sciences)
01.02.04 – Deformable Solid Mechanics (Physicomathematical Sciences)
01.02.06 – Dynamics, Strength of Machines, Gear, and Equipment (Engineering Sciences)
05.02.02 – Engineering Science, Drive Systems and Machine Parts (Engineering Sciences)
05.02.04 – Machine Friction and Wear (Engineering Sciences)
05.02.07 – Technology and Equipment of Mechanical and Physicotechnical Processing (Engineering Sciences)
05.02.08 – Engineering Technology (Engineering Sciences)
05.02.10 – Welding, Allied Processes and Technologies (Engineering Sciences)
05.02.11 – Testing Methods and Diagnosis in Machine Building (Engineering Sciences)
05.13.11 – Software and Mathematical Support of Machines, Complexes and Computer Networks (Engineering Sciences)
05.13.17 – Foundations of Information Science (Engineering Sciences)
05.13.18 – Mathematical Simulation, Numerical Methods and Program Systems (Engineering Sciences)

The journal is indexed and archived in the Russian Science Citation Index (RSCI), in the International Database EBSCO (Academic Search Ultimate Magazines and Journals), Dimensions, CyberLeninka, ROAD, Google Scholar. The journal is a member of Directory of Open Access Journals (DOAJ), Association of Science Editors and Publishers (ASEP) and CrossRef.

Certificate of mass media registration ЭЛ № ФС 77 – 78854 of 07.08.2020 is issued by the Federal Service for Supervision of Communications, Information Technology, and Mass Media

The issue is prepared by:

Inna V. Boyko, Gennady I. Rassokhin, Marina P. Smirnova (English version)

Founder's, Publisher's and Printery Address:

Gagarin Sq. 1, Rostov-on-Don, 344003, Russia. Phone: +7 (863) 2-738-372

E-mail: vestnik@donstu.ru <http://vestnik-donstu.ru/>



The content is available under Creative Commons Attribution 4.0 License

Editorial Board

Editor-in-Chief — **Besarion Ch. Meskhi**, Dr.Sci. (Eng.), professor, Don State Technical University (Russian Federation);

deputy chief editor — **Valery P. Dimitrov**, Dr.Sci. (Eng.), professor, Don State Technical University (Russian Federation);

executive editor — **Manana G. Komakhidze**, Cand.Sci. (Chemistry), Don State Technical University (Russian Federation);

executive secretary — **Nadezhda A. Shevchenko**, Don State Technical University (Russian Federation);

Evgeny V. Ageev, Dr.Sci. (Eng.), professor, South-Western State University (Russian Federation);

Sergey M. Aizikovich, Dr.Sci. (Phys.-Math.), professor, Don State Technical University (Russian Federation);

Kamil S. Akhverdiev, Dr.Sci. (Eng.), professor, Rostov State Transport University (Russian Federation);

Vladimir I. Andreev, member of RAACS, Dr.Sci. (Eng.), professor, National Research Moscow State University of Civil Engineering (Russian Federation);

Imad R. Antipas, Cand.Sci. (Eng.), Don State Technical University (Russian Federation);

Torsten Bertram, Dr.Sci. (Eng.), professor, TU Dortmund University (Germany);

Dmitry A. Bezuglov, Dr.Sci. (Eng.), professor, Rostov branch of Russian Customs Academy (Russian Federation);

Larisa V. Cherkesova, Dr.Sci. (Phys. -Math.), professor, Don State Technical University (Russian Federation);

Alexandr N. Chukarin, Dr.Sci. (Eng.), professor, Rostov State Transport University (Russian Federation);

Oleg V. Dvornikov, Dr.Sci. (Eng.), professor, Belarusian State University (Belarus);

Karen O. Egiazyryan, Dr.Sci. (Eng.), professor, Tampere University of Technology (Tampere, Finland);

Sergey V. Eliseev, corresponding member of Russian Academy of Natural History, Dr.Sci. (Eng.), professor, Irkutsk State Railway Transport Engineering University (Russian Federation);

Victor A. Eremeev, Dr.Sci. (Phys.-Math.), professor, Southern Scientific Center of RAS (Russian Federation);

Mikhail B. Flek, Dr.Sci. (Eng.), professor, "Rostvertol" JSC (Russian Federation);

Nikolay E. Galushkin, Dr.Sci. (Eng.), professor, Institute of Service and Business (DSTU branch) (Russian Federation);

LaRoux K. Gillespie, Dr.Sci. (Eng.), professor, President-elect of the Society of Manufacturing Engineers (USA);

Anatoly A. Korotkii, Dr.Sci. (Eng.), professor, Don State Technical University (Russian Federation);

Victor M. Kureychik, Dr.Sci. (Eng.), professor, Southern Federal University (Russian Federation);

Geny V. Kuznetzov, Dr.Sci. (Phys.-Math.), professor, Tomsk Polytechnic University (Russian Federation);

Vladimir I. Lysak, Dr.Sci. (Eng.), professor, Volgograd State Technical University, (Russian Federation);

Vladimir I. Marchuk, Dr.Sci. (Eng.), professor, Institute of Service and Business (DSTU branch) (Shakhty);

Igor P. Miroshnichenko, Cand.Sci. (Eng.), professor, Don State Technical University (Russian Federation);

Vladimir G. Mokrozub, Dr.Sci. (Eng.), associate professor, Rostov State Transport University (Russian Federation);

Murman A. Mukutadze, Cand.Sci. (Eng.), professor, Tambov State Technical University (Russian Federation);

Nguyen Dong Ahn, Dr.Sci. (Phys. -Math.), professor, Institute of Mechanics, Academy of Sciences and Technologies of Vietnam (Vietnam);

Petr M. Ogar, Dr.Sci. (Eng.), professor, Bratsk State University (Russian Federation);

Gennady A. Ougolnitsky, Dr.Sci. (Phys.-Math.), professor, Southern Federal University (Russian Federation);

Sergey G. Parshin, Dr.Sci. (Eng.), associate professor, St. Petersburg Polytechnic University (Russian Federation);

Valentin L. Popov, Dr.Sci. (Phys. -Math.), professor, Institute of Mechanics, Berlin University of Technology (Germany);

Nikolay N. Prokopenko, Dr.Sci. (Eng.), professor, Don State Technical University (Russian Federation);

Igor B. Sevostianov, Cand.Sci. (Phys. -Math.), professor, New Mexico State University (USA);

Vladimir N. Sidorov, Dr.Sci. (Eng.), Russian University of Transport (Russian Federation);

Arkady N. Solovyev, Dr.Sci. (Phys. -Math.), professor, Don State Technical University (Russian Federation);

Alexandr I. Sukhinov, Dr.Sci. (Phys.-Math.), professor, Don State Technical University (Russian Federation);

Mikhail A. Tamarkin, Dr.Sci. (Eng.), professor, Don State Technical University (Russian Federation);

Valery N. Varavka, Dr.Sci. (Eng.), professor, Don State Technical University (Russian Federation);

Igor M. Verner, Cand.Sci. (Eng.), Docent, Technion (Israel)

Batyr M. Yazyev, Dr.Sci. (Phys. -Math.), professor, Don State Technical University (Russian Federation);

Vilor L. Zakovorotny, Dr.Sci. (Eng.), professor, Don State Technical University (Russian Federation);

CONTENTS

MECHANICS

- Chistyakov A. E., Sidoryakina V. V., Protsenko S. V.* Development of algorithms for constructing two-dimensional optimal boundary-adaptive grids and their software implementation 222
- Saypulaev M. R., Merkuryev I. V., Solovyev A. V., Tarasov A. N.* Study on free oscillations of a micromechanical gyroscope taking into account the nonorthogonality of the torsion axes 231
- Galaburdin A. V.* An infinite plate loaded with a normal force moving along a complex open trajectory 239

MACHINE BUILDING AND MACHINE SCIENCE

- Issabekov Zh. N., Tsybrii I. K., Moroz K. A.* Organization of walking of the lower-extremity exoskeleton using the control of the supporting foot 247
- Glushko S. P.* Investigation of the electrospark coating, alloying and strengthening technology 253
- Maistrenko A. V.* Building structures thermal calculation 260
- Kruglova T. N.* Method for assessing the current and additional load on the parallel kinematic structure mechanisms electric drive system 268

INFORMATION TECHNOLOGY, COMPUTER SCIENCE, AND MANAGEMENT

- Dubanov A. A.* Analysis of the speed and curvature of the trajectory in the problem of pursuing a set of targets 275
- Galushka V. V., Fatkhi D. V., Gazizov E. R.* A method for generating a local network graph based on the analysis of address sets 284
- Baskakov A. A., Tarasov A. G.* To the problem of using an automated workplace by people with disabilities 290

MECHANICS



UDC 517.95, 519.6

<https://doi.org/10.23947/2687-1653-2021-21-3-222-230>**Development of algorithms for constructing two-dimensional optimal boundary-adaptive grids and their software implementation**A. E. Chistyakov ¹, V. V. Sidoryakina ², S. V. Protsenko ¹¹ Don State Technical University (Rostov-on-Don, Russian Federation)² Taganrog Institute Named after A.P. Chekhov, Rostov State University of Economics (RINH) branch, (Taganrog, Russian Federation)✉ cheese_05@mail.ru

Introduction. It is noted that the use of adaptive grids in calculations makes it possible to improve the accuracy and efficiency of computational algorithms without increasing the number of nodes. This approach is especially efficient when calculating nonstationary problems. The objective of this study is the development, construction and software implementation of methods for constructing computational two-dimensional optimal boundary-adaptive grids for complex configuration regions while maintaining the specified features of the shape and boundary of the region. The application of such methods contributes to improving the accuracy, efficiency, and cost-effectiveness of computational algorithms.

Materials and Methods. The problem of automatic construction of an optimal boundary-adaptive grid in a simply connected region of arbitrary geometry, topologically equivalent to a rectangle, is considered. A solution is obtained for the minimum set of input information: the boundary of the region in the physical plane and the number of points on it are given. The creation of an algorithm and a mesh generation program is based on a model of particle dynamics. This provides determining the trajectories of individual particles and studying the dynamics of their pair interaction in the system under consideration. The interior and border nodes of the grid are separated through using the mask tool, and this makes it possible to determine the speed of movement of nodes, taking into account the specifics of the problem being solved.

Results. The developed methods for constructing an optimal boundary-adaptive grid of a complex geometry region provides solving the problem on automatic grid construction in two-dimensional regions of any configuration. To evaluate the results of the algorithm research, a test problem was solved, and the solution stages were visualized. The computational domain of the test problem and the operation of the function for calculating the speed of movement of interior nodes are shown in the form of figures. Visualization confirms the advantage of this meshing method, which separates the border and interior nodes.

Discussion and Conclusions. The theoretical and numerical studies results are important both for the investigation of the grids qualitative properties and for the computational grid methods that provide solving numerical modeling problems efficiently and with high accuracy.

Keywords: particle dynamics method, computational two-dimensional grid, boundary-adaptive grid, numerical simulation.

For citation: A. E. Chistyakov, V. V. Sidoryakina, S. V. Protsenko. Development of algorithms for constructing two-dimensional optimal boundary-adaptive grids and their software implementation. Advanced Engineering Research, 2021, vol. 21, no. 3, pp. 222–230. <https://doi.org/10.23947/2687-1653-2021-21-3-222-230>

Funding information: the research is done with the financial support from RFFI (project no. 19–01–00701).

© Chistyakov A. E., Sidoryakina V. V., Protsenko S. V., 2021



Introduction. The grid construction was initially considered as a necessary auxiliary step in solving other problems [1–3]. In particular, when solving computational fluid dynamics problems, the construction of a computational grid is a considerably labor-intensive and lengthy process [4–6]. When studying the water areas of real reservoirs, we have to deal with the areas with an objectively predetermined boundary running along the coastline¹. The border nodes of the rectangular grid of Cartesian coordinates covering the reservoir may not exactly fall on the contour of the coastline. Therefore, a uniform grid should be very dense, so that the errors it introduces for setting the coastline are acceptable. For example, for the Azov Sea, a two-dimensional grid, as a rule, contains more than half a million nodes [7–11]. Note also that when using rectangular grids, the boundary conditions are set at points offset from the real boundary, or (when truncating the boundary grid cells) inhomogeneities associated with uneven steps in spatial directions are concentrated near the boundary². Taking into account the above, as well as the need to simplify data structures and algorithms for their processing, it is advisable to conduct numerical modeling of this type of problems on an optimal boundary-adaptive grid [12–14].

This paper presents an algorithm and a program developed for constructing quadrangular optimal boundary-adaptive computational grids based on the particle dynamics method in a two-dimensional formulation. This powerful computational method provides the grid nodes as charged particles and simulates the dynamics of a system consisting of a huge number of particles (up to a million). Using the example of text problems, the efficiency of the algorithm for areas with a complex boundary is demonstrated.

Materials and methods. Description of the method for constructing a 2D optimal boundary-adaptive grid. In the Cartesian coordinate system Oxy , we introduce area D . In area D , grid $\omega = \{(x_{i,j}, y_{i,j}), i = \overline{1, N_1}, j = \overline{1, N_2}\}$ is built according to the specified coordinates of the border nodes. The grid area divides area D into elementary subdomains in the form of quadrilaterals. The grid nodes are redistributed along the coordinate lines. Then, in the needed zones where node thickening is required, variables x, y are replaced with compressing variables ξ, η c using separated transformations:

$$(\xi, \eta) \rightarrow (x, y): x = x(\xi, \eta), y = y(\xi, \eta), \quad (1)$$

$$(x, y) \rightarrow (\xi, \eta): \xi = \xi(x, y), \eta = \eta(x, y). \quad (2)$$

Thus, grid $\omega = \{(\xi_{i,j}, \eta_{i,j}), i = \overline{1, N_1}, j = \overline{1, N_2}\}$, which is determined by the functions $x = x(\xi, \eta)$, $y = y(\xi, \eta)$, is constructed on the plane (ξ, η) .

The construction of the computational grid ω is based on the method of particle dynamics. This modeling technique is widely presented in the literature, so we will focus on it only briefly [15–17].

We represent nodes of grid ω as a collection of particles with charges q_{ij} and mass m_{ij} , that move in the calculated area D along and near its boundary. The particles interact with each other, and the interaction forces are of an electrical nature.

¹Sukhinov AI, Sukhinov AA. Reconstruction of 2001 ecological disaster in the Azov Sea on the basis of precise hydrophysics models. Parallel Computational Fluid Dynamics 2004, Multidisciplinary Applications. Amsterdam: Elsevier; 2005. P. 231–238. <https://doi.org/10.1016/B978-0-444-52024-1/50030-0>

²Sukhinov A, Chistyakov A, Sidoryakina V. Investigation of nonlinear 2D bottom transportation dynamics in coastal zone on optimal curvilinear boundary adaptive grids. In: Proc. XIII Int. Sci.-Tech. Conf. on Dynamic of Technical Systems. 2017;132:04003. <https://doi.org/10.1051/mateconf/201713204003>

According to Coulomb's law, repulsive force \vec{F}_{ij} acts on a single i -th particle from the side of j -th particle. Absolute magnitude of force F_{ij} is determined by the distance between these particles, and its vector is directed opposite to the radius-vector \vec{r}_{ij} , connecting the i -th and j -th charges (Fig. 1).

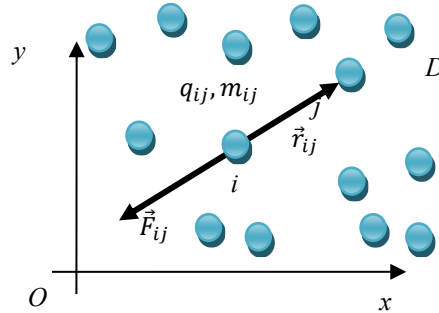


Fig. 1. Scheme of particle interaction

The trajectories of the charged particles determine the location of the grid nodes. Let us denote the coordinates of the i -th particle (x_{ij}, y_{ij}) , and j -th — (ζ_{ij}, η_{ij}) . The length of radius-vector \vec{r}_{ij} , that determines the movement of the node (x_{ij}, y_{ij}) to the node (ζ_{ij}, η_{ij}) , is calculated from the formula:

$$r_{ij} = r(x_{ij}, y_{ij}, \zeta_{ij}, \eta_{ij}) = \sqrt{(x_{ij} - \zeta_{ij})^2 + (y_{ij} - \eta_{ij})^2}. \quad (3)$$

Note the specificity of the transformation (1)–(2). If the distance is $r \neq 0$, then the node (ζ_{ij}, η_{ij}) repels from each of the neighboring ones. They, in turn, must either stand at the prescribed distance, or move away, being pulled to a neighboring node and freeing up space for the newly inserted one.

The type of transformation (1)–(2) that compresses coordinates x, y in zones of high gradients is determined by the solution to the problem. For this purpose, a model equation describing the potential is used in the direction of axes Ox, Oy :

$$F(x_{ij}, y_{ij}, \zeta_{ij}, \eta_{ij}) = \frac{l}{r(x_{ij}, y_{ij}, \zeta_{ij}, \eta_{ij})^\alpha}, \quad (4)$$

where l — proportionality factor between potential and distance r at a given node, α — a certain parameter.

Each node seeks to reduce potential energy, namely:

$$\sum_{m,n} F(x_{ij}, y_{ij}, x_{nm}, y_{nm}) \rightarrow \min, \quad i = \overline{1, N_1}, \quad j = \overline{1, N_2}, \quad n = \overline{1, N_1}, \quad m = \overline{1, N_2}. \quad (5)$$

Force $\vec{f}(x_{ij}, y_{ij})$ is related to potential $F = F(x_{ij}, y_{ij}, \zeta_{ij}, \eta_{ij})$ through the following relation:

$$\vec{f}(x_{ij}, y_{ij}) = \text{grad}(F) = - \sum_{m,n} \frac{al}{r(x_{ij}, y_{ij}, x_{nm}, y_{nm})^{\alpha+2}} \vec{r}. \quad (6)$$

When modeling the process of interaction of mobile particles, we assume that the grid nodes that fall outside the calculated domain are forced to move to a point on the boundary of the domain, the distance to which is minimal. The scheme of interaction between a mobile particle and a particle at the boundary is shown in Fig. 2.

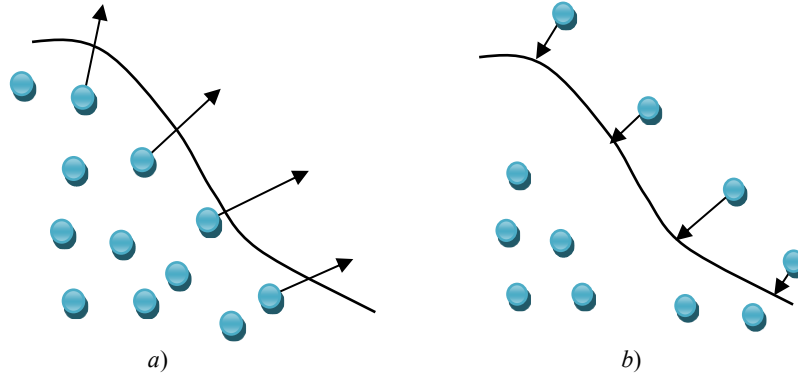


Fig. 2. Scheme of particle interaction at the boundary of computational domain D :

a) direction of movement of particles inside domain D ; b) direction of movement of particles outside domain D

The technology of numerical integration of the equations of motion is based on the algorithm presented in [17].

Description of the meshing software. The program consists of modules that implement five functions: a control one that calls the calculation functions a specified number of times, three calculation functions, and a visualization function. The calculation functions are the following: a function describing the speed at which nodes move; a function for moving nodes; a function for checking the exit of nodes beyond the boundary of the domain.

The data structure of the program: A — input array of sizes $[N, M]$; C — visualization array; B_x, B_y — arrays of sizes $[n, m]$, describing the location of nodes; B_m — array of sizes $[n, m]$, describing the masks of boundary conditions; u, v — components of the velocity vector of the nodes; i, j — counters; n, m — number of nodes in the directions Ox, Oy , respectively; l — proportionality coefficient between the potential and distance r at a given node; α — some parameter (degree at r). The control function resets the arrays and sets the initial location of the nodes.

Algorithm describing the node speed function.

Input arrays: B_x, B_y, B_m and parameter α (i.e., $\alpha = 3$). Output arrays: u, v .

1. Start of the loop on variables i, j . The counter values are set equal to $i = 0, \dots, n-1, j = 0, \dots, m-1$.
2. Separation of border and interior points of the computational domain. If mask = 1 — point on the domain boundary, go to item 3, if mask = 2 — point is inside the domain, go to item 4.
3. Algorithm describing the speed function of the border nodes
 - 3.1. Zeroing arrays u, v .
 - 3.2. Start of the loop on variables $i1, j1$. The counter values are set equal to $i1 = i-2, \dots, i+2, j1 = j-2, \dots, j+2$.
 - 3.3. Calculating the distance from one node to another:

$$r \leftarrow \sqrt{(Bx_{i,j} - Bx_{i1,j1})^2 + (By_{i,j} - By_{i1,j1})^2}.$$

- 3.4. Checking the condition. If $r > 0$, then go to item 3.5, otherwise, go to item 3.6.

- 3.5. Calculating u, v for $\alpha = 3$:

$$u_{i,j} \leftarrow u_{i,j} + \frac{(Bx_{i,j} - Bx_{i1,j1})}{r^\alpha} Bm_{i1,j1},$$

$$v_{i,j} \leftarrow v_{i,j} + \frac{(By_{i,j} - By_{i1,j1})}{r^\alpha} Bm_{i1,j1}.$$

- 3.6. Build up counters $i1, j1$ and go to item 3.3.

- 3.7. Build up counters i, j and go to item 3.1.

4. Algorithm describing the speed function of the interior nodes

4.1. Zeroing arrays u, v .

4.2. Start of the loop on variables $i1, j1$. The counter values are set equal to $i1 = i - 1, \dots, i + 1, j1 = j - 1, \dots, j + 1$.

4.3. Checking the condition. If $(i1 - i)(j1 - j) = 0$, then go to item 4.4, otherwise, go to item 4.8.

4.4. Calculating the distance from one node to another:

$$r \leftarrow \sqrt{(Bx_{i,j} - Bx_{i1,j1})^2 + (By_{i,j} - By_{i1,j1})^2}.$$

4.5. Checking the condition. If $r > 0$ is executed, then go to item 4.6, otherwise, go to item 4.7.

4.6. Calculating u, v for $k = 0.005$:

$$\begin{aligned} u_{i,j} &\leftarrow u_{i,j} - k(Bx_{i,j} - Bx_{i1,j1}), \\ v_{i,j} &\leftarrow v_{i,j} - k(By_{i,j} - By_{i1,j1}). \end{aligned}$$

4.7. Build up counters $i1, j1$ and go to item 4.4.

4.8. Build up counters i, j and go to item 4.1.

Algorithm describing the function of calculating the movement of nodes

Input arrays: B_x, B_y, u, v and parameter l (i.e., $l = 30$). Output arrays: B_x, B_y .

1. Start of the loop on variables i, j . The counter values are set equal to $i = 1, \dots, n - 2, j = 1, \dots, m - 2$.

2. Calculating arrays B_x, B_y :

$$\begin{aligned} Bx_{i,j} &\leftarrow Bx_{i,j} + lu_{i,j}, \\ By_{i,j} &\leftarrow By_{i,j} + lv_{i,j}. \end{aligned}$$

3. Build up counters i, j and go to item 2.

Algorithm describing the function of checking the exit of nodes beyond the domain boundary

Input arrays: B_x, B_y, A and parameter d (i.e., $d = 3$), that describes the size of the window in which the computational domain is presented in case node B_x, B_y goes beyond the boundary of the computational domain.

Output arrays: B_x, B_y .

1. Start of the loop on variables i, j . The counter values are set equal to $i = 1, \dots, n - 2, j = 1, \dots, m - 2$.

2. Finding indexes A , in the array corresponding to node $(Bx_{i,j}, By_{i,j})$:

$$i1 \leftarrow |Bx_{i,j}|, \quad j1 \leftarrow |By_{i,j}|.$$

3. The initial value of the distance to the boundary is set by the parameter value d :

$$r \leftarrow 2d.$$

4. Checking the condition for the exit of point $(i1, j1)$ beyond the computational domain boundary: if $A_{i1,j1} > 0$ is executed; otherwise, go to item 12.

5. Start of the loop on variables $i2, j2$. The counter values are set equal to $i2 = -d, \dots, d, j2 = -d, \dots, d$.

6. Checking point $(i2 + i1, j2 + j1)$ for belonging to the calculated domain: if $A_{i2+i1, j2+j1} = 0$ is executed; otherwise, go to item 10.

7. The distance from node $(Bx_{i,j}, By_{i,j})$ to point $(i2 + i1, j2 + j1)$ is found from the formula:

$$r1 \leftarrow \sqrt{(Bx_{i,j} - i2 - i1)^2 + (By_{i,j} - j2 - j1)^2}.$$

8. If $r1 > r$ is executed, then item 9 is performed; otherwise, go to item 10.

9. Remember the point of the computational domain closest to the node $(Bx_{i,j}, By_{i,j})$:

$$r \leftarrow r1, \quad i3 \leftarrow i2 + i1, \quad j3 \leftarrow j2 + j1.$$

10. Build up counters by variables $i2, j2$ and go to item 6.

11. Offset of the node $(Bx_{i,j}, By_{i,j})$ to the boundary of the computational domain:

$$Bx_{i,j} \leftarrow i3, \quad By_{i,j} \leftarrow j3.$$

12. Build up counters i, j and go to item 2.

Algorithm describing the visualization function.

Input arrays: B_x, B_y, A . Output array — C .

1. We put array A in the visualization array.

2. Start of the loop on variables i, j, k . The counter values are set equal to $i = 1, \dots, n-3, j = 1, \dots, m-2,$

$$k = |Bx_{i,j}| \dots |Bx_{i+1,j}|.$$

3. Draw vertical lines:

$$C \left[k, \left| By_{i,j} + \frac{By_{i+1,j} - By_{i,j}}{Bx_{i+1,j} - Bx_{i,j}} \cdot (k - Bx_{i,j}) \right| \right] \leftarrow 255.$$

4. Build up counters i, j, k and go to item 3.

5. Start of the loop on variables i, j, k . The counter values are set equal to $i = 1, \dots, n-2, j = 1, \dots, m-3,$

$$k = |By_{i,j}| \dots |By_{i,j+1}|.$$

6. Draw horizontal lines:

$$C \left[k, \left| Bx_{i,j} + \frac{Bx_{i+1,j} - Bx_{i,j}}{By_{i+1,j} - By_{i,j}} \cdot (k - By_{i,j}) \right| \right] \leftarrow 255.$$

7. Build up counters i, j, k and go to item 6.

The source file is BMP. On it, the geometry of the domain on which the grid is being built is indicated in black. The rest of the domain is marked in white. The source BMP file is written to an array, with black being 0, and white — 255. The output information includes arrays B_x, B_y , describing the location of the grid nodes, and array C , that stores the geometry of the source domain with the applied grid.

Research Results. The results of the algorithm demonstrate the solution to the test problem.

Input data: the source domain of the type shown in Fig. 3, as well as the calculated data $n = 12, m = 14, i = 1, \dots, 10, j = 1, \dots, 12, l = 30, d = 3, \alpha = 3$.

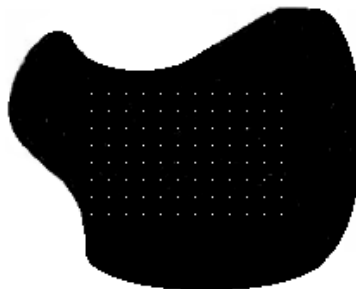


Fig. 3. Computational domain of the test problem

The initial location of the nodes is taken as the location of nodes of grid ω without adaptation to the boundary of the source domain. Visualization of the work of the function of moving interior nodes is shown in Fig. 4.

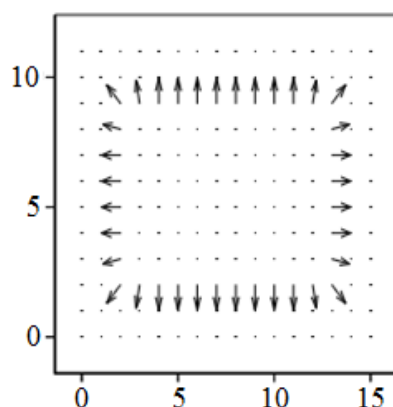


Fig. 4. Work of the function for calculating the speed of interior nodes

The result of constructing quadrangular boundary-adaptive grid ω , covering the source domain, is obtained on the basis of the presented algorithm (Fig. 5 a). Fig. 5 b shows the work of the program algorithm for the case when the border and interior nodes were not separated. A clear advantage of the grid shown in Fig. 5 a, consists in the fact that its cells are convex quadrilaterals. This requirement is not met for the grid of type 5 b.

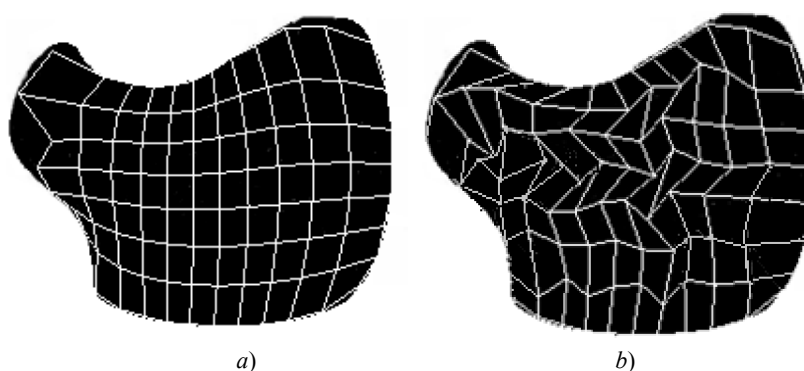


Fig. 5. Results of grid ω construction algorithm: a) image of grid ω , constructed when separating the border and interior grid nodes; b) image of grid ω , constructed without separating the border and interior nodes of grid ω

Discussion and Conclusions. A technology for constructing two-dimensional optimal boundary-adaptive grids based on the particle dynamics method is proposed. An algorithm for numerical calculation of quadrangular grids for complex configuration domains with preservation of the specified geometric features of the domain shape and boundary is developed and tested. Using the example of a test problem, the possibilities of the proposed algorithm were investigated. One of the advantages of this software implementation is the ability to automatically place nodes on the boundary of the computational domain and get convex cells. The presented approach has sufficient versatility and reliability and can be used for triangulation of the considered domains.

References

1. Downing-Kunz MA, Work PA, Schoellhamer DH. Tidal Asymmetry in Ocean-Boundary Flux and In-Estuary Trapping of Suspended Sediment Following Watershed Storms: San Francisco Estuary, California, USA. Estuaries and Coasts. 2021. URL: <https://doi.org/10.1007/s12237-021-00929-y> (accessed: 31.08.2021).
2. Ballent A, Pando S, Purser A, et al. Modelled transport of benthic marine microplastic pollution in the Nazaré Canyon. Biogeosciences. 2013;10(12):7957–7970. <https://doi.org/10.5194/bg-10-7957-2013>

3. Kirk B, Lipnikov K, Carey GF. Nested grid iteration for incompressible viscous flow and transport. *International Journal of Computational Fluid Dynamics*. 2003;17(4):253–262. <https://doi.org/10.1080/1061856031000173635>
4. Xiaoying Liu, Shi Qi, YuanHuang, et al. Predictive modeling in sediment transportation across multiple spatial scales in the Jialing River Basin of China. *International Journal of Sediment Research*. 2015;30(3):250–255. <https://doi.org/10.1016/j.ijsrc.2015.03.013>
5. Barnard PL, Jaffe BE, Schoellhamer DH (eds.). A multi-discipline approach for understanding sediment transport and geomorphic evolution in an estuarine-coastal system: San Francisco Bay. *Marine Geology*. 2013;345:1–326. <https://doi.org/10.1016/j.margeo.2013.09.010>
6. Alekseenko E, Roux B, Sukhinov A, et al. Coastal hydrodynamics in a windy lagoon. *Computers & Fluids*. 2013;77:24–35. <https://doi.org/10.1016/j.compfluid.2013.02.003>
7. Sukhinov AI. Pretsizionnye modeli gidrodinamiki i opyt ikh primeneniya v predskazanii i rekonstruktsii chrezvychaynykh situatsii v Azovskom more. *Izvestiya TRTU*. 2006;58(3):228–235. (In Russ.)
8. Sukhinov AI, Sidoryakina VV. Development and correctness analysis of the mathematical model of transport and suspension sedimentation depending on bottom relief variation. *Vestnik of Don State Technical University*. 2018;18(4):350–361. <https://doi.org/10.23947/1992-5980-2018-18-4-350-361> (In Russ.)
9. Sidoryakina VV, Sukhinov AI. Well-posedness analysis and numerical implementation of a linearized two-dimensional bottom sediment transport problem. *Computational Mathematics and Mathematical Physics*. 2017;57(6):978–994. <https://doi.org/10.1134/S0965542517060124>
10. Sukhinov AI, Sidoryakina VV, Sukhinov AA. Sufficient conditions for convergence of positive solutions to linearized two-dimensional sediment transport problem. *Vestnik of Don State Technical University*. 2017;17(1):5–17. <https://doi.org/10.23947/1992-5980-2017-17-1-5-17> (In Russ.)
11. Sukhinov AI, Vasiliev VS. Precise two-dimensional models for shallow water basins. *Mathematical Models and Computer Simulations*. 2003;15(10):17–34. (In Russ.)
12. Carey GF, Anderson M, Carnes B, et al. Some aspects of adaptive grid technology related to boundary and interior layers. *Journal of Computational and Applied Mathematics*. 2004;166(1):55–86. <https://doi.org/10.1016/j.cam.2003.09.036>
13. Owen SJ. A Survey of Unstructured Mesh Generation Technology. In: *Proc. 7th Int. Meshing Roundtable*. Dearborn, MI; 1998. P. 239–269.
14. Skovpen' AV. Improved algorithm for unstructured quadrilateral mesh generation. *Computational Mathematics and Mathematical Physics*. 2005;45(8):1506–1528. (In Russ.)
15. Krivtsov AM, Krivtsov NV. Method of particles and its application to mechanics of solids. *Far Eastern Mathematical Journal*. 2002;3(2):254–276. (In Russ.)
16. Belkin AA. On a modification of the method of molecular dynamics. *Journal of Applied and Industrial Mathematics*. 2006;9(4):27–32. (In Russ.)
17. Zheleznyakova AL, Surzhikov ST. Triangular mesh generation by molecular dynamics method. *Physical-Chemical Kinetics in Gas Dynamics*. 2011. Vol. 11. URL: <http://chemphys.edu.ru/issues/2011-11/articles/192/> (accessed: 31.08.2021). (In Russ.)

Received 28.06.2021

Revised 19.07.2021

Accepted 27.07.2021

About the Authors:

Chistyakov, Aleksandr E., professor of the Mathematics and Informatics Department, Don State Technical University (1, Gagarin sq., Rostov-on-Don, RF, 344003) Dr.Sci. (Phys.-Math.), professor, ResearcherID: O-1507-2016, ORCID: <https://orcid.org/0000-0002-8323-6005>, cheese_05@mail.ru

Sidoryakina, Valentina V., Head of the Mathematics Department, Taganrog Institute Named after A. P. Chekhov, Rostov State University of Economics (RINH) branch, (48, Initsiativnaya St., Taganrog, RF, 347936) Cand. Sci. (Phys.-Math.), associate professor, ORCID: <https://orcid.org/0000-0001-7744-015X>, cvv9@mail.ru

Protsenko, Sofya V., postgraduate student of the Mathematics and Informatics Department, Don State Technical University (1, Gagarin sq., Rostov-on-Don, RF, 344003) ORCID: <https://orcid.org/0000-0001-9656-8466>, rab55555@rambler.ru

Claimed contributorship

A. E. Chistyakov: academic advising; development of the calculation program; analysis of the research results. V. V. Sidoryakina: basic concept formulation; research objectives and tasks setting; conducting a computational experiment; text preparation. S. V. Protsenko: text preparation; formulation of conclusions.

All authors have read and approved the final manuscript.

MECHANICS



UDC 531.383

<https://doi.org/10.23947/2687-1653-2021-21-3-231-238>

Study on free oscillations of a micromechanical gyroscope taking into account the nonorthogonality of the torsion axes


M. R. Saypulaev ^{1,2}, I. V. Merkuriev ², A. V. Solovyev ¹, A. N. Tarasov ¹
¹ Kuznetsov Research Institute of Applied Mechanics, TsENKI division (Moscow, Russian Federation)

² National Research University «Moscow Power Engineering Institute» (Moscow, Russian Federation)

✉ saypulaevmr@mail.ru

Introduction. The paper is devoted to the study on free oscillations of the sensing element of a micromechanical R-R-type gyroscope of frame construction developed by the Kuznetsov Research Institute of Applied Mechanics, taking into account the nonorthogonality of the torsion axes. The influence of the instrumental manufacturing error on the accuracy of a gyroscope on a movable base in the case of free oscillations is studied. The work objective was to improve the device accuracy through developing a mathematical model of an R-R type micromechanical gyroscope, taking into account the nonorthogonality of the torsion axes, and to study the influence of this error on the device accuracy. The urgency of the problem of increasing the accuracy of micromechanical gyroscopes is associated with improving the accuracy of inertial navigation systems based on micromechanical sensors.

Materials and Methods. A new mathematical model that describes the gyroscope dynamics, taking into account the instrumental error of manufacturing the device, and a formula for estimating the error of a gyroscope, are proposed. The dependences of the state variables obtained from the results of modeling and on the basis of the experiment are presented. Methods of theoretical mechanics and asymptotic methods, including the Lagrange formalism and the Krylov-Bogolyubov averaging method, were used in the research.

Results. A new mathematical model of the gyroscope dynamics, taking into account the nonorthogonality of the torsion axes, is developed. The solution to the equations of small oscillations of the gyroscope sensing element and the estimate of the precession angle for the case of a movable base are obtained. A comparative analysis of the developed model and the experimental data obtained in the case of free oscillations of the gyroscope sensing element with a fixed base is carried out. The analysis has confirmed the adequacy of the constructed mathematical model. Analytical expressions are formed. They demonstrate the fact that the nonorthogonality of the torsion axes causes a cross-influence of the amplitudes of the primary vibrations on the amplitudes of the secondary vibrations of the sensing element, and the appearance of an additional error in the angular velocity readings when the gyroscope is operating in free mode.

Discussion and Conclusions. The results obtained can be used to improve the device accuracy using the algorithm for analytical compensation of the gyroscope error and the method for identifying the mathematical model parameters.

Keywords: gyroscope R-R type, gyro precession, gyro error estimation, micromechanical gyroscope, free oscillations.

For citation: M. R. Saypulaev, I. V. Merkuriev, A. V. Solovyev, A. N. Tarasov. Study on free oscillations of a micromechanical gyroscope taking into account the nonorthogonality of the torsion axes. Advanced Engineering Research, 2021, vol. 21, no. 3, pp. 231–238. <https://doi.org/10.23947/2687-1653-2021-21-3-231-238>

© Saypulaev M. R., Merkuriev I. V., Solovyev A. V., Tarasov A. N., 2021



Introduction. The development of high-precision micromechanical inertial sensors, including micromechanical gyroscopes (MMG), used to solve navigation problems and control the movement of aircraft and mobile robots, is an urgent task of instrument engineering [1]. The advantages of MMG include small weight and size,

as well as low cost compared to gyroscopes based on other physical principles. However, the main disadvantages of MMG are the variability of its metrological characteristics and the low accuracy of measuring the parameters of the angular motion of the object (angular rate and angle of rotation). The principle of operation of vibrating gyroscopes is based on the property of the Foucault pendulum to keep the plane of small vibrations motionless in inertial space [2].

Fundamentals of the theory of gyroscopes of the generalized Foucault pendulum class, which include MMG, are given in [2–5]. They describe various design schemes for the construction of MMG, and investigate the influence of instrumental manufacturing errors and changing operating conditions on the dynamics of the gyroscope. The principal feature of the gyroscopes of the generalized Foucault pendulum class is nonlinearity due to the finite vibrations of the sensing elements (SE) or physical nonlinearity associated with the features of the vibration control system [2–6].

Studies on the MMG dynamics and design were also published in the works of foreign authors [6–9]. For example, in publications [6, 9], a formula for estimating gyro drifts was obtained, based on the use of a developed mathematical model of motion that describes a slow change in the toroidal coordinates of the SE vibrations. In [7, 8], the issues on manufacturing MMG are discussed, and the equations of its small vibrations are analyzed. In paper [7], the equations of the MMG motion with angular (R-R-type) and linear (L-L-type) oscillatory types of the SE movement are compiled. In the above paper, a comparative analysis of the dynamics of such devices is carried out within the framework of linear models, and recommendations are given on the selection of MMG parameters, based on the conditions for increasing sensitivity and ensuring the required bandwidth, as well as the requirements for the linearity of the scale factor.

When designing MMG, the developers tend to use the phenomenon of internal resonance in the system, due to the combination of the natural frequencies of the SE vibrations [3, 4]. However, it is noted in [7, 8] that errors in the manufacturing technology, unknown and unpredictable deviations of structural elements from the design positions cause additional errors in the device measurements.

To improve the accuracy of the measurement of the angular rate of the MMG, the objective is set: to study free oscillations (in the absence of control) of the R-R-type MMG SE, taking into account the effects arising from the nonorthogonality of the torsion axes. This defect appears due to the imperfection of the manufacturing technology of the device. The tasks of developing a new mathematical model of the MMG dynamics considering the nonorthogonality of the torsion axes, evaluating the device drift, and describing the effect of the nonorthogonality of the torsion axes on the dynamics of the MMG SE, are set.

Materials and Methods. A model design of an R-R-type vibrating MMG — a design with an intermediate frame in accordance with the classification from the source is considered [3]. The kinematic scheme of the gyroscope (Fig. 1) is implemented in the form of a two-degree gimbal of the SE.

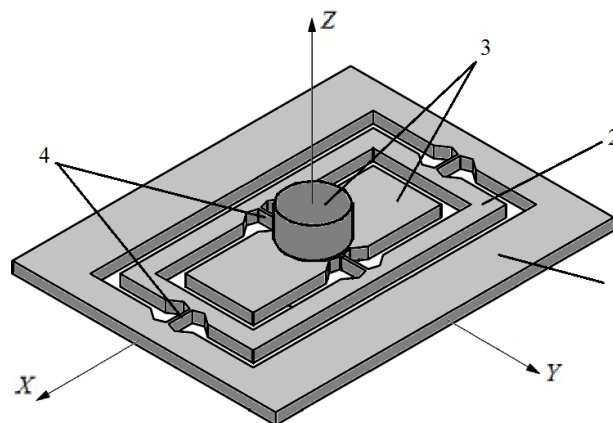


Fig. 1. Design diagram of the device: 1) base (body); 2) intermediate (external) frame; 3) sensing element consisting of balanced plate and inertial mass; 4) torsion bars

To describe the SE position, we introduce coordinate systems (Fig. 2) associated with: the device body — $OXYZ$; with the external frame of the elastic suspension of the gyroscope — $Ox_1y_1z_1$; with the balanced plate —

$Oxyz$. Moreover, OZ is the axis of sensitivity of the gyroscope, and the coordinate system $Ox_2y_2z_2$ differs from the system $Ox_1y_1z_1$ by turning by a constant angle of nonorthogonality of all torsions. In the presented systems, the origin of coordinates corresponds to point O and is located in the geometric center of the balanced plate.

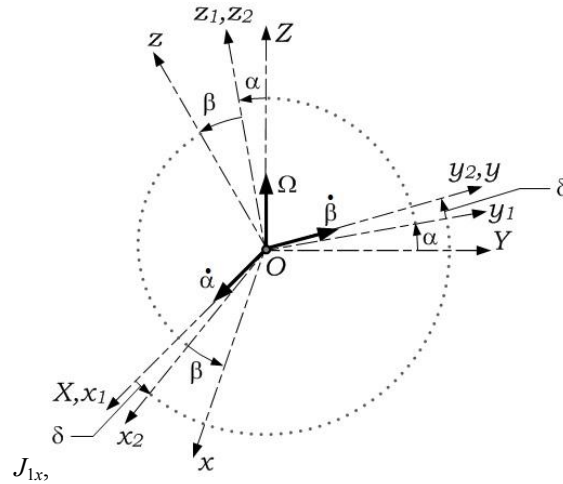


Fig. 2. Coordinate systems

In the system $Ox_1y_1z_1$ we will set the axial moments of inertia of the intermediate frame J_{1x}, J_{1y}, J_{1z} , and in the system $Oxyz$ — the axial moments of inertia of the SE J_{2x}, J_{2y}, J_{2z} . Note that in this paper, the axes of the coordinate systems $Ox_1y_1z_1$ and $Oxyz$ are considered the main central axes of inertia of the intermediate frame and SE, respectively.

When modeling the motion of the SE, the assumption is made that the torsion design provides infinite bending stiffness. The position of the SE relative to the base of the MMG is described by two generalized coordinates — angles α and β , as well as a small constant angle δ , that characterizes the nonorthogonality of the torsion axes (Fig. 2). The relative position of the coordinate systems is determined by a sequence of elementary rotations:

$$OXYZ \xrightarrow[x]{\alpha} Ox_1y_1z_1 \xrightarrow[z_1]{\delta} Ox_2y_2z_2 \xrightarrow[y_2]{\beta} Oxyz,$$

where under each arrow, the axis is indicated around which there is a counterclockwise rotation by the angle indicated above the corresponding arrow.

We will set up the equations of the dynamics of the MMG SE in the form of Lagrange equations of the 2nd kind [10, 11]:

$$\frac{d}{dt} \left(\frac{\partial L}{\partial \dot{\alpha}} \right) - \frac{\partial L}{\partial \alpha} = -\frac{\partial \Phi}{\partial \alpha}, \quad \frac{d}{dt} \left(\frac{\partial L}{\partial \dot{\beta}} \right) - \frac{\partial L}{\partial \beta} = -\frac{\partial \Phi}{\partial \beta}, \quad (1)$$

where $L = T - \Pi$ — the Lagrange function; T and Π — kinetic and potential energies of the system, respectively; Φ — dissipative function that characterizes the loss on internal friction. The expressions for these values have the form:

$$T = \frac{1}{2} (J_{2x} \omega_x^2 + J_{2y} \omega_y^2 + J_{2z} \omega_z^2) + \frac{1}{2} (J_{1x} \dot{\alpha}^2 + (J_{1y} \sin^2 \alpha + J_{1z} \cos^2 \alpha) \Omega^2),$$

$$\Phi = \frac{1}{2} d_\alpha \dot{\alpha}^2 + \frac{1}{2} d_\beta \dot{\beta}^2, \quad \Pi = \frac{1}{2} c_\alpha \alpha^2 + \frac{1}{2} c_\beta \beta^2, \quad (2)$$

where d_α, d_β — friction coefficients; c_α, c_β — torsion stiffness coefficients.

The expressions for the projections $\omega_x, \omega_y, \omega_z$ of the SE angular rate on the movable axes x, y, z have the form:

$$\omega_x = \dot{\alpha} \cos \beta \cos \delta - \Omega \cos \alpha \sin \beta + \Omega \sin \alpha \cos \beta \sin \delta,$$

$$\omega_y = \dot{\beta} + \Omega \sin \alpha \cos \delta - \dot{\alpha} \sin \delta,$$

$$\omega_z = \dot{\alpha} \sin \beta \cos \delta + \Omega \cos \alpha \cos \beta + \Omega \sin \alpha \sin \beta \sin \delta. \quad (3)$$

Given the smallness of angles α , β and δ , the trigonometric functions in expressions (2) and (3) from these angles can be replaced by Taylor series expansions, limiting the summands to the first order of smallness. Then we obtain the equations of small vibrations from the equations of motion (1), written with account for the expressions (2) and (3).

Using the Lagrange formalism [10] in the case of a constant angular rate of the base, we obtain the equations of small oscillations of the SE, written up to the terms of the first order of smallness in the form:

$$\ddot{\alpha} + \omega_\alpha^2 \alpha = j_1 \Omega \dot{\beta} - \frac{\omega_\alpha}{Q_\alpha} \dot{\alpha} + \frac{j_1}{j_2} \delta \ddot{\beta}, \quad \ddot{\beta} + \omega_\beta^2 \beta = -j_2 \Omega \dot{\alpha} - \frac{\omega_\beta}{Q_\beta} \dot{\beta} + \delta \ddot{\alpha}, \quad (4)$$

where the following notation is introduced (similar to how it is performed in paper [12]):

$$j_1 = \frac{J_{2x} + J_{2y} - J_{2z}}{J_{1x} + J_{2x}}, \quad j_2 = \frac{J_{2x} + J_{2y} - J_{2z}}{J_{2y}}, \quad \omega_\alpha = \sqrt{\frac{c_\alpha}{J_{1x} + J_{2x}}},$$

$$\omega_\beta = \sqrt{\frac{c_\beta}{J_{2y}}}, \quad Q_\alpha^{-1} = \frac{d_\alpha}{\omega_\alpha (J_{1x} + J_{2x})}, \quad Q_\beta^{-1} = \frac{d_\beta}{\omega_\beta J_{2y}}.$$

Here, j_1 , j_2 — dimensionless moments of inertia of the elastic suspension; ω_α , ω_β and Q_α , Q_β — natural frequencies of vibrations and Q-values at corners α , β , respectively.

When deriving the oscillation equations (4), the angular rate of the gyroscope body Ω was considered small relative to the natural frequency ω_α , i.e. $|\Omega| \ll \omega_\alpha$, and angle δ was also assumed to be a small value, i.e., $\delta \ll 1$. Note that in equations (4), the terms are dropped due to the presence of geometric nonlinearity of the MMG. The influence of the nonlinearity of the geometry of the SE motion on the dynamics of the R-R-type MMG is described in monograph [5].

Taking into account that the right-hand sides of equations (4) are small perturbations, i.e., $\ddot{\alpha} + \omega_\alpha^2 \alpha = O(\varepsilon)$, up to the terms of the first order of smallness, we can write: $\ddot{\alpha} = -\omega_\alpha^2 \alpha + O(\varepsilon)$. Thus, the second derivatives of angles α and β are excluded from the right part of equations (4).

We consider the case of an isotropic elastic suspension, i.e., the equality of natural oscillation frequencies and equal Q-factors:

$$\omega_\alpha = \omega_\beta = \omega_0, \quad Q_\alpha = Q_\beta = Q,$$

where ω_0 — the characteristic value of the natural frequency of vibrations; Q — the characteristic value of Q-factor.

It should be noted that the case of a difference in quality ($Q_\alpha \neq Q_\beta$) and a small difference in frequency ($\omega_\alpha \neq \omega_\beta$) under studying free oscillations of the MMG SE is considered in paper [12]. With the entered notation and the accepted assumptions, we write down the equations of the SE motion with an accuracy of the first-order terms of smallness in a dimensionless form:

$$\ddot{\alpha} + \omega_0^2 \alpha = j_1 \Omega \dot{\beta} - Q^{-1} \omega_0 \dot{\alpha} - \frac{j_1}{j_2} \delta \omega_0^2 \beta, \quad (5)$$

$$\ddot{\beta} + \omega_0^2 \beta = -j_2 \Omega \dot{\alpha} - Q^{-1} \omega_0 \dot{\beta} - \delta \omega_0^2 \alpha.$$

Note that the system of equations (5) is reduced to the standard form of writing a regularly perturbed system of differential equations with one fast angular variable [13, 14]. One of the most common ways to find solutions to regularly perturbed systems is to use asymptotic motion separation methods [13–16].

The solution to nonlinear equations (5) is obtained using the Krylov-Bogolyubov averaging method [14], and we will use Van der Pol variables as slowly changing variables [13] p_1, q_1, p_2, q_2 :

$$\alpha = p_1 \sin(\omega_0 t) + q_1 \cos(\omega_0 t), \quad \dot{\alpha} = \omega_0 p_1 \cos(\omega_0 t) - \omega_0 q_1 \sin(\omega_0 t),$$

$$\beta = p_2 \sin(\omega_0 t) + q_2 \cos(\omega_0 t), \quad \dot{\beta} = \omega_0 p_2 \cos(\omega_0 t) - \omega_0 q_2 \sin(\omega_0 t).$$

Using the averaging procedure [15, 16] over an explicitly incoming time, we obtain an averaged system of differential equations solved with respect to the derivatives of slow Van der Pol variables:

$$\begin{aligned} p_1' &= -\frac{1}{2}Q^{-1}p_1 + \frac{j_1\Omega}{2\omega_0}p_2 - \frac{j_1\delta}{2j_2}q_2, & q_1' &= -\frac{1}{2}Q^{-1}q_1 + \frac{j_1\Omega}{2\omega_0}q_2 + \frac{j_1\delta}{2j_2}p_2, \\ p_2' &= -\frac{1}{2}Q^{-1}p_2 - \frac{j_2\Omega}{2\omega_0}p_1 - \frac{\delta}{2}q_1, & q_2' &= -\frac{1}{2}Q^{-1}q_2 - \frac{j_2\Omega}{2\omega_0}q_1 + \frac{\delta}{2}p_1. \end{aligned} \quad (6)$$

The dash in equations (6) indicates the differentiation in dimensionless time $\tau = \omega_0 t$.

The resulting model in the form of linear differential equations describes the free oscillations of a gyroscope SE on a movable base. The solution to the system of equations (6) can be written as:

$$\begin{aligned} p_1(\tau) &= \exp\left(-\frac{\tau}{2Q}\right) \left[p_{10} \cos(\sqrt{\nu^2 + \gamma^2}\tau) + \sqrt{\frac{j_1}{j_2}} \cdot \frac{(\nu p_{20} - \gamma q_{20})}{\sqrt{\nu^2 + \gamma^2}} \sin(\sqrt{\nu^2 + \gamma^2}\tau) \right], \\ q_1(\tau) &= \exp\left(-\frac{\tau}{2Q}\right) \left[q_{10} \cos(\sqrt{\nu^2 + \gamma^2}\tau) + \sqrt{\frac{j_1}{j_2}} \cdot \frac{(\gamma p_{20} + \nu q_{20})}{\sqrt{\nu^2 + \gamma^2}} \sin(\sqrt{\nu^2 + \gamma^2}\tau) \right], \\ p_2(\tau) &= \exp\left(-\frac{\tau}{2Q}\right) \left[p_{20} \cos(\sqrt{\nu^2 + \gamma^2}\tau) - \sqrt{\frac{j_2}{j_1}} \cdot \frac{(\nu p_{10} + \gamma q_{10})}{\sqrt{\nu^2 + \gamma^2}} \sin(\sqrt{\nu^2 + \gamma^2}\tau) \right], \\ q_2(\tau) &= \exp\left(-\frac{\tau}{2Q}\right) \left[q_{20} \cos(\sqrt{\nu^2 + \gamma^2}\tau) - \sqrt{\frac{j_2}{j_1}} \cdot \frac{(\gamma q_{10} - \nu p_{10})}{\sqrt{\nu^2 + \gamma^2}} \sin(\sqrt{\nu^2 + \gamma^2}\tau) \right] \end{aligned} \quad (7)$$

where $p_{10} = p_1(0)$, $p_{20} = p_2(0)$, $q_{10} = q_1(0)$, $q_{20} = q_2(0)$ — initial conditions; dimensionless angular rate of the device base $\nu = \sqrt{j_1 j_2} \Omega / (2\omega_0)$; parameter characterizing the nonorthogonality of the torsion axes $\gamma = \sqrt{j_1} \delta / (2\sqrt{j_2})$.

The second terms in formulas (7) characterize the cross-influence of primary vibrations on secondary vibrations and vice versa. Note that in the case of orthogonal torsion axes, when $\gamma = 0$, solution (7) coincides with the results of paper [5].

The obtained analytical solutions (7) of the oscillation equations are of interest for the development of methods for identifying parameters, as well as predicting the gyro drift and considering it when using the method of algorithmic error compensation.

Research Results. To validate the developed model, we compare the simulation results calculated from formulas (7) and experimental data. The measurement information was obtained using an observation system. As the measurement information of electrostatic sensors, we have Van der Pol variables p_1, q_1, p_2, q_2 .

In the experiment, a sample device with the following parameters of a mathematical model with a fixed base ($\nu = 0$): $Q = 3856$, $j_1 = j_2 = 1$, $\gamma = 0.2 \cdot 10^{-5}$, as initial conditions for the Van der Pol variables, values equal to the measurements at the initial moment of time were selected:

$$p_{10} = 13.467 \cdot 10^{-3}, \quad q_{10} = 20.429 \cdot 10^{-3}, \quad p_{20} = 0.787 \cdot 10^{-3}, \quad q_{20} = 1.172 \cdot 10^{-3}.$$

Parameter γ value corresponds to the angle of nonorthogonality of torsion axes δ equal to one angular second. A graphical representation of the dependencies of Van der Pol variables $p_1(\tau)$, $q_1(\tau)$, $p_2(\tau)$, $q_2(\tau)$ that slowly change over a dimensionless time is shown in Fig. 3.

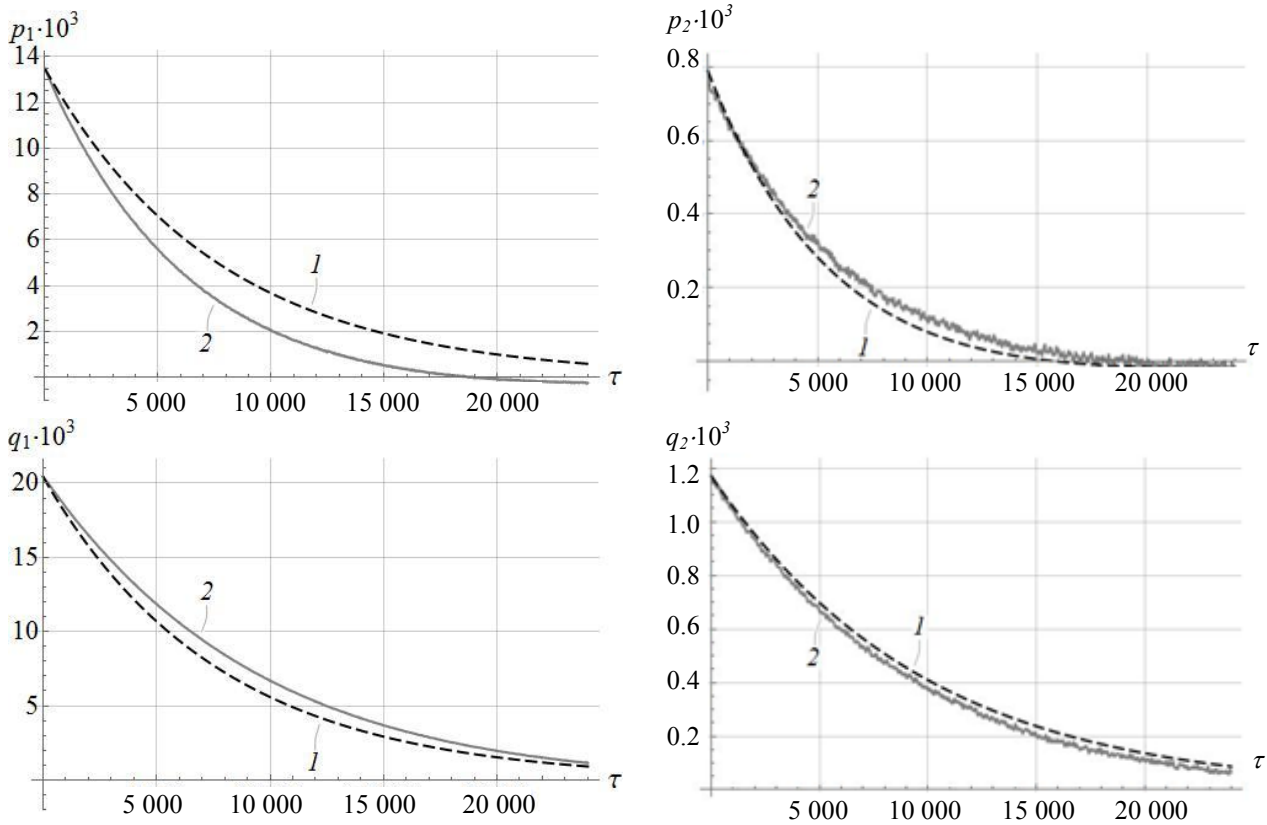


Fig. 3. Dependences of Van der Pol variables: 1 — simulation results; 2 — experimental data

The graphs (Fig. 3) show a significant coincidence of the dependencies for variables p_2 , q_2 , obtained from the simulation results with the experimental data. The dependences for variables p_1 , q_1 , obtained from the simulation results, are in qualitative agreement with the experimental data, and the observed small quantitative deviations may be due to nonlinear effects, such as the nonlinearity of the geometry of the SE motion [5], or the phenomena of variability of quality, variability of frequency, and the error of the inertial mass displacement [12]. Consideration of nonlinear effects affecting the dynamics of MMG in the construction of mathematical models of SE oscillations increases the accuracy of micromechanical sensors as part of the inertial navigation systems [2].

The gyro drift due to nonlinear effects and other instrumental errors will be estimated using the auxiliary functional I [5, 6, 9]:

$$I = \frac{2\sqrt{j_1 j_2} (q_1 q_2 + p_1 p_2)}{j_2 (q_1^2 + p_1^2) - j_1 (q_2^2 + p_2^2)}, \quad (8)$$

which is related to angle θ via the relation:

$$\theta = \frac{1}{2} \arctan(I).$$

Moreover, this parameter is proportional to the integral of the angular rate:

$$\theta = -\frac{\sqrt{j_1 j_2}}{2} \int_0^\tau \Omega(\tau_1) d\tau_1.$$

Using formula (8), taking into account solution (7), it is possible to estimate the gyroscope drift associated with the nonorthogonality of the torsion axes, which arose due to the imperfection of the manufacturing technology. Figure 4 shows the dependences of functional I on the dimensionless time according to the results of the experiment and the calculation according to formula (8).

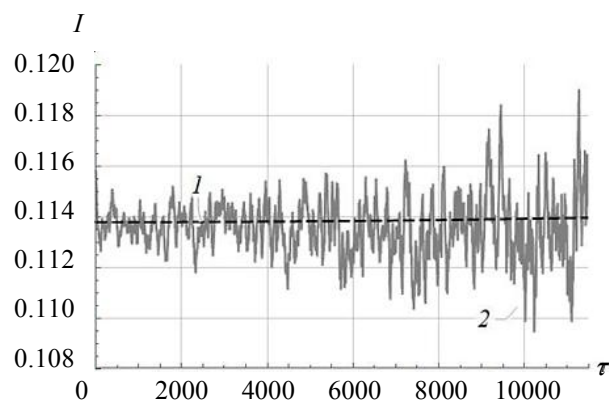


Fig. 4. Functional dependence $I(\tau)$: 1 — simulation results; 2 — experimental data

The proximity of the drift estimate (Fig. 4) and the Van der Pol variables (Fig. 3) obtained analytically with experimental data characterize good accuracy of the constructed model, especially if we take into account the fact that it neglected nonlinear effects, as well as the phenomena of variability of frequency and variability of quality. Despite these neglects, the model provides building methods for identifying parameters, with the help of which it is possible to clarify the dependences obtained under modeling. The application of methods for identifying the parameters of a mathematical model will cause an increase in the accuracy of the MMG in the forced oscillation mode, which is the operating mode of gyroscopes.

Discussion and Conclusions. A new mathematical model of the R-R-type MMG for the mode of free oscillations of the SE is constructed. The model takes into account the nonorthogonality of the torsion axes, which arises as a result of the technological impossibility to ensure high accuracy of the device manufacturing. The formula for estimating the precession angle with a movable base of the device is obtained. Through comparing the simulation results and the experimental data, the validation of the MMG mathematical model was carried out. It is shown that the nonorthogonality of the torsion axes causes a cross-influence of primary vibrations on the magnitude of secondary vibrations and vice versa. The research results can be used in the algorithm of analytical compensation of the gyroscope error to increase the accuracy of the MMG.

References

1. Peshekhonov VG. Gyroscopic navigation systems: Current status and prospects. *Gyroscopy and Navigation*. 2011;2(3):111–118.
2. Zhuravlev VF. Upravlyaemyi mayatnik Fuko kak model' odnogo klassa svobodnykh giroskopov. *Izvestiya RAN. Mekhanika Tverdogo Tela = Mechanics of Solids*. 1997;6:27–35. (In Russ.)
3. Raspopov VYa. *Mikromekhanicheskie pribory*. Moscow: Mashinostroenie; 2007. 400 p. (In Russ.)
4. Neapolitansky AS, Khromov BV. *Mikromekhanicheskie vibratsionnye giroskopy*. Moscow: Kogito-tsentr; 2002. 122 p. (In Russ.)
5. Merkur'yev IV, Podalkov VV. *Dinamika mikromekhanicheskogo i volnovogo tverdotel'nogo giroskopov*. Moscow: Fizmatlit; 2009. 228 p. (In Russ.)
6. Yongmeng Zhang, Tongqiao Miao, Kechen Guo, et al. Electronic Gain Error Compensation for Whole-Angle Coriolis Vibrating Gyroscopes With High Q Factor. In: *Proc. IEEE Int. Symposium on Inertial Sensors and Systems (INERTIAL)*. 2020. P. 1–4. <https://doi.org/10.1109/INERTIAL48129.2020.9090062>
7. Apostolyuk V. Theory and Design of Micromechanical Vibratory Gyroscopes. *MEMS/NEMS Handbook*. 2006;1(6):173–195. 10.1007/0-387-25786-1_6
8. Wei Wang, Xiaoyong Lv, Feng Sun. Design of a Novel MEMS Gyroscope Array. *Sensors*. 2013;13(2):1651–1663. <https://doi.org/10.3390/s130201651>
9. Sina Askari, Mohammad H. Asadian, Andrei M. Shkel. High quality factor MEMS gyroscope with whole angle mode of operation. In: *Proc. IEEE Int. Symposium on Inertial Sensors and Systems (INERTIAL)*. 2018;12(6):141–144. <https://doi.org/10.1109/ISISS.2018.8358148>
10. Markeev AP. *Theoretical mechanics*. Moscow, Izhevsk: RKhD; 2007. 592 p. (In Russ.)
11. Bolotin SV, Karapetyan AV, Kugushev EI, et al. *Theoretical mechanics*. Moscow: Akademiya; 2010. 432 p. (In Russ.)
12. Saipulaev MR, Merkur'yev IV. Dynamics and accuracy of a micromechanical gyroscope with provision for the displacement of inertial mass. *BSU Bulletin. Mathematics, Informatics*. 2020;3:49–62. <https://doi.org/10.18101/2304-5728-2020-3-49-62> (In Russ.)

13. Andrei L. Smirnov, Sergei Filippov, Petr E. Tovstik, et al. Asymptotic Methods in Mechanics of Solids. Birkhäuser Basel: International Series of Numerical Mathematics; 2015. 323 p. 10.1007/978-3-319-18311-4
14. Awrejcewicz J, Krysko VA. Introduction to asymptotic methods. Boca Raton FL: Chapman & Hall/CRC; 2006. 242 p.
15. Burd V. Method of Averaging for Differential Equations on an Infinite Interval: Theory and Applications. Chapman & Hall/CRC; 2007. 343 p.
16. Medvedev GN. Lektsii po metodu usredneniya. Moscow: Faculty of Physics of Moscow State University; 2019. 109 p. (In Russ.)

Received 28.06.2021

Revised 19.07.2021

Accepted 27.07.2021

About the Authors:

Saypulaev, Musa R., graduate student of the Department of Robotics, Mechatronics, Dynamics and Strength of Machines, National Research University “Moscow Power Engineering Institute” (14, Krasnokazarmennaya St., Moscow, 111250, RF), engineer of 1 category, Kuznetsov Research Institute of Applied Mechanics (12A, Prud-Klyuchiki St., Moscow, 111024, RF), ORCID: <http://orcid.org/0000-0002-5165-654X>, saypulaevmr@mail.ru

Merkuryev, Igor V., Head of the Department of Robotics, Mechatronics, Dynamics and Strength of Machines, National Research University “Moscow Power Engineering Institute” (14, Krasnokazarmennaya St., Moscow, 111250, RF), Dr.Sci. (Eng.), associate professor, ORCID: <http://orcid.org/0000-0001-7682-2228>, ScopusID: [35422634900](https://orcid.org/0000-0001-7682-2228), nir4s@ya.ru

Solovyev, Alexey V., Head of the Department of Inertial Devices and Sensors, Kuznetsov Research Institute of Applied Mechanics (12A, Prud-Klyuchiki St., Moscow, 111024, RF), Cand.Sci. (Eng.), ORCID: <http://orcid.org/0000-0003-1345-1778>, AV.Solovev@russian.space

Tarasov, Alexander N., Head of the Department of Inertial Devices and Sensors, Kuznetsov Research Institute of Applied Mechanics (12A, Prud-Klyuchiki St., Moscow, 111024, RF), Cand.Sci. (Eng.), ORCID: <https://orcid.org/0000-0002-3657-5733>, A.Tarasov@russian.space

Claimed contributorship

M. R. Saypulaev: basic concept formulation; research objectives and tasks; construction of a mathematical model and obtaining an analytical solution to the oscillation equations; conducting modeling; text preparation; formulation of conclusions. I. V. Merkuryev: academic advising; analysis of the research results; the text revision; correction of the conclusions. A. V. Solovyev: discussion of the research results; the text revision. A. N. Tarasov: verification of the comparative analysis of experimental data and simulation results; discussion of the research results.

All authors have read and approved the final manuscript.

MECHANICS



UDC 539.3

<https://doi.org/10.23947/2687-1653-2021-21-3-239-246>

An infinite plate loaded with a normal force moving along a complex open trajectory

A. V. Galaburdin  

Don State Technical University (Rostov-on-Don, Russian Federation)

 Galaburdin@mail.ru

Introduction. A method for solving the problem on the action of a normal force moving on an infinite plate according to an arbitrary law is considered. This method and the results obtained can be used to study the effect of a moving load on various structures.

Materials and Methods. An original method for solving problems of the action of a normal force moving arbitrarily along a freeform open curve on an infinite plate resting on an elastic base, is developed. For this purpose, a fundamental solution to the differential equation of the dynamics of a plate resting on an elastic base is used. It is assumed that the movement of force begins at a sufficiently distant moment in time. Therefore, there are no initial conditions in this formulation of the problem. When determining the fundamental solution, the Fourier transform is performed in time. When the Fourier transform is inverted, the image is expanded in terms of the transformation parameter into a series in Hermite polynomials.

Results. The solution to the problem on an infinite plate resting on an elastic base, along which a concentrated force moves at a variable speed, is presented. A smooth open curve, consisting of straight lines and arcs of circles, was considered as a trajectory. The behavior of the components of the displacement vector and the stress tensor at the location of the moving force is studied, as well as the process of wave energy propagation, for which the change in the Umov-Poynting energy flux density vector is considered. The effect of the speed and acceleration of the force movement on the displacements, stresses and propagation of elastic waves is investigated. The influence of the force trajectory shape on the stress-strain state of the plate and on the nature of the propagation of elastic waves is studied. The results indicate that the method is quite stable within a wide range of changes in the speed of force movement.

Discussion and Conclusions. The calculations have shown that the most significant factor affecting the stress-strain states of the plate and the propagation of elastic wave energy near the concentrated force is the speed of its movement. These results will be useful under studying dynamic processes generated by a moving load.

Keywords: infinite plate, moving load, arbitrary open trajectory, variable speed, energy of elastic waves.

For citation: A. V. Galaburdin. An infinite plate loaded with a normal force moving along a complex open trajectory. Advanced Engineering Research, 2021, vol. 21, no. 3, pp. 239–246. <https://doi.org/10.23947/2687-1653-2021-21-3-239-246>

© Galaburdin A. V., 2021



Introduction. The regularities of dynamic processes in solid media caused by the action of a moving load are of considerable interest, and solutions to such problems find numerous applications and involve the use of various methods. In a number of works, to exclude time from the number of independent variables, a mobile coordinate system was introduced [1–2] or a quasistatic formulation of the problem was considered [3–6]. The finite element method [7], variational methods [8–10], as well as direct methods [11–13] proved to be quite effective in solving these problems. In [14–15], the method of boundary integral equations was used, and in [16] — a method based on the application of fundamental solutions to the corresponding differential equations. In this paper, the given method is used to solve the problem of the action of a normal force moving along a freeform open curve on an infinite plate resting on an elastic base.

Problem statement. Following [17, 18], this problem is reduced to solving the equation:

$$\Delta^2 U + c^{-2} \partial_t^2 U + kU = \frac{P}{D}, \quad (1)$$

where U — the plate deflection; $D = \frac{EH^3}{12(1-\mu^2)}$; E — the Young's modulus; μ — the Poisson's ratio; H — the plate thickness; $c^{-2} = \frac{\rho H}{D}$; ρ — the density of the plate material; $k = \frac{k_o}{D}$; k_o — the stiffness coefficient of the elastic base.

The solution to this equation corresponds to the energy flow directed from the excitation sources to infinity. We will assume:

$$P = \delta(x - x_o(t))\delta(y - y_o(t)).$$

This force moves along an open trajectory γ , whose beginning and end go to infinity. The parametric setting of the trajectory has the form: $\begin{cases} x = x(t) \\ y = y(t) \end{cases}$, where t — time. It is assumed that the force starts to move at the beginning of the trajectory, located at a sufficient distance from the place where its effect on the plate is being studied at the moment of time $t = -\infty$. Therefore, there are no initial conditions in such a statement.

Materials and Methods. Consider the fundamental solution to equation (1), which can be obtained from the equation:

$$\Delta^2 W + c^{-2} \partial_t^2 W + kW = \frac{1}{D} \delta(x - x_o) \delta(y - y_o) \delta(t - \tau). \quad (2)$$

It is known that the solution to equation (1) can be presented as:

$$U(x, y, t) = \int_{-\infty}^{\infty} \iint_{R^2} W(x, x_o, y, y_o, t - \tau) P(x_o, y_o, \tau) dx_o dy_o d\tau.$$

In our case, taking into account a specific type of moving force, we have:

$$U(x, y, t) = \int_{-\infty}^{\infty} W(x, x_o(\tau), y, y_o(\tau), t - \tau) d\tau.$$

Applying the Fourier transform in time to equation (2), we obtain the differential equation:

$$\Delta^2 W_o - \omega^2 c^{-2} W_o + kW_o = \frac{1}{D} \delta(x - x_o) \delta(y - y_o) e^{i\omega\tau}. \quad (3)$$

Using the limiting absorption principle and the Fourier transform with respect to variables x and y , and under the condition $k > \frac{\omega^2}{c^2}$ we can obtain a solution to the equation (3):

$$W_o \left(x, x_o, y, y_o, \frac{\omega^2}{c^2} \right) = \frac{i}{4\pi\chi^2 D} [K_0(\alpha_1 R) - K_0(\alpha_2 R)],$$

where $R = [(x - x_o)^2 + (y - y_o)^2]^{1/2}$; $\chi = \sqrt{k - \omega^2/c^2}$; $\alpha_1 = \chi e^{i\pi/4}$; $\alpha_2 = \chi e^{-i\pi/4}$; $K_0(z)$ — the Macdonald function.

Under the condition $k \leq \frac{\omega^2}{c^2}$ the solution to equation (3) looks like this:

$$W_o(x, x_o, y, y_o, \omega^2/c^2) = \frac{i}{4\pi\chi^2 D} \left[\frac{\pi i}{2} H_0^{(1)}(\chi R) - K_0(\chi R) \right],$$

where $\chi = \sqrt[4]{\frac{\omega^2}{c^2} - k}$; $H_0^{(1)}(z)$ — the Hankel function.

To reverse the Fourier transform, the solution $W_0(x, x_0, y, y_0, \omega^2/c^2)$ is expanded by variable $\frac{\omega}{c}$ into series according to the system of orthogonal functions $\left\{e^{-\omega^2/c^2} H_k\left(\frac{\omega}{c}\right)\right\}$, where $H_k(z)$ — Hermit polynomials.

Given that function $W_0\left(x, x_0, y, y_0, \frac{\omega^2}{c^2}\right)$ is even in $\frac{\omega}{c}$, only even terms will be present in the expansion. Then:

$$W_0(x, x_0, y, y_0, \omega^2/c^2) = \sum_{k=0}^{\infty} w_{2k}(x, x_0, y, y_0) e^{-\omega^2/2c^2} H_{2k}\left(\frac{\omega}{c}\right), \text{ где}$$

$$w_{2k}(x, x_0, y, y_0) = \frac{1}{(2k)! 2^{2k} \sqrt{\pi}} \int_{-\infty}^{\infty} W_0(x, x_0, y, y_0, z^2) e^{-z^2/2} H_{2k}(z) dz.$$

Given the ratio:

$$\int_{-\infty}^{\infty} e^{-\omega^2/2c^2} H_{2k}\left(\frac{\omega}{c}\right) e^{-i\omega t} d\omega = 2c \sqrt{\frac{\pi}{2}} (-1)^k e^{-c^2 t^2/2} H_{2k}(ct),$$

we get:

$$W_0(x, x_0, y, y_0, t) = 2c \sqrt{\frac{\pi}{2}} \sum_{k=0}^{\infty} (-1)^k w_{2k}(x, x_0, y, y_0) e^{-c^2 t^2/2} H_{2k}(ct).$$

In this case, the solution to the original differential equation will have the form:

$$U(x, y, t) = 2c \sqrt{\frac{\pi}{2}} \sum_{k=0}^{\infty} (-1)^k w_{2k}(x, x_0(\tau), y, y_0(\tau)) e^{-c^2(t-\tau)^2/2} H_{2k}(c(t-\tau)) d\tau.$$

Through replacing the integration variable, we get:

$$U(x, y, t) = \sum_{k=0}^{\infty} \int_{-\infty}^{\infty} \int_{-\infty}^{\infty} W_0\left(x, x_0\left(t - \frac{s\sqrt{2}}{c}\right), y, y_0\left(t - \frac{s\sqrt{2}}{c}\right), 2\tau^2\right) \frac{2\sqrt{2}(-1)^k}{(2k)! 2^{2k}} e^{-(s^2+\tau^2)} H_{2k}(s\sqrt{2}) H_{2k}(\tau\sqrt{2}) ds d\tau.$$

This type of solution allows us to use the Gauss-Hermite quadrature formula to calculate the integral.

To improve the convergence of the series, the Kummer method was used. Following this method, it is required to select a series whose sum is known, and the difference between the original series and the selected series should represent a rapidly converging series. As such a series, you can take:

$$U^*(x, y, t) = \sum_{k=0}^{\infty} \int_{-\infty}^{\infty} \int_{-\infty}^{\infty} W_0\left(x, x_0\left(t - \frac{s\sqrt{2}}{c}\right), y, y_0\left(t - \frac{s\sqrt{2}}{c}\right), q\right) \frac{2\sqrt{2}(-1)^k}{(2k)! 2^{2k}} e^{-(s^2+\tau^2)} H_{2k}(s\sqrt{2}) H_{2k}(\tau\sqrt{2}) ds d\tau,$$

where q — some nonnegative value.

Through integrating on variable τ and summing, we get:

$$U^*(x, y, t) = \pi c \sqrt{2} W_0(x, x_0(t), y, y_0(t), q).$$

Finally, to solve equation (1), we obtain the following expression:

$$U(x, y, t) = U^*(x, y, t) +$$

$$+ \sum_{k=0}^{\infty} \int_{-\infty}^{\infty} \int_{-\infty}^{\infty} (W_0(x, x_0(t - \frac{s\sqrt{2}}{c}), y, y_0(t - \frac{s\sqrt{2}}{c}), 2\tau^2) - W_0(x, x_0(t - \frac{s\sqrt{2}}{c}), y, y_0(t - \frac{s\sqrt{2}}{c}), q)) \times$$

$$\times \frac{2\sqrt{2}(-1)^k}{(2k)! 2^{2k}} e^{-(s^2+\tau^2)} H_{2k}(s\sqrt{2}) H_{2k}(\tau\sqrt{2}) ds d\tau.$$

To sum the series, the arithmetic mean method was used. At the same time, the following was supposed: $q = 0$.

Having determined the plate deflections, it is possible to calculate the remaining components of the displacement vector and the stress tensor at any point of it using known formulas. To analyze the energy displacement of elastic waves in the plate, the Umov-Poynting energy flux density vector was calculated:

$$\vec{E} = -(\sigma_x \dot{u} + \sigma_{xy} \dot{v}) \vec{l} - (\sigma_{xy} \dot{u} + \sigma_y \dot{v}) \vec{j}.$$

Research Results. Calculations are carried out for the case when the force moves along a trajectory consisting of straight lines and arcs of circles (Fig. 1). The following parameter values were taken: $H = 0.25$ m; $c = 221$ m/s; $E = 232469$ N/m²; $\mu = 0.36$; $K = 1.864$ m⁻⁴.

The parameters of the law of motion of the force along the trajectory were selected in such a way that at the time under consideration, the force was always at the same point of the trajectory marked with an asterisk, having different values of speed v and acceleration a , as well as at different values of the radius of trajectory R_2 . To study the stress-strain state of the plate, displacements and stresses near the point of application of force were calculated.

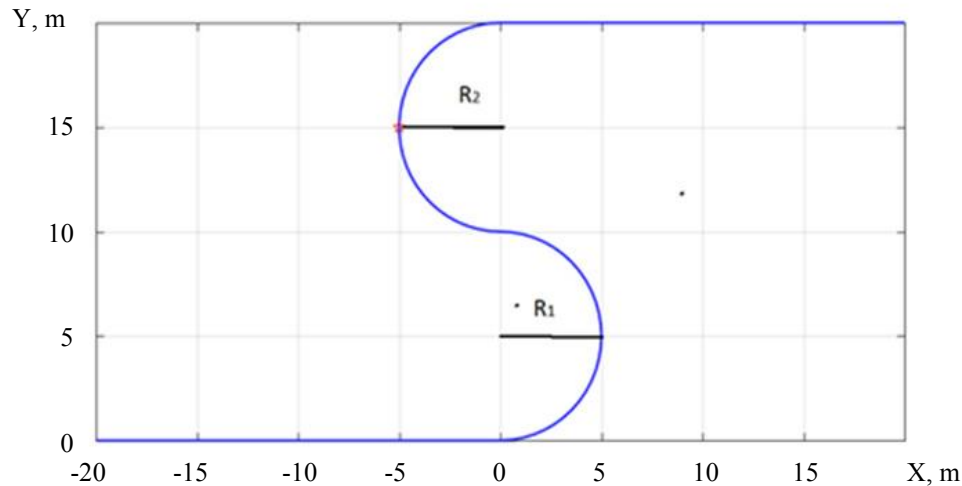


Fig. 1. Trajectory of the concentrated force

Figures 2 and 3 show the change in displacements and stresses during the movement of a concentrated force along a given trajectory at $v = 25$ m/s, $a = 0$ m/s², $R_2 = 5$ m. The change of these values along the Y-axis does not practically differ from their change along the X-axis.

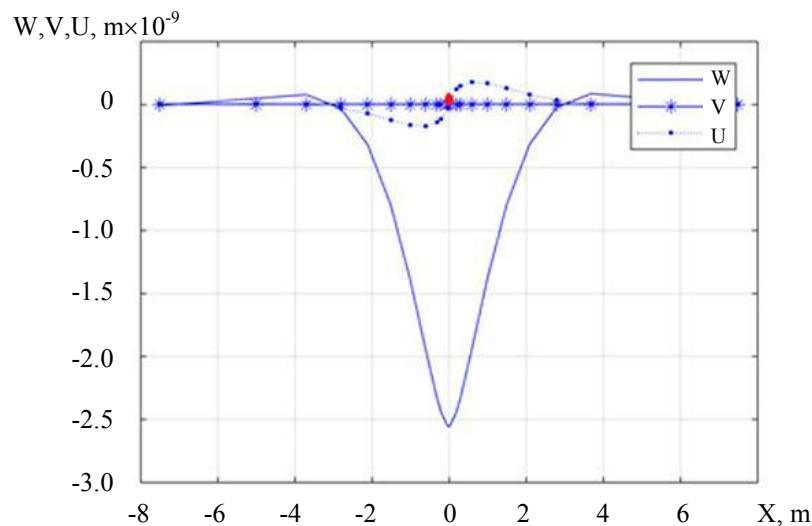


Fig. 2. Change in displacements: W — vertical; U — along the X axis; V — along the Y axis

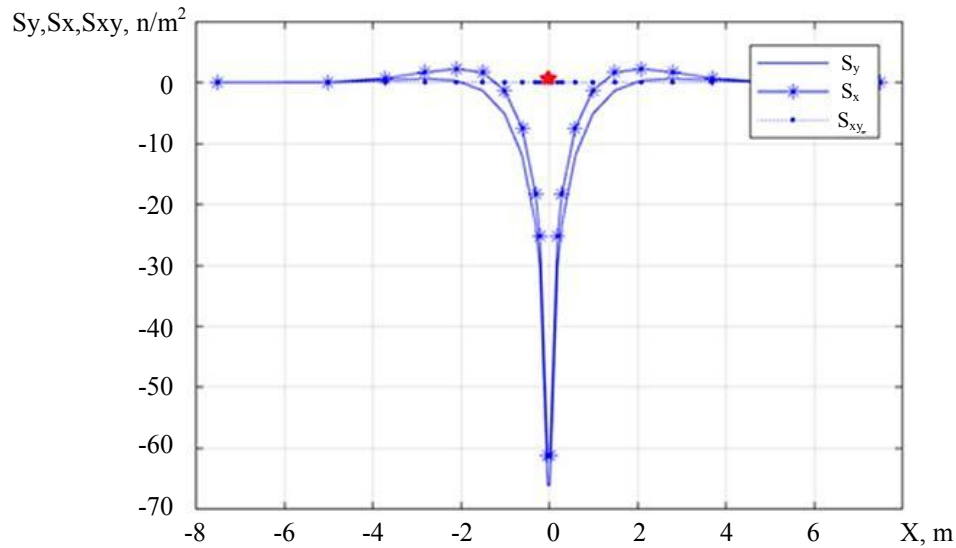


Fig. 3. Change in voltages: W — vertical; U — along the X axis; V — along the Y axis

Figure 4 shows the movement of the energy of elastic waves near the concentrated force, whose position on the trajectory is marked with a red dot. The vectors determine the amount and direction of energy transfer at a given point.

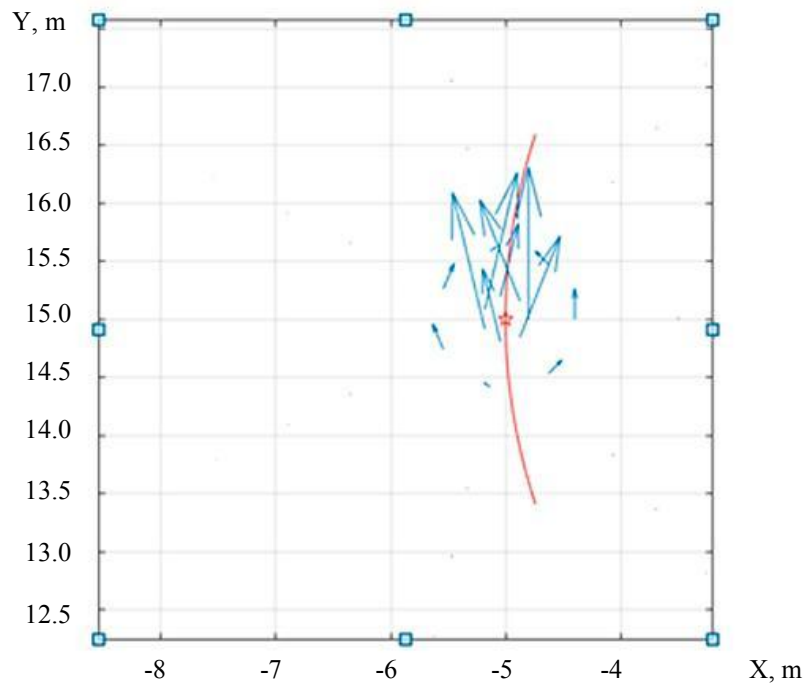


Fig. 4. Energy flux density vector at $v = 25 \text{ m/s}$, $a = 0 \text{ m/s}^2$, $R_2 = 5 \text{ m}$

The calculations have shown that with an increase in the speed of the force movement, there is no qualitative change in displacements and stresses, but only their quantitative growth occurs. A slight change in the qualitative behavior of displacements and stresses is observed only at sufficiently high speeds, when the condition $v > c$ is met. This follows from Fig. 5, 6 ($a = 0 \text{ m/sc}^2$, $R_2 = 5 \text{ m}$).

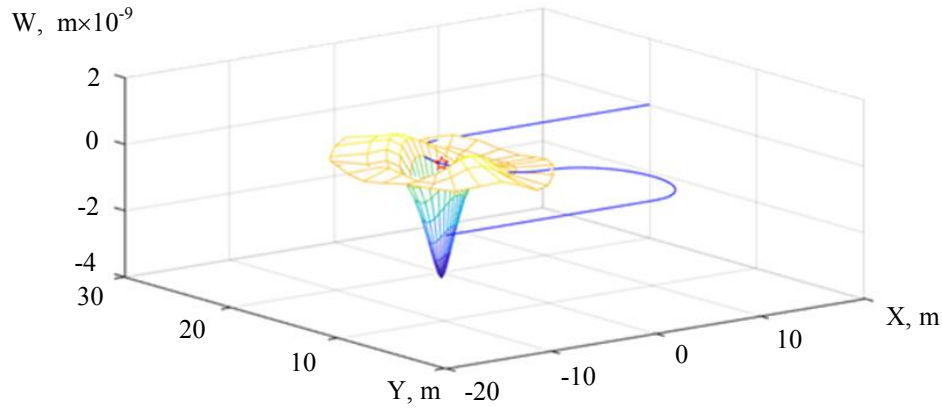


Fig. 5. Changing vertical movements at $v = 275$ m/s

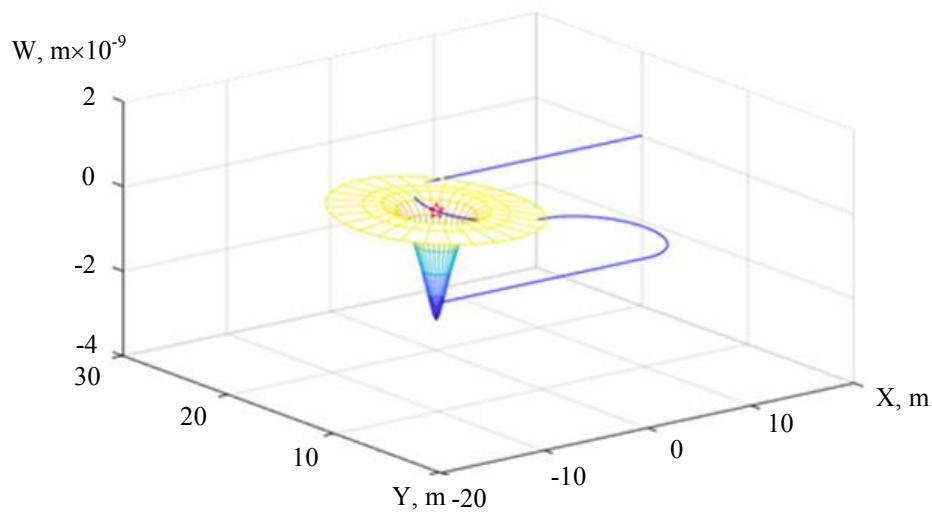


Fig. 6. Changing vertical movements at $v = 75$ m/s

Figures 7 and 8 show the change in the maximum vertical displacements W and stresses S_x , S_y depending on the speed of the force movement at $a = 0$ m/s², $R_2 = 5$ m. The remaining components of displacements and stresses assumed sufficiently low values and therefore were not of constructive interest when analyzing the stress-strain state of the plate.

Calculations performed at different values of acceleration and radius R_2 , have shown that these factors have little effect on the stress-strain state of the plate. The qualitative picture of wave energy propagation near the concentrated force also weakly depends on these factors.

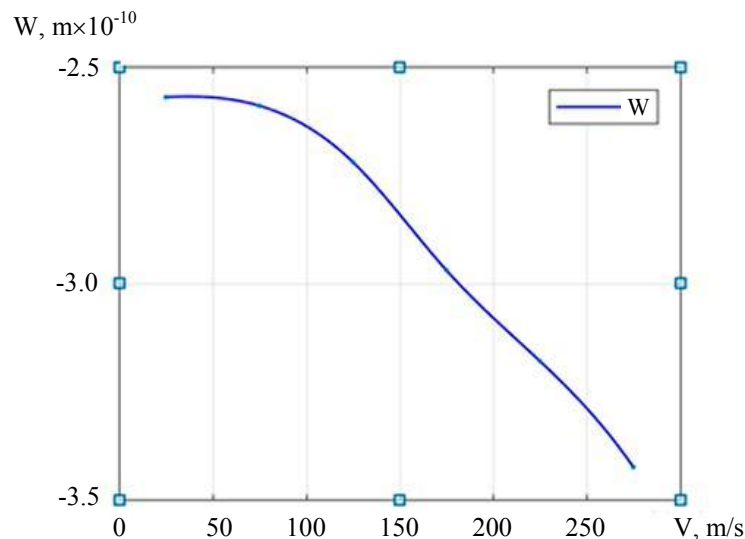


Fig. 7. Dependence of maximum vertical displacements on concentrated force movement speed

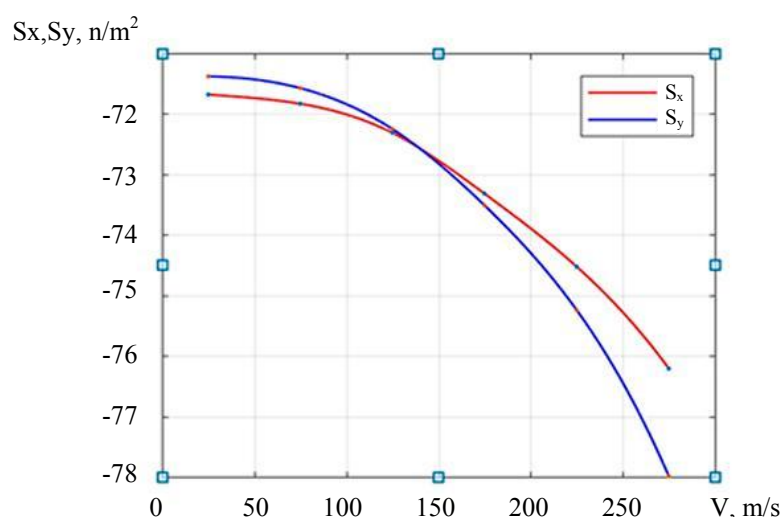


Fig. 8. Dependence of maximum voltages on concentrated force movement speed

Discussion and Conclusions. The most significant effect on the stress-strain state of the plate and the propagation of elastic wave energy near the concentrated force is exerted by the speed of its movement. The radius of curvature of the trajectory and the acceleration of the force movement do not significantly affect.

The calculation results indicate that the method of solving problems on the action of a moving load is quite stable within a wide range of changes in the speed of its movement. The method is economical and simple, because it uses already known fundamental solutions.

References

1. Onur Şahin, Barış Erbaş, Nihal Ege. Response of a 3D elastic half-space to a distributed moving load. *Hacettepe Journal of Mathematics and Statistics*. 2017;46(5):817-828. <https://doi.org/10.15672/HJMS.2017.434>
2. Kalinchuk VV, Belyankova TI, Schmid C, et al. Dynamic of layered half space under the action of moving and oscillating load. *Vestnik SSC RAS*. 2005;1(1):3–11. (In Russ.)
3. Yuyan Chen, Niki D. Beskou, Jiang Qian. Dynamic response of an elastic plate on a cross-anisotropic poroelastic halfplane to a load moving on its surface. *Soil Dynamics and Earthquake Engineering*. 2018;107:292-302. <https://doi.org/10.1016/j.soildyn.2018.01.038>
4. Kaplunov J, Prikazchikov DA, Rogerson GA. The edge wave on an elastically supported Kirchhoff plate. *The Journal of the Acoustical Society of America*. 2014;136(4):1487-1490. <https://doi.org/10.1121/1.4894795>
5. Egorychev OO. Vozdeistvie podvizhnoi nagruzki na mnogosloinuyu vyzkoupругuyu plastinu, lezhashchuyu na vyzkoupругom osnovanii. *Vestnik MGSU*. 2007;1:39–42. (In Russ.)
6. Doszhanov MZh, Iskak EN, Saktaganov BZh, et al. Dynamic behavior of infinite elastic plate affected by mobile load. *The Way of Science*. 2016;11(33):26–28. (In Russ.)
7. Shishmarev KA. Problem formulation of ice plate viscoelastic oscillations in a channel caused by a moving load. *Izvestia of Altai State University*. 2015;1/2(85):189–194. [https://doi.org/10.14258/izvasu\(2015\)1.2-35](https://doi.org/10.14258/izvasu(2015)1.2-35). (In Russ.)
8. Dyniewicz B, Pisarski BD, Bajer CI. Vibrations of a Mindlin plate subjected to a pair of inertial loads moving in opposite directions. *Journal of Sound and Vibration*. 2017;386:265-282. <https://doi.org/10.1016/j.jsv.2016.09.027>
9. Esen I. A new finite element for transverse vibration of rectangular thin plates under a moving mass. *Finite Elements in Analysis and Design*. 2013;66:26-35. <https://doi.org/10.1016/j.finel.2012.11.005>
10. Song Qinghua, Shi Jiahao, Liu Zhanqiang. Vibration analysis of functionally graded plate with a moving mass. *Applied Mathematical Modelling*. 2017;46:141-160. <https://doi.org/10.1016/j.apm.2017.01.073>
11. Qinghua Song, Zhanqiang Liu, Jiahao Shi, et al. Parametric study of dynamic response of sandwich plate under moving loads. *Thin-Walled Structures*. 2018;123:82-99. <https://doi.org/10.1016/j.tws.2017.11.012>

12. Yegao Qu, Wenming Zhang, Zhike Peng, et al. Time-domain structural-acoustic analysis of composite plates subjected to moving dynamic loads. *Composite Structures*. 2019;208:574-584. <https://doi.org/10.1016/j.compstruct.2018.09.103>
13. Foyouzat MA, Estekanchi HE, Mofid M. An analytical-numerical solution to assess the dynamic response of viscoelastic plates to a moving mass. *Applied Mathematical Modelling*. 2018;54:670-696. <https://doi.org/10.1016/j.apm.2017.07.037>
14. Galaburdin AV. Applying of boundary integral equation method to the decision of flat problems of thermoelasticity with mobile load. *Bulletin of Higher Education Institutes. North-Caucasian region. Natural Sciences*. 2012;4:29–31. (In Russ.)
15. Galaburdin AV. Application of a method of the boundary integral equations to the decision of problems on moving loading. *Bulletin of Higher Education Institutes. North-Caucasian region. Natural Sciences*. 2015;1:9–11. (In Russ.)
16. Galaburdin AV. The problem of infinite plate loaded with normal force following a complex trajectory. *Vestnik of Don State Technical University*. 2019;19(3):208–213. <https://doi.org/10.23947/1992-5980-2019-19-3-208-213> (In Russ.)
17. Babakov IM. *Teoriya kolebanii*. Moscow: Nauka; 1968. 560 p. (In Russ.)
18. Brebbia K, Telles J, Vroubel L. *Metody granichnykh uravnenii*. Moscow: Mir; 1987. 524 p. (In Russ.)

Received 26.07.2021

Revised 09.08.2021

Accepted 25.08.2021

About the Author:

Galaburdin, Alexander V., associate professor of the Mathematics and Computer Sciences Department, Don State Technical University (1, Gagarin sq., Rostov-on-Don, 344000, RF), Cand.Sci. (Phys.-Math.), associate professor, ORCID: <http://orcid.org/0000-0003-0411-6724>, Galaburdin@mail.ru

The author has read and approved the final manuscript.

MACHINE BUILDING AND MACHINE SCIENCE



UDC 681.5

<https://doi.org/10.23947/2687-1653-2021-21-3-247-252>


Organization of walking of the lower-extremity exoskeleton using the control of the supporting foot



Zh. N. Issabekov ¹, I. K. Tsybrii ², K. A. Moroz  ³

¹Satbayev University (Almaty, Republic of Kazakhstan)

^{2,3}Don State Technical University (Rostov-on-Don, Russian Federation)

 Leramoroz@mail.ru

Introduction. The development of robotics in many advanced countries has raised various industries to a high level. The demand for robots increases the share of their use in production tasks, mainly in the motor-vehicle and electronics industries. Advanced robotics can increase productivity in many industries by 30%, while reducing labor costs. Automation of technological processes of electronics production has a positive impact on the use of robots. Robots are used in construction, logistics, oil and gas, aerospace, plant engineering and construction, mining, healthcare, etc. The authors consider robots from the point of view of their application in medicine for the rehabilitation of musculoskeletal patients. This paper describes the mechanisms for controlling the feet and the center of mass of a humanoid robot.

Materials and Methods. The authors chose the simplest algorithm for searching for the law of motion control of a humanoid robot. The robot movement was presented as a reverse pendulum. Using the large kinematic redundancy of walking robots, we have developed a way to control the robot in such a way as to bring the dynamics of its movement to the reverse pendulum as close as possible. At the same time, the problem of determining the generalized coordinates is considered, at which a given position and orientation of the transferred foot and a given position of the projection of the center of mass (CM) of the robot onto the reference surface are provided.

Results. The authors have developed a digitalized automatic control scheme for the movement of the feet and the center of mass of the human exoskeleton, which will largely reduce the load on a sick person.

Discussion and Conclusions. When discussing the results, comparing the data of the tables obtained during the calculation, the following conclusion was made. The scheme for controlling the feet movement of a human exoskeleton developed by the authors is most effective when designing an automatic scheme for controlling the movement of the feet and the center of mass of a human exoskeleton using digital technology, which will largely reduce the load on a sick person.

Keywords: center, mass, supporting foot, exoskeleton, robot, human, movement dynamics, reverse pendulum.

For citation: Zh. N. Issabekov, I. K. Tsybrii, K. A. Moroz. Organization of walking of the lower-extremity exoskeleton using the control of the supporting foot. Advanced Engineering Research, 2021, vol. 21, no. 3, pp. 247–252. <https://doi.org/10.23947/2687-1653-2021-21-3-247-252>

© Issabekov Zh. N., Tsybrii I. K., Moroz K. A., 2021



Introduction. In many advanced countries, the successful introduction of robotics has raised various industries to a high level. The demand for robots has increased the share of their use in production tasks to 25–45 %, mainly in the motor-vehicle and electronics industries. Advanced robotics can increase productivity in many industries by 30 %, while reducing labor costs by 18–33 %. Modern robotics can significantly change the entire value chain of products. It is estimated that there are about 1.8 million industrial robots operating in the world production systems today, representing a global market of about \$35 billion: the possibilities of robotics continue to grow, and the costs of manufacturing robots continue to fall (they have decreased by about 25 % over the past decade). In production, the largest number of robots are used for packaging, grabbing and moving (in Russia, almost 40 % of the 1.7 million), and this application has the highest annual growth rate (on average, 11 % per year for 2010-2014). The second common

application is in the production of cars, where robots are used primarily for welding. The use of robots for assembly is also a fast-growing segment (the average annual growth rate in 2010–2014 was 10 %) due to the growing number of electronics/electrical industry products that seek miniaturization and require increased accuracy in manufacturing.

At Russian enterprises, the density of production robotization is more than 20 times lower than the global average. According to the statistics of the International Federation of Robotics, in Kazakhstan, as well as in Russia, there are only three industrial robots per 10000 workers, while on average there are 69 worldwide, and more than 100 – in the leading countries in the field of digitalization. For example, the share of the Russian market of industrial robots is only 0.25 % of the global volume, the main consumers are China (27 %), South Korea (15 %), Japan (14 %) and North America (about 14 %). There is also a lag in the share of machines with numerical control: in Japan it is more than 90 %, in Germany and the USA – more than 70 %, in China – about 30 % [1–3].

Modern robotics has been successfully developed in Kazakhstan. Modern factories are being built, where robots perform monotonous work. The growth of investments in robotics is increasing every year in Kazakhstan. Currently, Kazakhstani enterprises are given a chance to reduce the gap with world leaders. The great flexibility and intelligence of robots allow them to be used in various industries where they have not been traditionally used, including the production of food and beverages, consumer goods and pharmaceuticals.

New concepts have emerged, such as wearable electronics and virtual reality, which can be used for quality control, work instructions, training, workflow management, various operations, security, logistics, and maintenance. In addition, the increased accuracy of these technologies provides improving the profitability of the enterprise by increasing productivity. And the instability of quality can be reduced by shortening downtime, defects and waste while decreasing the lead time [2]. The development of new technologies will significantly change production processes: it is most effective in those industries where it is important to adapt the product to customer requirements, and components are produced in small volumes and have a high cost. Therefore, the production of consumer goods and the motor-vehicle industry, medical and aerospace industries are priorities in the Republic of Kazakhstan, especially in the use of 3D printing technologies, the production of highly reliable medical devices: hearing aids, dental and other prostheses.

Materials and Methods. Among all types of robotics, the authors distinguish the medical field. They are engaged in the development of exoskeletons of bipedal walking machines (BWM) [4–8]. For BWM, it is generally accepted to distinguish two types of walking: static and dynamic. At the static walking, the robot movements are so slow that it is possible to neglect the forces of inertia. This allows using a control algorithm built on the basis of only equations describing the kinematics of the robot. However, the device speed depends on its size, dynamic parameters, kinematic scheme. For many walking machines, this is the main method of control. Figure 1 shows an image of an exoskeleton that is being developed by the authors.

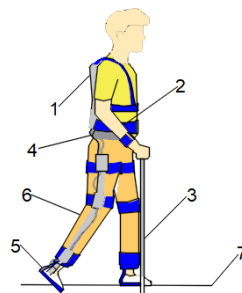


Fig. 1. Functional scheme of the exoskeleton:

1 — backpack with a microprocessor; 2 — arm; 3 — crutches; 4 — trunk; 5 — foot; 6 — leg; 7 — reference surface

The equations describing the dynamics of the robot are complex and require the use of well-known methods for solving variational problems of large dimension. A simpler algorithm for finding the law of movement control of a human robot is needed. The authors from the Bauman Moscow State Technical University proposed the simplest way – to imagine the robot as a reverse pendulum and, using the large kinematic redundancy of BWM, control the robot in such a way as to bring the dynamics of its movement to the reverse pendulum as close as possible [4–5].

Let us consider the problem of determining the generalized coordinates at which a given position and orientation of the transferred foot and a given position of the projection of the center of mass (CM) of the robot on the reference surface 7 are provided (Fig. 1). The position and orientation of the supporting foot will be considered known. Let S be a vector of a given position of the robot foot 5 and CM 6, having dimension 8,

$$S = (X_F, Y_F, Z_F, \alpha_F, \beta_F, \gamma_F, x_{CM}, y_{CM})^T.$$

It is required to determine the vector q with dimension 14 BWM, which has 14 controlled mobility stages.

The task is complicated by the fact that BWM has 14 degrees of mobility, the vector S is 8, and there are kinematic restrictions in the mobility stages, the external connections imposed on the feet of BWM change during each step.

In this case, various methods are used to solve the inverse problem. For example, an iterative method based on minimizing the objective function, and a method for solving the inverse problem in increments based on using the Jacobi matrix. However, to control the robot, whose kinematics is represented as a kinematic tree not attached to the rack, it is necessary to solve the inverse problem for the supporting foot, the transferred foot, and the projection of the center of mass on the reference surface [11–13].

The objective function used has the form: $f = f_{F1} + f_{F2} + f_{CM} + f_P$ where f_{F1} and f_{F2} – the components of the objective function that determine the feet positions; f_{CM} – a component of the objective function that determines the position of the projection of the center of mass; f_P – a penalty function that allows bringing the solution closer to the optimal one by some criterion.

On the trajectories of the feet movement and the projection of the center of mass, points are selected so that they can then be applied to restore the original trajectory using interpolation with a given accuracy. T_i is the matrix of the actual position of the foot, and T_i^0 – the specified position matrix. These matrices are equal if any three points that do not match in the connected system have, respectively, the same coordinates in the absolute system [5–9].

$$\begin{cases} T_i^i x_1 = T_i^0 x_1 \\ T_i^i x_2 = T_i^0 x_2 \\ T_i^i x_3 = T_i^0 x_3 \end{cases}$$

Setting the vectors $^i x_1, ^i x_2, ^i x_3$ as:

$$\begin{aligned} x_1 &= ri \\ ^i x_2 &= rj \\ ^i x_3 &= rk \end{aligned}$$

i, j, k – the directing vectors of the coordinate axes;

r is a parameter that determines the ratio of the accuracy of solving the inverse problem in angular and linear coordinates

$$\Delta T = T_i - T_i^0$$

we get

$$f_F = tr(\Delta T H \Delta T)$$

where the matrix H has the form:

$$H = \begin{bmatrix} r^2 & 0 & 0 & r \\ 0 & r^2 & 0 & r \\ 0 & 0 & r^2 & r \\ r & r & r & 3 \end{bmatrix}$$

consider the component of the objective function that determines the position of the projection of the center of mass of BWM on the reference surface. The coordinates of the projection of the center of mass are determined by the formula:

$$S = \begin{pmatrix} x_{CM} \\ y_{CM} \end{pmatrix} = \frac{1}{M} \left(\sum_{i=6}^N m_i P T_i^0 r_{cmi} \right),$$

where M – robot weight; N – the total number of degrees of mobility of the human robot; m – mass of an individual link; r_{CM} – vector of the CM link; P – the projecting matrix.

$$P = \begin{bmatrix} 1 & 0 & 0 & 0 \\ 0 & 1 & 0 & 0 \end{bmatrix}$$

The index i changes from 6, because the links of the kinematic tree with smaller numbers are fictitious and have zero mass. If $\Delta S_{CM} = (x_{icm}, y_{icm})^T$ is the target position of the projection of the center of mass, and $\Delta S_{CM} = S_{CM} - S_{CM}^0$, then $f_{CM} = \Delta S_{CM}^2$.

Penalty function $f_P = \Delta q^T A \Delta q$, where q – change of the generalized coordinates when moving to a new point; A – a diagonal matrix of weight coefficients.

Physically, the penalty function f_P is proportional to the work performed by the drives when moving to a new point [10].

When considering the robot movement as the motion of an inverse pendulum, the following equations were adopted (Fig. 2):

$$\begin{aligned} x - x_0 &= l \sin \alpha, \quad \alpha = \arcsin \frac{x_0}{l} \\ \omega &= \frac{x_0}{l \cos \alpha}, \quad \varepsilon = \frac{M}{J} = \frac{g \sin \alpha}{l} \end{aligned}$$

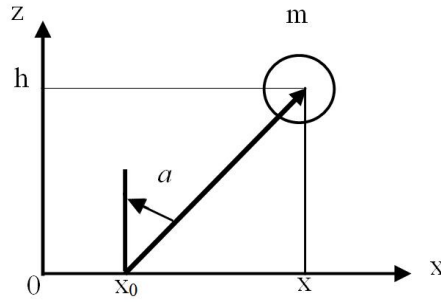


Fig. 2. The motion of the reverse pendulum with a constant height of the center of mass

The pendulum motion along the horizontal x axis is described by the equations

$$mx = mg \frac{x - x_0}{h}$$

$$x - \frac{g}{h}x = -\frac{gx_0}{h}$$

take $X_0 = 0$ and denote

$$\lambda = \sqrt{\frac{g}{l}}$$

We obtain a homogeneous linear differential equation

$$x(t) = c_1 e^{-\lambda t} + c_2 e^{\lambda t}$$

Substituting the initial conditions, we get

$$c_1 = \frac{\lambda x_0 - x_0}{2\lambda e^{-\lambda t_0}}$$

$$c_2 = \frac{\lambda x_0 + x_0}{2\lambda e^{\lambda t_0}}$$

The equation will take the form

$$x(t) = \frac{\lambda x_0 - x_0}{2\lambda} e^{-\lambda(t-t_0)} + \frac{\lambda x_0 + x_0}{2\lambda} e^{\lambda(t-t_0)}$$

At small angles of inclination of the pendulum, the solution to this equation is close to the solution to the nonlinear one written for a pendulum of constant length. Under different conditions, only the expression λ [3, 10, 11, 12] will change.

Research Results. When analyzing the calculations with various options, it was concluded that the matrix method is quite time-consuming, takes a lot of time, and does not give measurement accuracy, whereas modern methods provide considering the dynamics of the foot movement and the center of mass with greater accuracy, and divide the study not into eight or twelve points, but into more, bringing closer to more accurate results.

Discussion and Conclusions. When discussing the results, comparing the data of the tables obtained during the calculation, it was concluded that the scheme for controlling the feet movement of a exoskeleton-human developed by the authors is most effective when designing an automatic scheme for controlling the movement of the feet and the center of mass of an exoskeleton-human using digital technology. As a result of the obtained equations, an automatic control scheme using digital technology was developed, which is shown in Fig. 3 and works as follows.

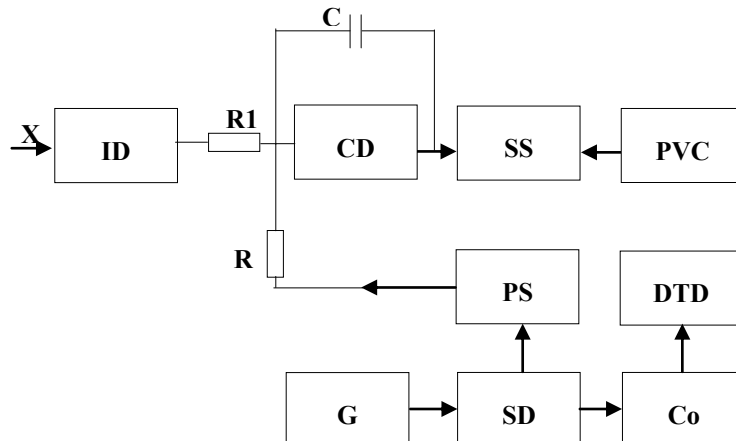


Fig. 3. Block diagram of the exoskeleton control

The control device (CD) sets the measurement cycle of the T_C and generates a pulse of the first cycle with duration of T_I . During the time interval T_I , the electronic key SA is in the initial state, and the measured position of the feet and CM through the input device ID goes to the integrator and informs the capacitor (C) the amount of electricity

$$q_s = \frac{T_I}{R} U_x$$

At the end of the pulse T_I , the CD opens the SD key, and the counter Co starts receiving pulses from the generator G . At the same time, the SD key is transferred to the second stable state, and the reference value λ of the reverse polarity is received by the integrator. The capacitor C is discharged to the initial state during the time interval

$$T_x \cdot q_p = \frac{T_x}{R} U_x$$

At the end of the discharge of the capacitor, the voltage at both inputs SS are equal to zero, the SS gives the command to open S . The receipt of pulses to the counter stops. Their number determines the T_x . Since the amount of electricity during the charge and discharge of the capacitor is the same, then

$$U_x = \frac{T_x}{T_I} U_c$$

Therefore, the measurement result is proportional to the parameters. The time interval T_x does not depend on the time constant of the integrator, i.e., no chains with highly stable elements are required to implement the double integration method. The duration of the first cycle of integration T_I and the value of the reference values can be kept constant with high accuracy, and therefore the error of converting voltage into a time interval is insignificant with this method. The noise immunity at the multiplicity of the time of the first integration cycle T_I to the interference period reaches 60 dB or more.

References

1. Issabekov ZhN. Razrabotka kinemacheskoi skhemy drevovidnogo ispolnitel'nogo mekhanizma ehkzoskeleta v MGTU im. N. E. Baumana. Molodezhnyi nauchno-tekhnicheskii vestnik. 2016;11:16. (In Russ.)
2. Jackson RW, Dembia ChL, Delp SL, et al. Muscle-tendon mechanics explain unexpected effects of exoskeleton assistance on metabolic rate during walking. Journal of Experimental Biology 2017;220(11):2082–2095. <https://doi.org/10.1242/jeb.150011>
3. John Schulman, Yan Duan, Jonathan Ho, et al. Motion planning with sequential convex optimization and convex collision checking. International Journal of Robotics Research. 2014;33(9):1251–1270. <https://doi.org/10.1177/0278364914528132>
4. Issabekov ZhN. Mathematical model of kinematics and dynamics of powered exoskeleton tree actuator. Polytechnical Student Journal, Bauman Moscow State Technical University. 2016;4(4):8. <https://doi.org/10.18698/2541-8009-2016-4-34>. (In Russ.)
5. Issabekov ZhN, Kovalchuk AK, Zhetenbayev NT. Lower limb exoskeletons: Brief review. The Bulletin of KazATC. 2019;108(1):78–83. (In Kazakh)
6. Song S, Collins SH. Optimizing Exoskeleton Assistance for Faster Self-Selected Walking. In: IEEE Transactions on Neural Systems and Rehabilitation Engineering. 2021;29:786–795. <https://doi.org/10.1109/TNSRE.2021.3074154>
7. Kang HG, Dingwell JB. Effects of walking speed, strength and range of motion on gait stability in healthy older adults. Journal of Biomechanics. 2008;41(14):2899–2905.
8. Rosen J, Brand M, Fuchs MB, et al. A myosignal-based powered exoskeleton system. In: IEEE Trans. On Systems, Mann, and Cybernetics. Part A: Systems and Humans. 2001;31(3):210–222. <https://doi.org/10.1109/3468.925661>
9. Lavrovskii EK, Pismennaya EV, Komarov PA. On the problem of the organization of the lower limb exoskeleton walk with the help of control in the knee joints. Russian Journal of Biomechanics. 2015;19(2):158–176. (In Russ.)
10. Lapierre L, Soetanto D. Nonlinear path-following control of an AUV. Ocean Engineering. 2007;34(11-12):1734–1744. <https://doi.org/10.1016/j.oceaneng.2006.10.019>
11. Kapitan'yuk YuA, Chepinsky SA. Control of mobile robot following a piecewise-smooth path. Gyroscopy and Navigation. 2013;4(4):198–203. <https://doi.org/10.1134/s207510871304007x>
12. Wang J, Chepinskiy SA, Krasnov AJ, et al. Geometric path following control for an omnidirectional mobile robot. In: Proc. 21st Int. Conf. on Methods and Models in Automation and Robotics, MMAR. Miedzyzdroje, Poland; 2016. P. 1063–1068. <https://doi.org/10.1109/mmar.2016.7575285>

Received 02.08.2021

Revised 16.08.2021

Accepted 30.08.2021

About the Authors:

Issabekov, Zhanibek N., PhD student, Satbayev University (22a, Satbayev St., Almaty, 050013, Republic of Kazakhstan), ORCID: <https://orcid.org/0000-0003-2900-8025>, zh.issabekov@satbayev.university

Tsybrii, Irina K., associate professor of the Tool Engineering and Biomedical Engineering Department, Don State Technical University (1, Gagarin sq., Rostov-on-Don, 344003, RF), Cand.Sci. (Eng.), Senior Scientist Researcher, ORCID: <https://orcid.org/0000-0002-6281-1832>, irconst@mail.ru

Moroz, Kaleriya A., Head of the Tool Engineering and Biomedical Engineering Department, Don State Technical University (1, Gagarin sq., Rostov-on-Don, 344003, RF), Cand.Sci. (Eng.), associate professor, ORCID: <https://orcid.org/000-0001-8624-0184>, Leramoroz@mail.ru

Claimed contributorship

Zh. N. Issabekov: basic concept formulation; research objectives and tasks setting; conducting the research. I. K. Tsybrii: development of research methods; text preparation; formulation of conclusions. K. A. Moroz: academic advising; correction of the conclusions.

All authors have read and approved the final manuscript.

MACHINE BUILDING AND MACHINE SCIENCE



UDC 621.793.182

<https://doi.org/10.23947/2687-1653-2021-21-3-253-259>

Investigation of the electrospark coating, alloying and strengthening technology

S. P. Glushko  

Kuban State Technological University (Krasnodar, Russian Federation)

 sputnik_s7@mail.ru

Introduction. The work objectives were the analysis and application of the technology of electrospark deposition of wear-resistant metal coatings on cutting tools or machine parts for their hardening or dimensional restoration.

Materials and Methods. The technology, device and principle of operation of the modernized installation intended for electric spark application of wear-resistant metal coatings with composites T15K6, VK8 and VK6 are considered.

Results. To determine the parameters of the upgraded electrospark alloying plant, experiments were carried out on hardening of polished samples made of steel 45 with hard alloy T15K6 with dimensions of 25×25×25 mm. As a result of using the experiment planning method, the possibility of selecting and adjusting the installation parameters was confirmed. The following parameters were selected for hardening samples made of steel 45 with hard alloy T15K6: current $I = 1\text{--}2\text{ A}$, voltage $U = 40\text{--}75\text{ V}$, capacitor bank capacity = 60–100 μF .

Discussion and Conclusions. The use of carbon dioxide as a protective medium enables to increase the number of passes and, accordingly, the number of coating layers to twenty, to obtain a total thickness of up to 0.3 mm with a dense structure without oxides. Coatings of this thickness make it possible not only to strengthen, but also to restore the dimensions of worn machine parts. The parameters of the technological modes of electrospark alloying significantly affect the intensity of coating application and the quality of the resulting surface. A rise in the electrical parameters causes an increase in the intensity of each individual discharge and, within certain limits, contributes to an increase in the amount of the transferred coating material, as well as to deeper transformations of the coated surface in the discharge zone. Thus, an electrospark alloying plant equipped with monitoring and diagnostic tools, as well as with a protective gas supply system, can be used for hardening and restoring machine parts and cutting tools.

Keywords: electrospark alloying, machine parts, cutting tool, hardening, wear resistance coating, restoration of machine parts.

For citation: S. P. Glushko. Investigation of the electrospark coating, alloying and strengthening technology. Advanced Engineering Research, 2021, vol. 21, no. 3, pp. 253–259. <https://doi.org/10.23947/2687-1653-2021-21-3-253-259>

© Glushko S. P., 2021



Introduction. The introduction of technology for manufacturing machine parts and cutting tools with high mechanical characteristics is an important component of mechanical engineering in general and the production of metal-cutting equipment in particular. The basic requirements for this technology are accessibility, cost-effectiveness, and efficiency.

The materials used for manufacturing machine parts and cutting tools, as a rule, do not fully meet the requirements of operation, so they must be made of high-quality structural materials. But in this case, their production can be very expensive. In addition, it is also impossible to guarantee full satisfaction of operational requirements in this

case. These problems are sufficiently eliminated through applying coatings with a thickness of fractions of a millimeter to several millimeters to the working surfaces of machine parts and tools of various functional purposes [1–4].

The quality of such coatings is evaluated, as a rule, according to several specific criteria, on the basis of which a complex criterion is formed. Studies using the experimental planning method [5], in turn, enable to establish the relationship of quality criteria and the parameters of the coating process [6], optimize these parameters, and predict the properties of bimetal compositions [7].

Coating layers can have various chemical compositions and structural-phase states that differ from the base material. Coating materials provide high performance properties or a set of properties to the working surfaces of cutting tools or machine parts [5, 8–18]. In addition, a small amount of expensive materials is consumed on thin coatings, which gives a high economic effect when they are used in production practice.

Currently used various metal parts (bearings, shafts, axles, drills, turning tools, milling cutters, etc.) require increasing their wear resistance and strength. One of the inexpensive ways of applying thin metal coatings to their working surfaces is the electric spark processing method — electric spark alloying (ESA) [1–4]. In addition, this technology can be used to restore steel parts of machines with minor wear of their working surfaces — up to 0.2 mm.

Materials and Methods. ESA enables to harden the cutting tool and restore the steel parts of machines with wear-resistant composites such as T15K6, VK8, VK6, and coatings of other composition [8–18]. This technology allows increasing the hardness, wear resistance, corrosion resistance of metal surfaces and provides a good bond with the base material. ESA is implemented on relatively simple equipment, whose performance does not depend on the hardness and other physical characteristics of the materials used.

Until now, various models of the process have been proposed, which to one degree or another explained individual experimental data [1–4]. Figure 1 shows a model of the ESA technology, which is designed for high voltages and small values of the short-circuit current ($I_{K.3} < 10\text{--}20\text{ A}$). Providing that the short-circuit current $I_{K.3} > 10\text{ A}$ and the no-load voltage of the power supply $U_{xx} < 50\text{ V}$, it will be required to refine such a model, since due to the low potential between the electrodes, the interelectrode gap in this case should be significantly reduced.

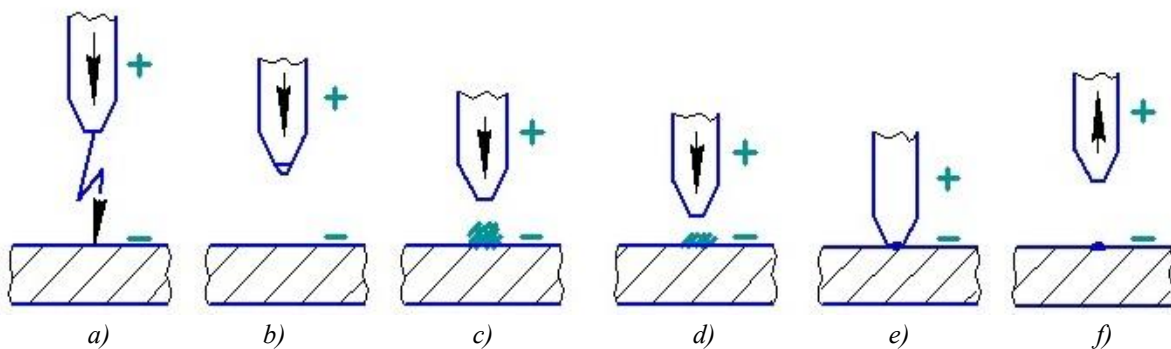


Fig. 1. Electric spark alloying model: a) moment of the interelectrode gap breakdown;

b) detachment of a molten metal drop from the anode; c) explosion of a drop of molten metal; d) deposition of molten anode metal on the cathode; e) contact of electrodes (mechanical shock of the anode on the cathode); f) separation of electrodes

As the movable electrode (anode) approaches the cathode (substrate), the electric field strength increases. At a certain distance, the voltage reaches a value at which a spark discharge occurs, and a through conduction channel is obtained. An electron beam from the cathode (substrate) passes through this channel, hits on the anode surface in a focused manner (Fig. 1 a), and the current density increases. The electrons abruptly release the accumulated kinetic energy, which is converted into thermal energy released in the surface layer of the anode. At the point of the electric discharge breakdown, the anode melts, a drop of molten metal separates from it and moves to the cathode (Fig. 1 b), ahead of the moving anode.

The falling drop, breaking away from the anode, heats up to a high temperature, boils and explodes. The current circuit in the channel is interrupted, the compressive forces of the electromagnetic field disappear. The metal particles, formed after the explosion of the drop, are no longer focused by the electromagnetic field and fall on the substrate with a wide front (Fig. 1 c), and when they reach the cathode, they are welded with it, partially penetrating

into its surface (Fig. 1 *d*). Following the molten metal of the electrode, the electrode-anode itself moves. In the meantime, the capacitor bank has time to charge, and the electric field strength in the interelectrode gap will increase accordingly. This is followed by a mechanical shock of the electrode on the surface of the substrate, while the electrical circuit is closed.

The anode material in the presented ESA model is transferred in the liquid crystal state, starting from the moment of the interelectrode gap breakdown and until the anode comes into contact with the cathode surface. In the liquid crystal state, the mesophases of a substance are characterized by anisotropic properties and combine the rheological properties of liquid bodies (fluidity) with the properties of solid crystals (anisotropy of physical properties). In the mesomorphic state, the fluidity of a substance is limited since there is a certain ordering of the arrangement and mutual orientation of its molecules, which approaches the ordered arrangement of the structure of solid crystals. A second pulse passes through the particles of the anode material lying on the cathode that have not cooled down. Pulse discharges have a high current density — up to 10^5 – 10^6 A/mm².

During mechanical contact of the mobile electrode and the substrate, the particles of the electrode material are welded to each other and to the surface of the substrate, which is heated, and the electrode material diffuses into it. Together with the diffusion process, chemical reactions occur between the materials of the electrode particles and the substrate. The mechanical shock of the movable electrode forges the heated coating material (Fig. 1 *d*), increasing its uniformity and density. Thus, a coating with an alloying effect is formed on the surface of the substrate that is firmly connected to it (Fig. 1 *e*). Then the next cycle begins, and the electrode moves up.

The coating process in ESA occurs under the influence of the following factors:

- gravity, under the influence of which a drop of molten metal rushes from the anode to the cathode when they are open;
- mechanical vibration of the electrodes;
- electrical polarity, under the influence of which ions of the coating material settle on the substrate.

An important characteristic of coating with the help of ESA is the bond strength of the coating and the base, which provides reliable and long-term operation of the cutting tool or part. During the formation of the coating and while ensuring the connection of the coating and the base, the interaction of the liquid phases of the electrode materials occurs. A chemical bond is formed between them, volumetric processes of diffusion of the anode into the substrate in the solid phase develop, intermetallides are formed.

Physical and chemical transformations in the surface layer of the substrate occur at high temperatures and high-speed plastic deformation. Interaction of the anode and substrate materials, crystallization of the molten anode material on the substrate surface, and diffusion in its surface layer occur under nonequilibrium conditions. High temperatures in the interelectrode gap and alloying elements of the electrode make it possible to increase and dope the surface of the substrate, improving its physical and chemical properties. Therefore, ESA can be used to restore complex-shaped machine parts and alloying cutting tools.

ESA advantages:

- spot heating, in which there is no deformation of the substrate (base);
- local (spot) coating, including on complex-shaped substrates;
- possibility of alloying the surfaces of machine parts and cutting tools.

Physical and mechanical properties of the surface of the tool or part being processed can be varied through changing the material of the electrodes. At the same time, the composition of the coating and its physico-chemical properties may differ significantly from the alloying material of the anode, and the alloyed base material.

After ESA processing, the steel base consists of three areas: the white layer, the transition zone, and the basic material. The thin white layer contains refractory compounds with a fine-grained structure, which are formed under conditions of fast heat dissipation. In the transition zone of the steel base there is a diffusion layer, a heat-affected zone, and a transition layer. The diffusion layer is a martensitic-carbide structure. The heat-affected zone is an austenitic-martensitic-carbide structure. The transition layer has an austenitic-sorbitol-martensitic structure. An austenitic structure is formed on the interface of ferrite carbide phases under rapid cooling and during diffusion saturation of steel with air

nitrogen if the ESA is carried out without the use of a shielding gas. It should be taken into account that the less nitrogen penetrates into the transition zone, the more martensitic structures will be formed under cooling. The transition layer is followed by the structure of the base, which is not subject to changes. The thickness and structure of the zones depend on the process conditions, the composition of the coating and base materials, as well as the composition of the environment.

The performance of the ESA process, the quality of the coating, the grain size of the base can be adjusted through changing the borehole and the frequency of electrical discharges. For electrodes, it is recommended to use materials with high hardness and wear resistance, for example, tungsten and titanium carbides, gray or white cast iron, hard alloys based on titanium carbide with various bonds based on molybdenum, nickel, intermetallides and steel. It should be noted that the microhardness of the hardened layers obtained on hardened steels is significantly higher than on non-hardened ones. This is due to the active influence of the base materials on the formation of the coating.

The ESA electrical parameters determine the degree of hardening, the purity of the coating surface, and the performance of the process. The electrical modes used can be conditionally divided into coarse, medium, and fine. They cover a significant range of power required for both finishing and rough ESA processes. Rough modes are characterized by a voltage of 100-200 V and a large capacity of the capacitor bank (100-300 μF). Medium modes are implemented through reducing the capacitance of the capacitor bank to 90-100 μF or by reducing the voltage at the same capacity. Fine modes can be obtained through reducing the voltage to 10-30 V or by reducing the capacitance of the capacitor bank to 0.5-10 μF . Accordingly, the short-circuit current increases or decreases.

The disadvantages of the ESA technology include the limited thickness of the applied coating layers and the significant roughness of their surfaces. Let us consider the disadvantages with specific examples.

Example 1. The installation operates in rough mode: the capacity of the capacitor bank $C = 200 \mu\text{F}$, the short-circuit current $I_{\text{к.з.}} = 3 \text{ A}$, voltage $U = 150 \text{ V}$, vibration frequency of the vibrator with the electrode is 100 Hz. Assume that the capacitor bank is charged to 99 % of the power supply voltage. In this case, the charging time of the capacitors is 0.05 s. However, since the vibrator closes the electrodes every 0.01 seconds and a discharge occurs, the voltage on the capacitors has time to rise only to 65 V.

Example 2. The installation operates in soft mode: the capacity of the capacitor bank $C = 4 \mu\text{F}$, the short-circuit current $I_{\text{к.з.}} = 0.5 \text{ A}$, voltage $U = 150 \text{ V}$, the capacitors are charged to 99 % of the voltage of the power source. In this case, the charging time of the capacitor is 0.005 s, but the vibrator will close the electrodes only after 0.01 s. In this case, the process is idle waiting for the next short circuit of the electrodes for about 50 % of the time.

One of the major causes for the limited thickness of the coating layer is the occurrence of chemical reactions between the electrode material and its environment during doping. The experimental data have shown that the greater the inertia of the environment, the higher the permissible specific duration of doping and the more coating material can be applied to the cathode. However, even in inert media, with an increase in the duration of doping, a decrease in the amount of material deposited on the cathode is observed.

The application of vacuum to eliminate the influence of chemical elements of the protective environment on the composition of the coating will require a significant complication and increase in the cost of electric spark alloying installations. Therefore, the use of a protective environment, e.g., carbon dioxide for ESA is preferable.

To study the ESA technology, an upgraded EFI-25 installation was used (Fig. 2). The basis of its power part is a single-phase transformer with increased scattering, a selenium rectifier, and a capacitor bank. The primary winding of the transformer is powered from a single-phase AC network of industrial frequency with a voltage of 220 V through 5A fuse and a two-pole switch. The installation rectifier is full wave. The cathode (the processed part) is grounded.

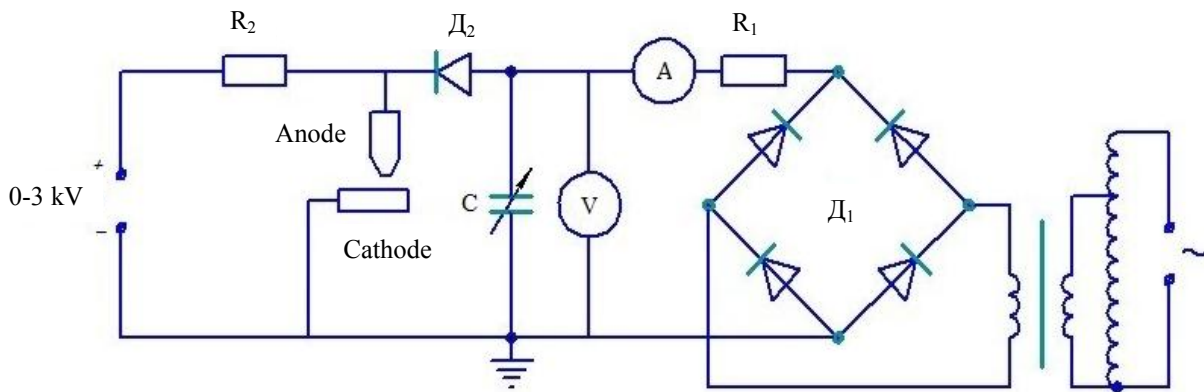


Fig. 2. Electric circuit of the power supply of the interelectrode gap of the electrosark alloying installation: \mathcal{D}_1 — selenium rectifier; C — capacitor bank; R_1 — ballast resistance; R_2 — current limiting resistance; \mathcal{D}_2 — valves; A — ammeter; V — voltmeter

At the output of the rectifier, the voltage changes from 15 to 220 V through switching the secondary winding. The valves separate the low-voltage and high-voltage parts of the installation, which prevents the breakdown of high voltage into the RC generator, which is designed to produce a spark discharge. The generator generates current pulses in the frequency range of 100-600 Hz. These are the optimal frequencies that are determined during experiments with different materials. The operation of the ESA installation outside this range causes performance degradation.

Automation of the ESA process and constant monitoring of its parameters provide high productivity and obtaining a high-quality carbide coating. This is provided, in particular, by ammeter A, designed to monitor the current in the power supply circuit of the interelectrode gap, and voltmeter V — for monitoring the voltage in the power supply circuit of the interelectrode gap (Fig. 2).

An autotransformer is installed as a power source on the upgraded installation, which provides stepless voltage regulation at the interelectrode gap up to 200 V. A panel of switches of the bank capacity is installed for stepwise changing the capacity of the interelectrode discharge power source. The total capacity of the bank is 120 μF , the number of switching stages is 16.

The safety of operation at the installation is provided by a separation transformer with a transformation coefficient $K = 1:1$ between the transformer and the electrodes of the installation. The technological modes of operation of ESA installations for coating, alloying and hardening, mainly set the following parameters:

- voltage at the interelectrode gap;
- capacitor bank capacity;
- charging current or the percentage of charging capacitors from the circuit voltage.

Research Results. To determine the possibility of regulating the ESA parameters, which should be provided by the upgraded installation, experiments were carried out on electric spark hardening with T15K6 hard alloy of polished samples made of steel 45 with dimensions of $25 \times 25 \times 25$ mm. The experiments were carried out without using a protective gas in the coating area; carbon dioxide was used as a protective medium. As a result, the possibility of selecting and adjusting the ESA parameters was confirmed. $I = 1-2$ A, voltage $U = 40-75$ V, 60-100 μF .

The results of experiments without using carbon dioxide have shown the following: when applying a hard alloy to the surface of steel 45 at a minimum voltage and minimum current, the surface of the material is strengthened unevenly due to the adhesion of the electrode to the treated surface; the minimum voltage causes a sharp increase in the porosity of the applied coating; the thickness of the applied layer is small and does not exceed 0.1 mm. The surface is uneven, loose, with traces of oxides, and the number of arbitrary passes of the alloying electrode, i.e., passes at which the thickness of the hardened layer increases, does not exceed eight. This is due to an increase in thermal stresses caused by local temperature drops at the interface between the cladding layer and the base, and mainly to the adhesive nature of the bonding of the cladding layer and the base. In addition, the hardness of the cladding layer is lower than the hardness of the electrode. For example, the T15K6 hard alloy plates used in the experiments had a hardness of 85–90 HRC, and in the cladding layer, this material has a hardness of 80–85 HRC.

In the next set of experiments, carbon dioxide was supplied to the coating area to prevent oxidation. This made it possible, with the same electrical parameters, to increase the number of passes, respectively, the number of coating layers applied, to twenty, and to obtain a total coating thickness of up to 0.3 mm with a dense structure and without oxides. Obtaining a coating of such thickness makes it possible not only to strengthen, but also to restore the dimensions of worn machine parts.

Discussion and Conclusions. It is possible to increase the operational characteristics of machine parts and cutting tools without compromising economic indicators through applying coatings on their working surfaces using the ESA method. The considered technology, due to point heating, in which there is no deformation of the substrate (base), and local coating, enables to restore the dimensions of complex-shaped parts lost as a result of wear. This is possible due to the use of a protective environment in the form of carbon dioxide for ESA since it provides increasing the thickness of the coating to 0.3 mm and achieving its dense structure that does not have oxides.

Values of the electric spark alloying parameters significantly affect the intensity of coating application and the quality of the resulting surface. A rise of the electrical parameters causes an amplification of the intensity of each individual electric discharge and, within certain limits, contributes to an increase in the amount of the transferred coating material and deeper transformations in the coated surface (in the discharge zone).

Thus, an electric spark alloying installation equipped with monitoring and diagnostic tools, as well as a protective gas supply system, can be used for hardening and restoring machine parts and cutting tools.

References

1. Grigoryev SN, Volosova SN. Nanesenie pokrytii i poverkhnostnaya modifikatsiya instrumenta. Moscow: MSUT STANKIN Publ. House; 2007. 324 p. (In Russ.)
2. Avdeichik SV, Vorontsov AS, Davydov VM, et al. Progressivnye tekhnologii naneseniya pokrytii. Moscow: Spektr; 2012. 272 p. (In Russ.)
3. Korotaev DN. Tekhnologicheskie vozmozhnosti formirovaniya iznosostoikikh nanostruktur ehlektroiskrovym legirovaniem. Omsk: Izd-vo SiBADI; 2009. 256 p. (In Russ.)
4. Verkhoturlov AD, Gordienko PS, Dostovalov VA, et al. Vyskoehnergeticheskoe lokal'noe vozdeistvie na vol'framsoderzhashchie materialy i metally. Vladivostok: Publ. House of Far Eastern Federal University; 2012. 472 p. (In Russ.)
5. Makarichev YuA, Ivannikov YuN. Metody planirovaniya ehksperimenta i obrabotki dannykh. Samara: Samara Polytech Publ. House; 2016. 131 p. (In Russ.)
6. Glushko SP, Denisenko SG. Sintez kriteriya kachestva bimetallicheskih podshipnikov skol'zheniya. In: Proc. All-Russian Sci. Conf. Volgograd: Dom nauki i tekhniki; 1990. P. 202–204. (In Russ.)
7. Denisenko SG, Glushko SP. Optimizatsiya tekhnologii proizvodstva podshipnikov skol'zheniya iz bimetalla stal'-bronz. In: Proc. IV Ukrainian Republican Sci.-Tech. Conf. Kharkiv: KhADI Publ. House; 1990. P. 70–71. (In Russ.)
8. Nikolenko SV. Novye ehlektrodnye materialy dlya ehlektroiskrovogo legirovaniya. Vladivostok: Dal'nauka; 2005. 219 p. (In Russ.)
9. Nikolenko SV, Gostishev VV, Lebukhova NV. Synthesis of materials on the basis of borides tungsten and zirconium in regime of burning. Voprosy Materialovedeniya = Materials Science Issues. 2011;68(4):89–94. (In Russ.)
10. Nikolenko SV, Kuz'menko AP, Timalov DI, et al. Nanostructuring a steel surface by electrospark treatment with new electrode materials based on tungsten carbide. Electronic Processing of Materials. 2011;47(3):28–35. (In Russ.)
11. Zheng Chen, Yixiang Zhou. Surface modification of resistance welding electrode by electro-spark deposited composite coatings: Part I. Coating characterization. Surface & Coatings Technology. 2006;201(3):1503–1510. [10.1016/j.surfcoat.2006.02.015](https://doi.org/10.1016/j.surfcoat.2006.02.015)
12. Jun Liu, Ruijun Wang, Yiyu Qian. The formation of a single-pulse electrospark deposition spot. Surface & Coatings Technology. 2005;200(7):2433–2437. [10.1016/j.surfcoat.2004.07.104](https://doi.org/10.1016/j.surfcoat.2004.07.104)

13. Zamulaeva EI, Levashov EA, Kudryashov AE, et al. Electrospark coatings deposited onto an Armco iron substrate with nano- and microstructured WC–Co electrodes: Deposition process, structure, and properties. *Surface & Coatings Technology*. 2008;202:3715–3722. <https://doi.org/10.1016/j.surfcoat.2008.01.008>
14. Agafii VI, Petrenko VI, Fomichev VM, et al. Electrospark alloying for deposition on aluminum surface of Al–Sn coatings and their wear resistance under dry friction. *Surface Engineering and Applied Electrochemistry*. 2013;49(3):1–8. <https://doi.org/10.3103/S1068375513030022>
15. Ribalko AV, Orhan Sahin, Kemal Korkmaz. A modified electrospark alloying method for low surface roughness. *Surface & Coatings Technology*. 2009;203(23):3509–3515. <https://doi.org/10.1016/j.surfcoat.2009.05.002>
16. Kornienko LP, Chernova GP, Mihailov VV, et al. Use of the electrospark alloying method to increase the corrosion resistance of a titanium surface. *Surface Engineering and Applied Electrochemistry*. 2011;47(1):9–17.
17. Feldshtein E, Kardapolova MA, Gaida R. Tribological properties of electrospark-deposited and further laser-hardened coatings. *Journal of Friction and Wear*. 2013;34(2):137–141. [10.3103/S1068366613020049](https://doi.org/10.3103/S1068366613020049)
18. Topala P, Ojegov A, Ursaki V. Nanostructures obtained using electric discharges at atmospheric pressure. In: *Nanostructures and Thin Films for Multifunctional Applications*. Springer, 2016. P. 43–83.

Received 19.07.2021

Revised 02.08.2021

Accepted 18.08.2021

About the Author:

Glushko, Sergey P. associate professor of the Control Systems and Technological Complexes Department, Kuban State Technological University (2, Moskovskaya St., Krasnodar, 350072, RF), Cand.Sci. (Eng.), associate professor, ORCID: <https://orcid.org/0000-0002-7087-6572>, sputnik_s7@mail.ru

The author has read and approved the final manuscript.

MACHINE BUILDING AND MACHINE SCIENCE




UDC 697.1

<https://doi.org/10.23947/2687-1653-2021-21-3-260-267>

Building structures thermal calculation

A. V. Maistrenko  

Don State Technical University (Rostov-on-Don, Russian Federation)

 anatol-maystrenko@yandex.ru

Introduction. The thermal calculation of a volumetric structure using the finite element method is considered. According to the plans of the Ministry of Energy of the Russian Federation, a powerful wind energy industry will be created in the country in the coming years. In this regard, calculations in the production of building structures of wind power plants are currently becoming a challenge. The production of such fiberglass structures is a complex thermochemical process, including the polymerization of the binder under strictly specified thermal conditions. The work objective is to develop a method for three-dimensional finite element calculation of the non-stationary heating mode of a complex-shaped composite structure.

Materials and Methods. The determination of the temperature fields of a complex-shaped structure made of inhomogeneous materials causes using numerical methods and, first of all, the finite element method. The finite element modeling of the behavior of composite materials under molding is still incomplete. For its partial solution, the well-known heat conduction equation is adapted for a specific problem based on the first law of thermodynamics. New finite element models describing the thermal fields in the structure during its manufacture are proposed. The accuracy of modeling thermal processes is specified. Numerical simulation of heating is carried out.

Results. The solution to the problem was performed in the multifunctional software complex ANSYS with the implementation of the calculation method in the parametric programming language APDL. The temperature fields of the blade elements of wind power plants at the stage of their manufacture were calculated, which made it possible to identify the characteristic features of the production process of these structures and to obtain recommendations for clarifying the process of their gluing.

Discussion and Conclusions. The results obtained can be used in thermal calculations of elements of complex layered structures made of composite materials in wind power, mechanical engineering, aircraft, shipbuilding, instrumentation, etc.

Keywords: finite element calculation, temperature field, nonmetallic structure, technological process, modeling.

For citation: A. V. Maistrenko. Building structures thermal calculation. Advanced Engineering Research, 2021, vol. 21, no. 3, p. 260–267. <https://doi.org/10.23947/2687-1653-2021-21-3-260-267>

© Maistrenko A. V., 2021



Introduction. Thermal calculations in the production of building structures of wind power plants are currently becoming a challenge. According to the plans of the Ministry of Energy of the Russian Federation¹, the wind power industry will be created in the country in the coming years. In 2016–2017, large Russian and foreign investors came to it, who committed themselves to the development of the technological and production base. The major disadvantages of blade wind power plants are eliminated through improving their design and manufacturing technique. First of all, this applies to the blades, which are the main elements of the wind turbine. They concentrate the key intellectual component of the installation. The production of a fiberglass blade is a complex thermochemical process, including the polymerization of the binder under a strictly specified thermal regime. In this regard, the exact calculation of the temperature fields in the body of the blade during its molding is of great practical importance.

¹Renewable energetics in Russia has established itself as an industry. Ministry of Energy of the Russian Federation. URL: <https://minenergo.gov.ru/node/10307/> (accessed: 04.02.2021). (In Russ.).

The determination of the temperature fields of a complex-shaped structure made of inhomogeneous materials causes the need to use numerical methods in calculations and, first of all, the finite element method (FEM). The problem of finite element modeling of composite materials under molding remains unresolved to date. This is due to complexity of the behavior of the composite as an inhomogeneous material with pronounced thermally dependent physical properties, including rheological ones, residual internal phenomena, aging, etc.

Modern models take into account the anisotropy of the material, its plastic behavior under a complex stress-strain state, etc. Thus, the temperature properties of composite materials were studied in [1, 2]. To substantiate and confirm the influence of the distribution and orientation of strengthening particles on the coefficient of thermal expansion of the material, the authors performed finite element modeling. Under the geometric construction, a real microstructure was taken as the basis. Calculations have established that the experimentally detected anisotropy of temperature properties is explained by internal stresses in the composite that depend on the filler orientation.

Many studies consider the calculations of two-dimensional models of reinforced composite materials. To analyze and optimize the properties of the composite, a calculated finite element scheme is proposed that takes into account its temperature properties [3]. With the help of FEM, the fields of residual stresses formed in the matrix as a result of thermal processing for a composite model including reinforcing fibers are calculated [4]. The effective elastic characteristics of a multilayer composite material were calculated using a finite element model, with each layer being described by its own thermomechanical properties [5]. Modeling of the behavior of anisotropic materials and other issues of thermal loading are also analyzed in [6–13].

Most of the studies based on finite element analysis were performed using the universal software system ANSYS, which provides solving linear and nonlinear, stationary and non-stationary spatial problems of heat transfer and heat exchange. For example, using ANSYS, the following tasks are solved:

- non-stationary heating of the structure with time-dependent convection coefficient²;
- thermal expansion of the elements under intense heating³;
- heat release during plastic deformation⁴;
- heat transfer in multilayer structures through the interface of media⁵, etc.

S. N. Shevtsov's works are devoted to the study of the processing of polymer composite materials, e.g., in [14]. Despite a large number of works on numerical thermal calculations, assessment of the thermal mode of forming the structures of blade units is still relevant. Increasing requirements for the quality of production of wind turbine elements necessitates further refinement of mathematical finite element models of heat transfer based on a more complete account of external and internal factors.

The work objective is to study the non-stationary temperature fields of a composite structure of a complex volumetric shape of a blade element of a wind power plant in the process of its manufacture, taking into account physical features and geometric nonlinearities. One of the structures consists of a spar and a tail section, whose parts are made of fiberglass, rubber, foamed plastic, etc. The tail section is manufactured using adhesive technology in a special device, which consists of upper and lower half-body with powerful stiffeners. A blade element is laid between them. For its high-quality gluing, it is required to strictly maintain the heating speed and the holding temperature in the glue lines. Setting the thermal mode is carried out by placing the device with a section in the heating furnace.

The task statement of the study is as follows. It is required to create a finite element model of heating a blade element during its molding, calculate the volumetric temperature fields at any moment of the process, determine the accuracy of modeling thermal processes in the body of the structure, and also form a graph of the temperature rising in the furnace, providing the required heating mode for the glue zones of the section.

Materials and Methods. The basis of thermal calculations is the statement of the first law of thermodynamics that the amount of heat received by an isolated system is spent on changing its internal energy. Applied to an elementary volume, this statement can be expressed mathematically:

$$\rho c (\partial T / \partial t + \{V\}^T \{L\} T) + \{L\}^T \{q\} = q_v, \quad (1)$$

where ρ — material density; c — specific heat capacity; T — temperature; t — time; $\{q\}$ — heat flux vector; q_v — heat release per unit volume.

² Thermal Time-Transient Loading and Solution in Ansys. SimuTechGroup. simutechgroup.com — URL: <https://www.simutechgroup.com/tips-and-tricks/fea-articles/97-fea-tips-tricks-thermal-transient> (accessed: 04.02.2021).

³ Extreme Thermal Expansion Modeling in Ansys Mechanical Workbench. SimuTechGroup. simutechgroup.com — URL: <https://www.simutechgroup.com/tips-and-tricks/fea-articles/139-extreme-thermal-expansion-modeling-in-ansys-mechanical> (accessed: 04.02.2021).

⁴ Heat Generation in Plastic Deformation Using Ansys Mechanical APDL and Workbench V14.5: Application of the New Act Module. SimuTechGroup. simutechgroup.com — URL: <https://www.simutechgroup.com/tips-and-tricks/fea-articles/171-fea-tips-tricks-ansys-heat-generation-plastic-deformation> (accessed: 04.02.2021).

⁵ Heat Conduction Across a Contact Element Gap in Ansys Workbench Mechanical. SimuTechGroup. simutechgroup.com — URL: <https://www.simutechgroup.com/tips-and-tricks/fea-articles/229-fea-tips-tricks-heat-conduction-contact-element-gap-ansys-workbench-mechanical> (accessed: 04.02.2021).

Vector operator $\{L\}$ and velocity vector $\{V\}$ for heat transfer realized by mass:

$$\{L\} = \begin{Bmatrix} \frac{\partial}{\partial x} \\ \frac{\partial}{\partial y} \\ \frac{\partial}{\partial z} \end{Bmatrix}, \quad \{V\} = \begin{Bmatrix} V_x \\ V_y \\ V_z \end{Bmatrix},$$

where x, y, z — coordinates.

According to Fourier's law, the heat flow is associated with the temperature gradient:

$$\{q\} = -[D]\{L\}T, \quad (2)$$

where $[D]$ — thermal conductivity matrix:

$$[D] = \begin{bmatrix} \lambda_x & 0 & 0 \\ 0 & \lambda_y & 0 \\ 0 & 0 & \lambda_z \end{bmatrix}.$$

Combining (1) and (2), we get:

$$\rho c (\partial T / \partial t + \{V\}^T \{L\} T) = \{L\}^T ([D] \{L\} T) + q_v. \quad (3)$$

Opening (3), we get:

$$\rho c \left(\frac{\partial T}{\partial t} + V_x \frac{\partial T}{\partial x} + V_y \frac{\partial T}{\partial y} + V_z \frac{\partial T}{\partial z} \right) = q_v + \frac{\partial}{\partial x} \left(\lambda_x \frac{\partial T}{\partial x} \right) + \frac{\partial}{\partial y} \left(\lambda_y \frac{\partial T}{\partial y} \right) + \frac{\partial}{\partial z} \left(\lambda_z \frac{\partial T}{\partial z} \right).$$

The basic equation of thermal conductivity is supplemented by boundary conditions:

1. Setting the surface temperature: $T = T^*$.
2. Setting the heat flow on the surface:

$$\{q\}^T \{n\} = -q^*,$$

where $\{n\}$ — surface normal unit vector; q^* — specific heat flux.

Heat transfer corresponds to Newton's law (surface convection):

$$\{q\}^T \{n\} = \alpha_f (T_s - T_b),$$

where α_f — heat transfer coefficient, T_s — surface temperature, T_b — temperature of the bordering medium.

For the case of constant thermophysical coefficients, the studied thermal processes are described by the three-dimensional equation of non-stationary thermal conductivity (the Fourier equation):

$$\rho c \frac{\partial T}{\partial t} = \lambda \left(\frac{\partial^2 T}{\partial x^2} + \frac{\partial^2 T}{\partial y^2} + \frac{\partial^2 T}{\partial z^2} \right),$$

where λ — heat conductivity factor.

Due to the symmetry of the problem, the calculation is carried out only for half of the design. The boundary conditions for the section plane are determined from the condition: $q = 0$.

On the docking interfaces, it is assumed that there is an ideal thermal contact, the absence of thermal resistance:

$$T|_{-0} = T|_{+0}; \quad \lambda_1 \frac{\partial T}{\partial x}|_{-0} = \lambda_2 \frac{\partial T}{\partial x}|_{+0}.$$

Convective heat flows are supplied to the external surfaces of the device. Internal heat generation during heating is not taken into account. The initial conditions assume the fixation of a constant temperature over the entire area under investigation: $T = T_0$.

The problem is solved by the finite element method in the multifunctional software complex ANSYS in the parametric programming language APDL. The structure is heated from the outer surface through convection. The results of the division of the device and the section into blocks, as well as into three-dimensional tetragonal finite elements, are shown in Fig. 1.

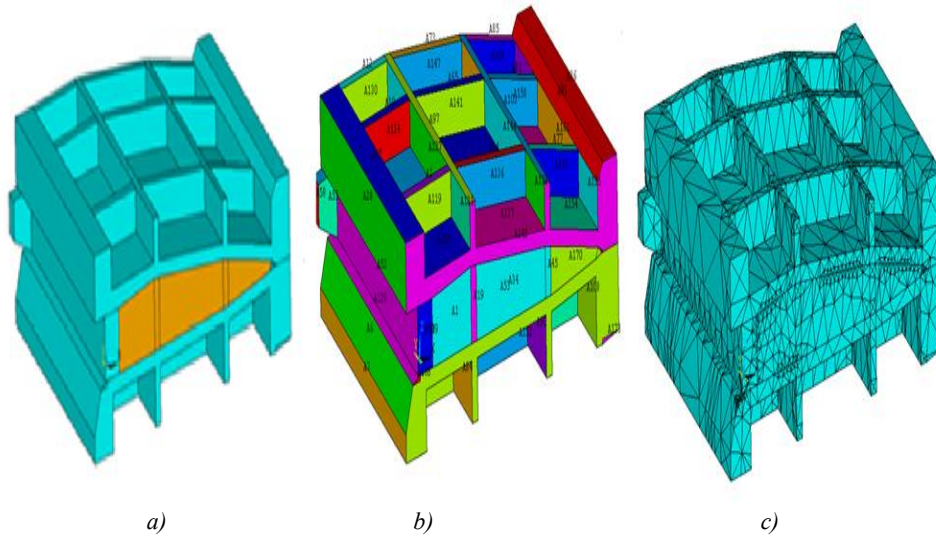


Fig. 1. Bonding device with a tail section: a) general view; b) model surfaces with their numbers; c) division of the analyzed area into finite elements

The thermophysical properties of the materials used in the calculations are given in Table 1.

Table 1

Thermophysical properties of the materials

Material	λ , W/(m·K)	c , J/(kg·K)	ρ , kg/m ³
Fiberglass	0.38	1230	1710
Al-alloy	176	798	2700

The program created to solve this problem determines the temperature values in each calculation node throughout the entire bonding process.

The calculation algorithm consists of the following steps:

- setting the initial data (geometry, thermophysical properties, initial temperature, etc.);
- division of the area into finite elements;
- application of heat sources;
- determining the temperature of the area at the end of the heating steps;
- output of calculation results (heat flows, temperature fields) to print.

To validate the program, it was tested. Figure 2 shows the experimental and calculated dependences of temperature on time in the adhesive zone (lower curves) and in the furnace itself (upper curves). The absolute error in calculating the temperature at the bonding point does not exceed 5° C, the relative error for really significant temperatures is no more than 6 %.

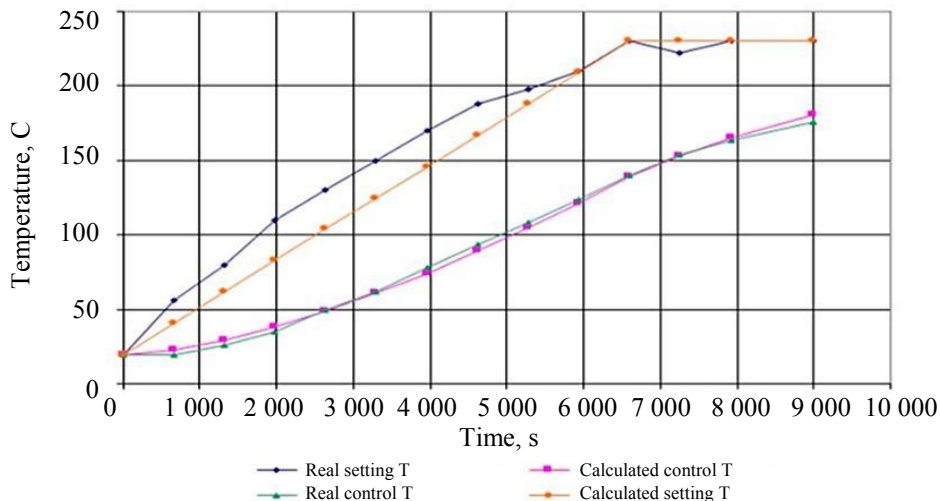


Fig. 2. Dependences of calculated and measured temperatures at the control and reference points on the time

Research Results. The processing includes a monotonous, continuous heating of the bonding device and the blade element to a certain temperature and its maintenance for a specified time. The calculation results are shown in Fig. 3–7. So, Figure 3 shows the volume distribution at a certain time of heat fluxes in vector form, and the total amount of heat in the body of the device with a section.

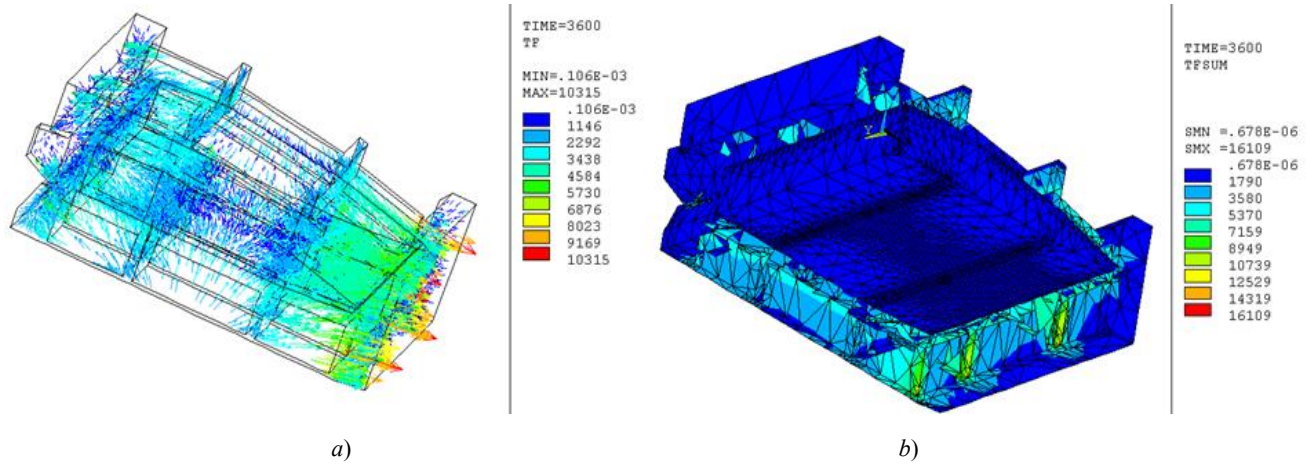


Fig. 3. Heat flows (a) and total heating (b) of the device with a section

Since the heating rate of the device is relatively small, the heat flows are redistributed evenly over its volume and turn out to be approximately the same in all directions. minor exceptions apply only to the stiffeners. Convective heat flows are supplied from the sides having a large area, and are carried away by thermal conductivity into the body of the half-bodies through a narrow cross-section.

Figure 4 shows the temperature gradients in the body of the device with a section at one of the heating moments. It can be seen that the heat spreads from the outer surfaces of the device to the inner areas. Heat flows are most actively supplied in places close to the side brass and move simultaneously both from the side brass and from the upper and lower half-bodies of the device. Also, Figure 4 shows a three-dimensional view of the temperature field at the same time. Since the blade section is non-metallic, its thermal conductivity is low, and the temperature distribution is uneven.

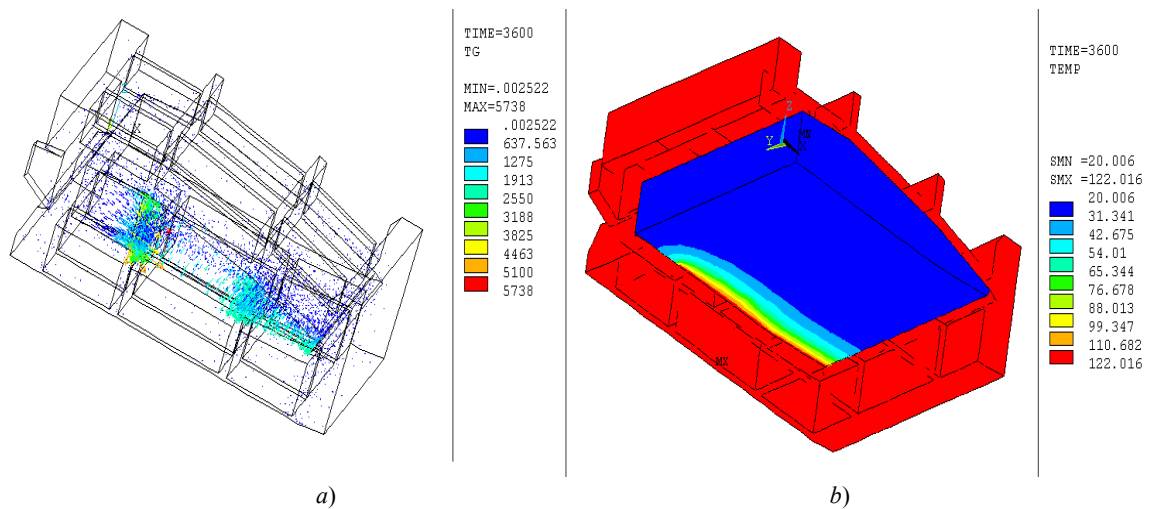


Fig. 4. Vector fields of the temperature gradient (a) and temperature (b) in the body of the device with a blade section

The temperature and time dependences at particular points of the bonding zone are shown in Fig. 5-7. It is possible to obtain maximum compliance of the schedule for setting and holding the temperature in the bonding zones with the requirements of the process through changing the values of the setting ambient temperatures and the number of their switches.

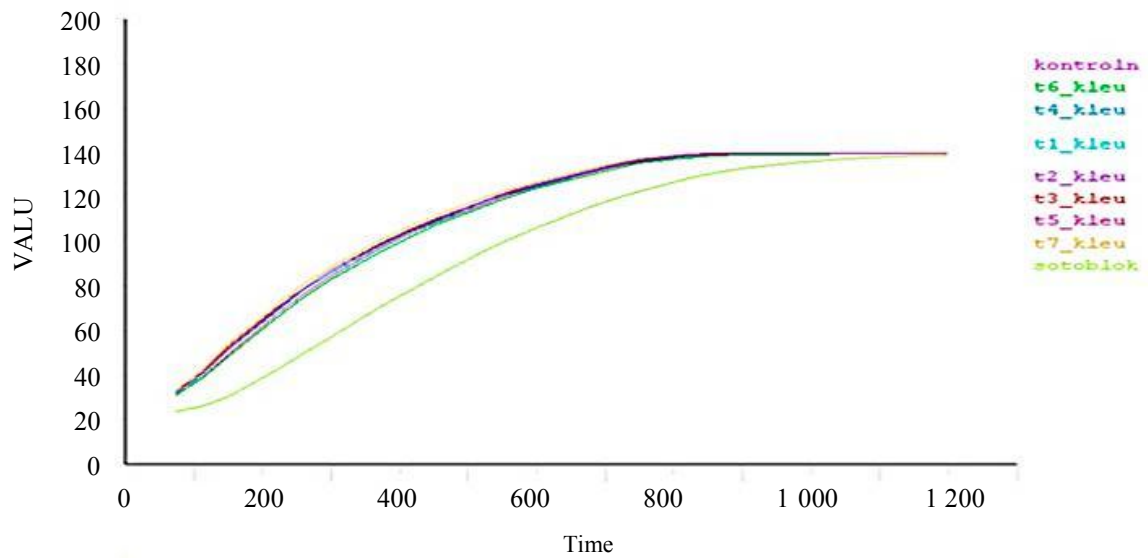


Fig. 5. Temperature versus time dependences at the characteristic points of the bonding zones and in the block (green line) for the technological mode, which includes two switches at the setting temperatures of 160 and 140 °C

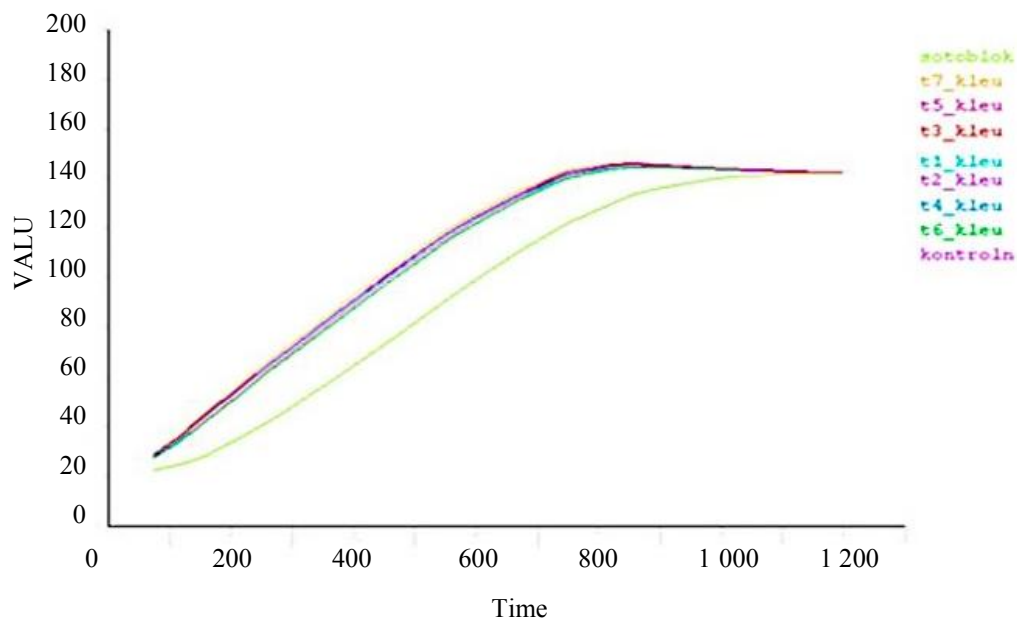


Fig. 6. Temperature versus time dependences at the characteristic points of the bonding zones and in the block (green line) for the technological mode, which includes four switches with an accuracy of setting the temperature up to 10 °C

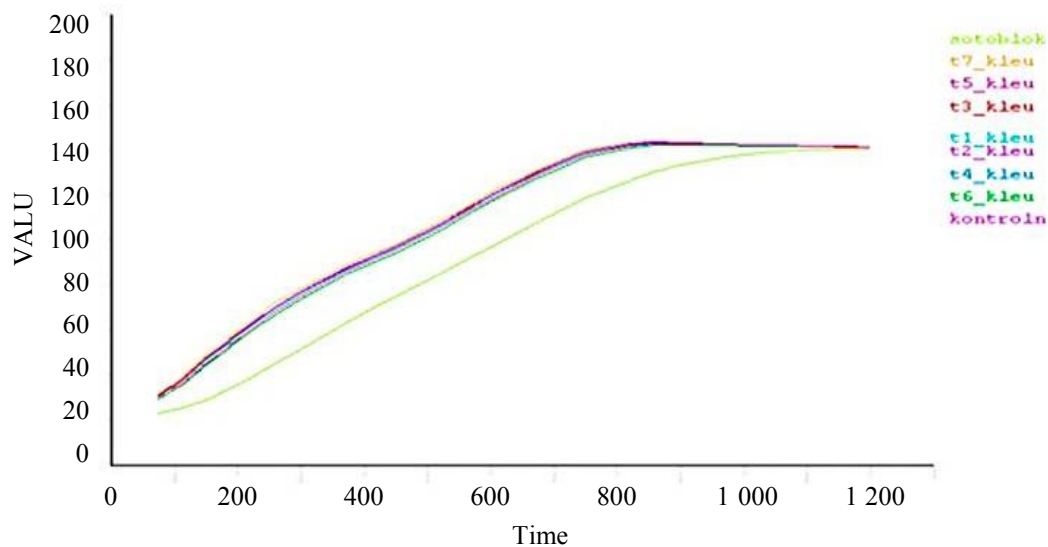


Fig. 7. Temperature versus time dependences at the characteristic points of the bonding zones and in the block (green line) for the technological mode, which includes three switches

Discussion and Conclusions. The performed thermal calculation of the elements of building structures of wind power plants at the manufacturing stage made it possible to identify the characteristic features of heating and obtain recommendations for clarifying the parameters of their bonding process.

References

1. Chawla N, Deng X, Schnell DRM. Thermal expansion anisotropy in extruded SiC particle reinforced 2080 aluminum alloy matrix composites. *Material Science and Engineering A*. 2006;426:314–322. [10.1016/j.msea.2006.04.054](https://doi.org/10.1016/j.msea.2006.04.054)
2. Chawla KK, Chawla N. Thermal Shock Behavior of Ceramic Matrix Composites. *Encyclopedia of Thermal Stresses*. John Wiley & Sons, Hoboken, New Jersey; 2014. P. 370-374. https://doi.org/10.1007/978-94-007-2739-7_94
3. Boguszewski T, Ciupinski L, Kurzydowski K. Design rules for optimizing microstructures of composite for thermal management. In: *Proc. Int. Conf. on Advanced Processing for Novel Functional Materials — APNFM 2008*. 2012. URL: <https://www.sfet.pl/doc/design-rules-drezden.pdf> (accessed: 29.04.2019).
4. Maligno A, Warrior NA. Finite element investigations on the microstructure of fibre-reinforced composites. *eXPRESS Polymer Letters*. 2008;2(9):665–676. [10.3144/expresspolymlett.2008.79](https://doi.org/10.3144/expresspolymlett.2008.79)
5. Xu YJ, Zhang WH, Domaszewski M. Microstructure modeling and prediction of effective elastic properties of 3D multiphase and multilayer braided composite. *Materials Science and Technology*. 2011;27(7):1213–1221.
6. Sudhanshu S. Singh, Yang Jiao, Jason J, et al. Modeling Anisotropic Multiphase Heterogeneous Materials via Directional Correlation Functions: Simulations and Experimental Verification. *Metallurgical and Materials Transactions A*. 2012;43(12):4470-4474. [10.1007/s11661-012-1451-7](https://doi.org/10.1007/s11661-012-1451-7)
7. Kyle E. Yazzie, Jonathan Topliff, Nikhilesh Chawla. The Asymmetric Growth Behavior of Intermetallic Compound Layers During Extended Reflow of Sn-rich Alloy on Cu. *Metallurgical and Materials Transactions A*. 2012;43:3442-3446.
8. Williams JJ, Segurado J, LLorca J, et al. Three-dimensional (3D) Microstructure-Based Modeling of Interfacial Decohesion in Particle Reinforced Metal Matrix Composites. *Material Science and Engineering: A*. 2012;557:113–118. [10.1016/j.msea.2012.05.108](https://doi.org/10.1016/j.msea.2012.05.108)
9. Shen Y-L, Blada CB, Williams JJ, et al. Cyclic Indentation Behavior of Metal-Ceramic Nanolayered Composites. *Material Science and Engineering: A*. 2012;557:119-125. [10.1016/j.msea.2012.05.103](https://doi.org/10.1016/j.msea.2012.05.103)
10. Zhang J, An Y, Yazzie KE, et al. Finite Element Simulation of Swelling-Induced Crack Healing in Gels. *Soft Matter*. 2012;31:8107-8112.
11. Lotfian S, Molina-Aldareguia JM, Yazzie KE, et al. High Temperature Nanoindentation Behavior of Al/SiC Multilayers. *Philosophical Magazine Letters*. 2012;92(8):362-367.
12. Bonakdar A, Wang F, Williams JJ, et al. Environmental Effects on Fatigue Crack Growth in 7075 Aluminum Alloy. *Metallurgical and Materials Transactions A*. 2012;43(8):2799-2809. [10.1007/s11661-011-0810-0](https://doi.org/10.1007/s11661-011-0810-0)
13. Walters JL, Williams JJ, Chawla N. Influence of Thermal Aging on the Microstructure and Mechanical Behavior of Sintered Dual Phase Stainless Steels. *Metallurgical and Materials Transactions A*. 2012;43:124-135.

14. Shevtsov SN, Sibirskiy VV, Chigrinets EG. Increase in efficiency of quality and hole-making in glass-reinforced titanium laminate by reducing drilling vibroactivity. Vestnik of Don State Technical University. 2016;16(1):119-126. <https://doi.org/10.12737/18273>

Received 05.07.2021

Revised 26.07.2021

Accepted 04.08.2021

About the Author:

Maistrenko, Anatolii V., associate professor of the Information Systems in Construction Department, Don State Technical University (1, Gagarin Sq., Rostov-on-Don, 344003, RF), Cand.Sci. (Eng.), associate professor, ScopusID: 57204525180, ORCID: <https://orcid.org/0000-0002-8391-7169>, anatol-maystrenko@yandex.ru

The author has read and approved the final manuscript.

MACHINE BUILDING AND MACHINE SCIENCE



UDC 621.8-1/-9

<https://doi.org/10.23947/2687-1653-2021-21-3-268-274>

Method for assessing the current and additional load on the parallel kinematic structure mechanisms electric drive system

T. N. Kruglova  

Platov South-Russian State Polytechnic University (Novocherkassk, Russian Federation)

 tatyana.kruglova.02@mail.ru

Introduction. The problem of the load on an electric drive system in a parallel kinematic structure is considered. The task of developing a fault-tolerant system that provides performing a given process in case of a failure of one or more drives is described. The work objective is to create a method for estimating the current and additional load on each drive of the mechanism of a parallel kinematic structure. The solution enables to correct the operating mode when performing a given process without compromising serviceable drives.

Materials and Methods. Previously, a diagnostic method was developed. It is based on the calculation and analysis of the coefficients of straight lines that approximate the envelopes of the values of the wavelet transform coefficients of electric motor current signals, taking into account the characteristic scales. This makes it possible to determine the current technical condition of the electric motor and find malfunctions. The logical continuation of this approach is the proposed method for assessing the current and additional load. It provides finding the current load on the drive based on the coefficients of the lines approximating the envelopes of the wavelet coefficients of the current signal. To calculate the additional load, the number and location of faulty drives are taken into account.

Results. For each scale of the wavelet coefficients, the relative coefficients and the current load on each drive are determined. The possibility of redistributing the load to two adjacent jacks was checked; the behavior of the system in this case was investigated. The load moved by the faulty jack is redistributed to two adjacent jacks in equal shares — 14.76 % each. The total load on the drives is 44.28 %, which is safe for the servo. The load on the drive of the fourth jack does not change (29.52 %). The drives have a sufficient safety margin. It is established that all three operating modes are acceptable for the studied servo drive, and they do not cause dynamic overloads and premature failure.

Discussion and Conclusions. The experimental studies on the method of assessing the current and additional load have shown its adequacy and high efficiency. It was found that when the drives were disconnected from one of the racks of the mechanism, the system performed a load redistribution on the drives. Thus, it was possible to avoid their dynamic overloads and premature failure. This means that the solution is able to ensure the reliable functioning of the complex at the time of renovation work.

Keywords: parallel kinematic structure mechanism, drive system, assessment of the current and additional load, wavelet transform, fuzzy logic apparatus.

For citation: T. N. Kruglova. Method for assessing the current and additional load on the power drive system of parallel kinematic structure mechanisms. Advanced Engineering Research, 2021, vol. 21, no. 3, pp. 268–274.. <https://doi.org/10.23947/2687-1653-2021-21-3-268-274>

© Kruglova T. N., 2021



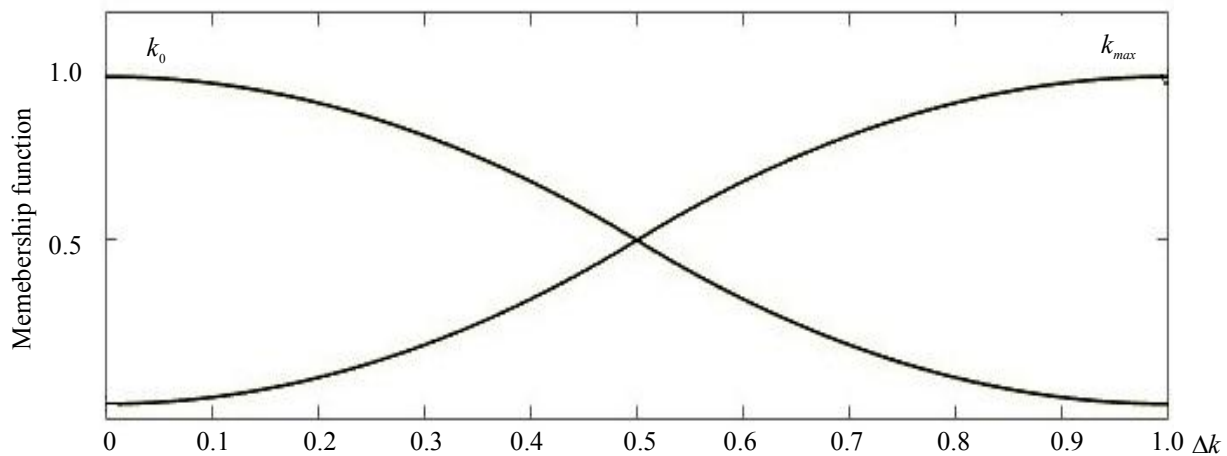
Introduction. During the operation of the mechanisms of the parallel kinematic structure, failures of one or more drives are possible. Among the likely consequences: the tilt of the platform, the curvature or jamming of the rack, unacceptable overloads, premature failure of the mechanism, production stoppage, and significant financial losses. To solve this problem, it is required to create a fault-tolerant system of drives of the parallel kinematic structure mechanisms that makes it possible to adjust the operating mode considering the technical condition. To this end, we need to determine the current load on each serviceable drive, and then, knowing the number and relative location of faulty drives, calculate the additional load on each serviceable drive.

Materials and Methods. Proper operation of drive systems of mechanisms of parallel kinematic structure is ensured through constant monitoring and evaluation of the technical condition of each actuator in real time [1]. For this purpose, a highly effective diagnostic method has been developed based on the analysis of the electric motor current using the wavelet transform [2]. The principle of the method can be described as follows: taking into account the characteristic scales, the values of the wavelet coefficients of the electric motor current are calculated, then the envelope is constructed, and its approximating line is calculated. The analysis of coefficients k and b of the resulting straight line enables to determine the current technical condition of the drive. If for all characteristic scales, $k < 0$, then the drive is serviceable, if $k \geq 0$, it is faulty. Thus, knowing the signs of coefficients k of the approximating lines, it is possible to determine the current state of each drive, calculate the number and location of faulty drives relative to each other [3].

For the subsequent adjustment of the operating mode of the parallel kinematic structure mechanism, it is required to determine the current and additional loads on each drive of the system. The calculation of the current load on the drive is based on the analysis of all the parameters of the approximating line for a known serviceable unloaded electric drive operating in nominal mode. The obtained data are reference coefficients k_0, b_0 , to which the current values of parameters k, b are compared. The value of the maximum permissible coefficients k_{max}, b_{max} can be calculated from the overload capacity of the electric motor by current K_T [4].

$$\Delta k = \frac{k - k_0}{k_{max} - k_0}, \Delta b = \frac{b - b_0}{b_{max} - b_0}. \quad (1)$$

To determine the possibility of increasing the load on the system drives, a model based on a fuzzy logic device has been developed. The inputs of the model are relative coefficients $\Delta k, \Delta b$ (Fig. 1), the output is the corresponding coefficient showing the percentage of load on the engine. If this parameter is zero, the drive operates in the rated mode without load. If it is equal to 100 %, then the engine has a maximum load and it is necessary to change its operating mode.



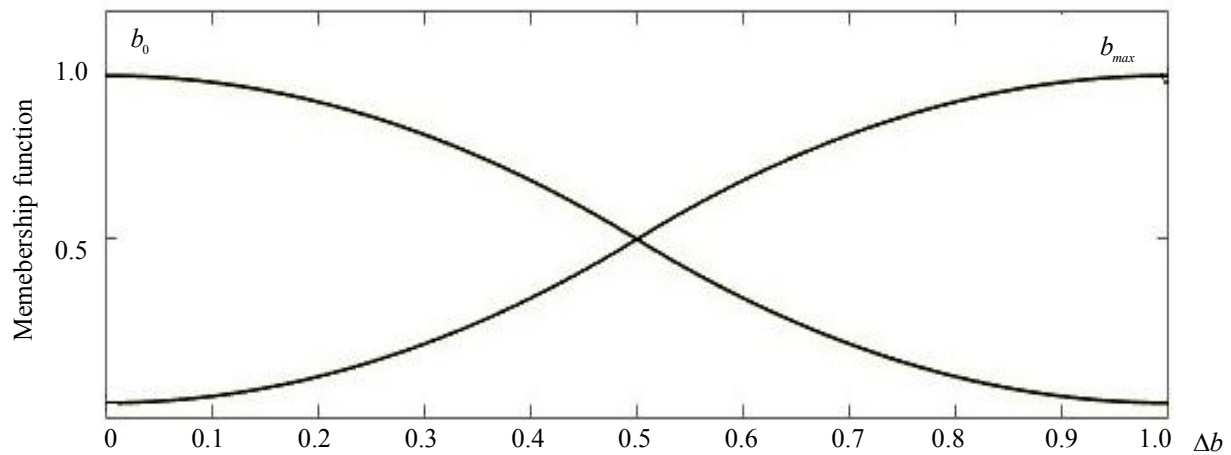


Fig. 1. Input data of the fuzzy model for determining the load on the electric drive

The correlation of the entered sets can be written using the following fuzzy rules:

R_1 : if k is k_0 and b is b_0 , then $Load_{\Pi D}=l_1$;

R_2 : if k is k_{max} and b is b_{max} , then $Load_{\Pi D}=l_2$.

The fuzzy inference algorithm *Sugeno* [5–14] is used to determine the value of the output variable.

The proposed model enables to determine the current load on the electric drive as a percentage of the maximum permissible load based on the analysis results of the coefficients of the straight line approximating the envelope of the values of the wavelet coefficients. In case of failure of one or more drives of the system and the permissible current load on the serviceable drives, it is possible to adjust the operating mode and redistribute the released load on the serviceable drives. To do this, we need to develop a model for calculating the additional load.

Let us consider the solution to this problem on the example of a platform with twelve parallel racks, each of which is an electromechanical jack. The uniform lifting of the platform is ensured by the synchronous, uniform movement of all racks at a given speed. To fulfill this condition, when designing mechanisms of a parallel kinematic structure, equal loading of lifting columns is laid. In this case, when the mechanism is operating properly, all the drives should have approximately the same external load

$$Load_{\Pi D1} \approx Load_{\Pi D2} \approx \dots \approx Load_{\Pi Dn}. \quad (2)$$

If one of the drives fails, the load moved by it is redistributed to two neighboring drives in approximately equal proportions (Fig. 2).

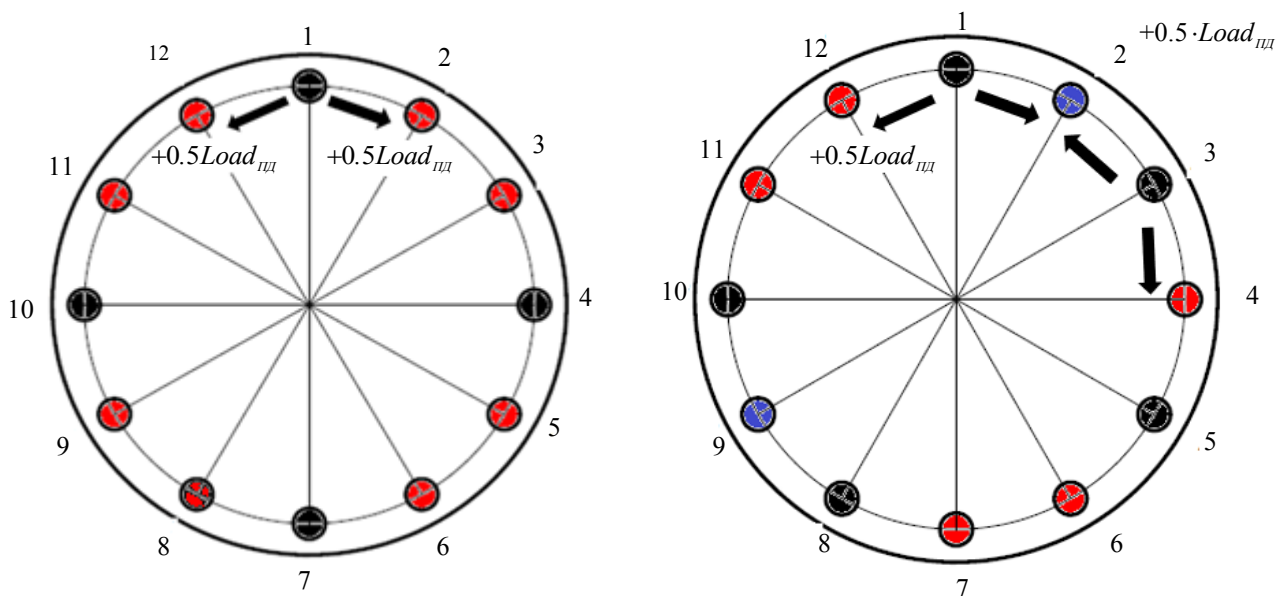


Fig. 2. Relative position of faulty jack drives and possible load correction

In this case, the additional load is calculated from ratio (3) and depends on the load change factor (L_{ch})

$$\Delta Load_{\Pi D j} = L_{ch} \cdot Load_{\Pi D i}. \quad (3)$$

This coefficient depends on the number and relative position of faulty jack drives. Theoretically, the coefficient varies in the range from 0 to n in 0.5 increments. The load increase factor is decisive when calculating the additional load on the mechanism drive. For its calculation, a model based on the use of the fuzzy logic apparatus has been developed [7]. The inputs of the model are the technical condition of each drive of the parallel kinematic structure mechanism, the outputs — the load change factor of the drive of each jack. As a result of diagnostics, the current technical condition of the drives is established: “serviceable” or “faulty”. Therefore, for each input of the system in the interval $[0, 1]$, Z- and S-shaped membership functions are set (Fig. 3 a). The serviceable drive will correspond to the input value 1, the faulty one — 0. Growth of the load increase factor greater than 2 causes critical overloads of the jack, so we set five triangular membership functions in the range $L_{ch} \in [0, 2]$ in 0.5 increments (Fig. 3 b).

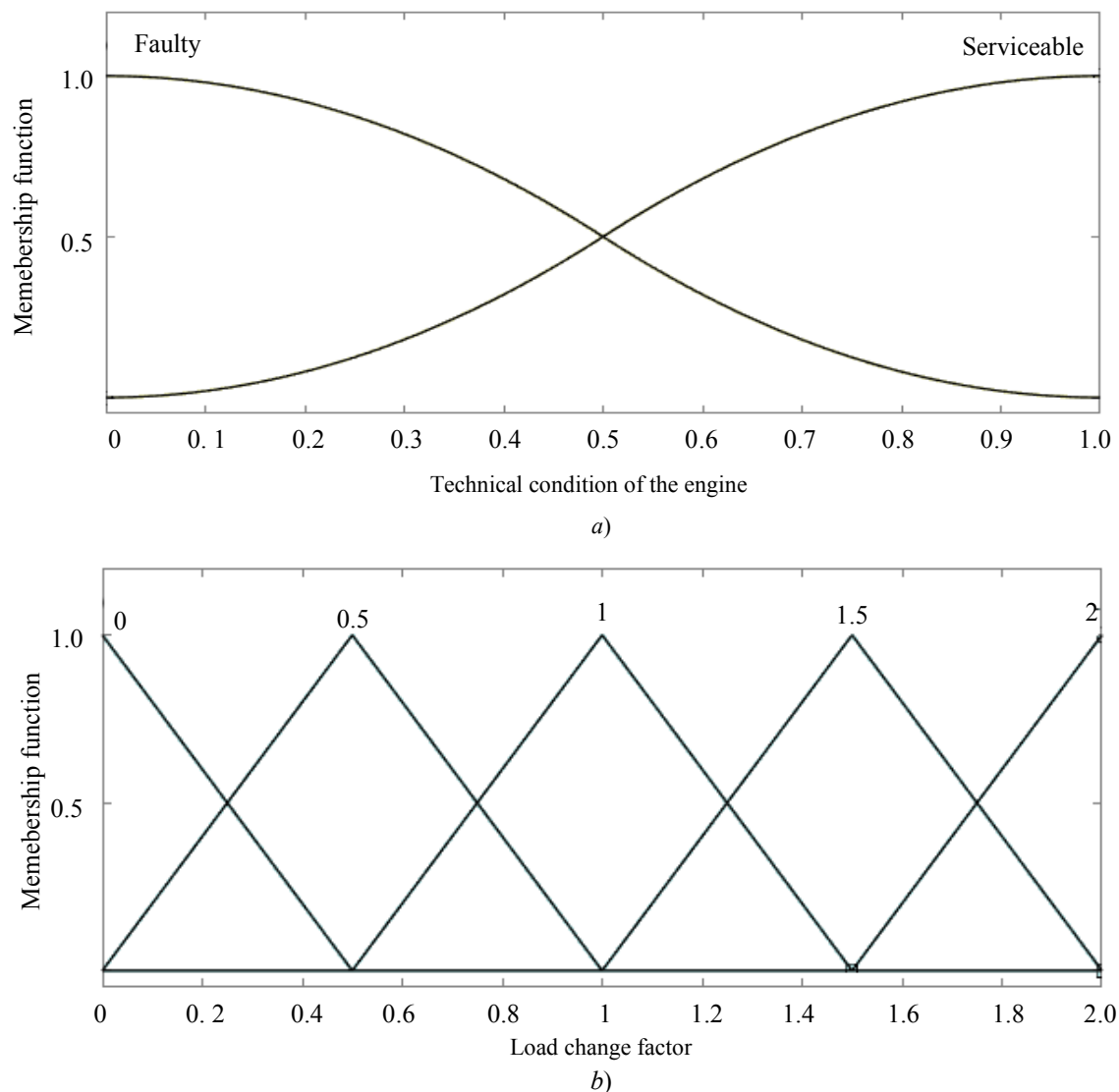


Fig. 3. Membership functions of the fuzzy model for calculating

Mamdani algorithm was used to calculate the load increase factor for the electric drives of the parallel kinematic structure mechanisms [8–10]. The resulting model is based on the analysis of the number and relative position of faulty racks of the parallel kinematic structure mechanism. This data enables to determine the additional load factor for each serviceable drive.

The relationship between the entered sets is recorded in the form of a knowledge base, whose fragment is shown in Table 1.

Table 1

Fuzzy knowledge base of the model for calculating the additional load factor

Jack number								Change factor of the jack load							
1	2	3	4	5	6	...	n	1	2	3	4	5	6	...	n
1	1	1	1	1	1	0	0	0	0	0	0
1	0	1	1	1	1	0.5	0	0.5	0	0	0
1	0	0	1	1	1	1	0	0	1	0	0
1	0	0	0	1	1	1.5	0	0	0	1.5	0
1	0	0	0	0	1	2	0	0	0	0	2
1	0	1	0	1	1	0.5	0	1	0	0.5	0
...

Combining the two developed models, we obtain a general model for determining the current and additional loads on the drives of the parallel kinematic structure mechanism (Fig. 4).

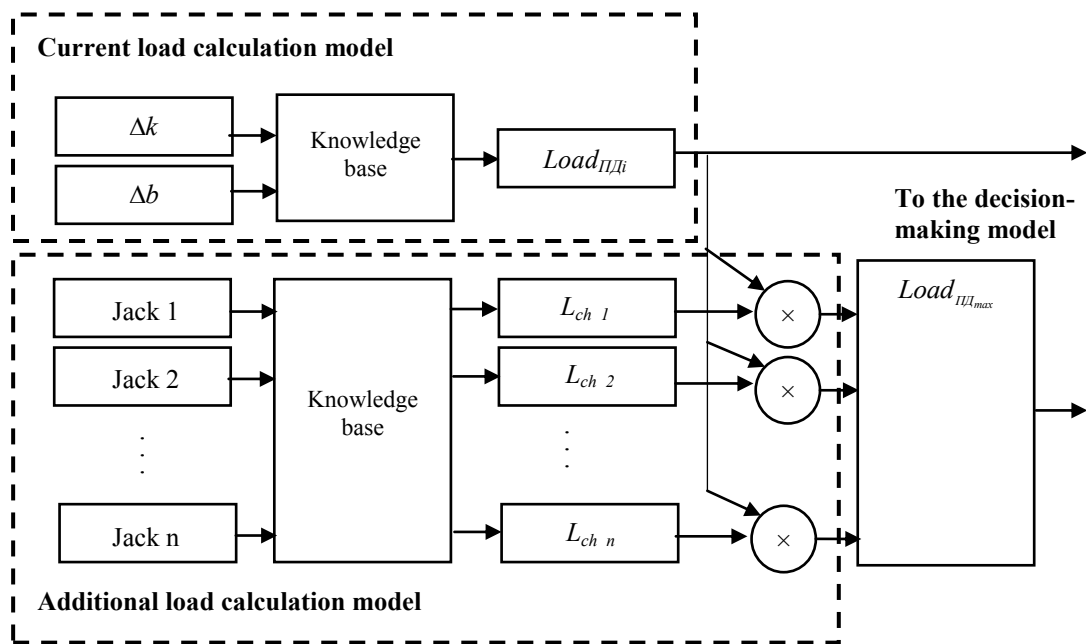


Fig. 4. Structure of the model for calculating current and additional loads on the drives of the parallel kinematic structure mechanism

The given model is based on the number and relative position of serviceable drives of the parallel kinematic structure mechanism. At the same time, taking into account the characteristic scales, the relative coefficients of the lines approximating the envelopes of the values of the wavelet transform coefficients of the electric motor current are analyzed. This data and the fuzzy logic device help to determine the current and additional load to ensure the reliability of electric motors.

Research Results. To check the operability of the proposed method for calculating the current and additional load, a stand was used (Fig. 5). It consisted of four electromechanical lifting jacks with a DC drive KY110AS0415-15B-D2 synchronously moving the load.

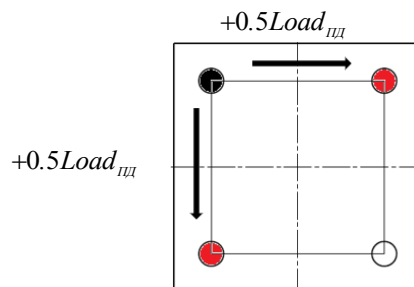


Fig. 5. Location of the faulty jack and a possible option for correcting the operating mode of the parallel kinematic structure mechanism

The current load on the drives is estimated based on the analysis of all parameters of the straight line approximating the envelopes of the wavelet transform coefficients, taking into account the characteristic scales for a

known serviceable drive operating in nominal mode. In our case, we are talking about the results of the first measurement of the current signal of the drives when they are installed on electromechanical jacks. The obtained data is used as reference k_0, b_0 . The current values of measured parameters k, b are compared to them.

Relative coefficients $\Delta k, \Delta b$ for each scale of the wavelet coefficients are calculated, and the current load on each drive is determined. The calculations have shown that the average load on all drives is approximately the same — 29.52% of the maximum. The experiment objective is to test the possibility of redistributing the load to two adjacent jacks, and to study the system behavior in this case. The load moved by a faulty jack is redistributed to two adjacent jacks in equal shares — 14.76 % each. Then, the total load on drives 1 and 3 (Fig. 5) is 44.28 %. According to the load diagram, it is safe for the servo. The load on the drive of the fourth jack remains unchanged — 29.52 %. Since coefficient k is negative for all drives, and their absolute values are significantly greater than 0, the drives have a sufficient safety margin.

To determine the impact of this load redistribution on the technical condition of the drives, the mechanical and electromechanical characteristics of the servos are analyzed. It is established that all three operating modes are acceptable for the servo drive under consideration. They do not cause dynamic overloads and premature failure. This makes it possible to ensure the reliable functioning of the complex during repair work.

Discussion and Conclusions. A model for estimating the current and additional load on the electric drives of the parallel kinematic structure mechanisms is developed. The data obtained in this way is required for correcting the operating mode of the drive system in the event of a failure of the actuators. To calculate the load, the coefficients of the straight line approximating the envelope of the current wavelet coefficients are used, taking into account the characteristic scales. In addition, the number and mutual position of the faulty jacks relative to each other are taken into account. The experiments validate the adequacy of the methods presented.

References

1. Alwan HM, Slosch AV. Decomposition of forces analysis problems of multi links parallel robotic mechanisms. *Teoriya mekhanizmov i mashin*. 2005;3(1):35–39. (In Russ.)
2. Kruglova TN. Study of the technical condition of electric drive under different loading conditions. *Bulletin of BSTU (named after V.G. Shukhov)*. 2019;3:106–116. (In Russ.)
3. Bulgakov AG, Kruglova TN. Diagnosis of the technical condition of electric drive on the basis of application of wavelet transformations. *Bulletin of Construction Equipment (BST)*. 2019;8(1020):46–50. (In Russ.)
4. Aksenov Y, Arces I, Noe G. On line PD Diagnostic on Medium Voltage Motors and Cable Lines: Useful Tool for the Maintenance Manager. *IEEE Xplore*. URL: <https://ieeexplore.ieee.org/document/1380497> (accessed: 24.08.2021). [10.1109/ELINSL.2004.1380497](https://doi.org/10.1109/ELINSL.2004.1380497)
5. Isermann R. Fault-Diagnosis Applications. Model-Based conditions monitoring: Actuators, drives, plants, sensors and fault-tolerant systems. Berlin: Springer; 2011. 466 p.
6. Cruz SMA, Cardoso AJM. Rotor cage fault diagnosis in three-phases induction motors by extended Park's Vector Approach. *Electric Machines & Power Systems*. 2000;28(4):289–299.
7. Gaskarov DV. *Iskusstvennyye informatsionnyye sistemy*. Moscow: Vysshaya shkola; 2003. 435 p. (In Russ.)
8. Zade LA. *Ponyatie lingvisticheskoi peremennoi, ego primeneniye k prinyatiyu priblizhennykh reshenii*. Moscow: Mir; 1976. 77 p. (In Russ.)
9. Kruglov VV, Borisov VV. *Iskusstvennyye neironnyye seti. Teoriya i praktika*. Moscow: Telekom; 2002. 382 p. (In Russ.)
10. Kliman GB, Koegl RA, Stein J, et al. Noninvasive detection of broken rotor bars in operating induction motors. *IEEE Transactions on Energy Conversion*. 1988;3(4):873–879. [10.1109/60.9364](https://doi.org/10.1109/60.9364)
11. Jee-Hoon Jung, Jong-Jae Lee, Bong-Hwan Kwon. Online Diagnosis of Induction Motors Using MCSA. *IEEE Transactions on Industrial Electronics*. 2006;53(6):1842–1852. [10.1109/TIE.2006.885131](https://doi.org/10.1109/TIE.2006.885131)
12. Jiyu Zhang, Alessandro Amodio, Bilin Aksun Guvenc, et al. Investigation of torque security problems in electrified vehicles. In: *Proc. ASME 2015 Dynamic Systems and Control Conf.* URL:

www.researchgate.net/publication/281295777_DSCC2015-9627_investigation_of_torque_security_problems_in_electrified_vehicles (accessed: 24.08.2021).

13. Jiyu Zhang, Hongyang Yao, Giorgio Rizzoni. Fault diagnosis for electric drive systems of electrified vehicles based on structural analysis. IEEE Transactions on Vehicular Technology. 2016;66(2):1027–1039. URL: https://www.researchgate.net/publication/301571844_Fault_Diagnosis_for_Electric_Drive_Systems_of_Electrified_Vehicles_Based_on_Structural_Analysis (accessed: 24.08.2021). [10.1109/TVT.2016.2556691](https://doi.org/10.1109/TVT.2016.2556691)

14. Thomson WT, Fenger M. Current signature analysis to detect induction motor faults. IEEE Industry Applications Magazine. 2001;7(4):26–34. [10.1109/2943.930988](https://doi.org/10.1109/2943.930988)

Received 28.06.2021

Revised 19.07.2021

Accepted 27.07.2021

About the Author:

Kruglova, Tatyana N., associate professor of the Mechatronics and Hydropneumatic Automatics Department, Platov South-Russian State Polytechnic University (NPI) (132, ul. Prosveshcheniya, Novocherkassk, Rostov Region, 346428, RF), Cand.Sci. (Eng.), associate professor, Researcher ID: F-4200-2018, Scopus ID 57170357700, ORCID: <https://orcid.org/0000-0001-8801-8368>, tatyana.kruglova.02@mail.ru.

The author has read and approved the final manuscript.

INFORMATION TECHNOLOGY, COMPUTER SCIENCE, AND MANAGEMENT




UDC 004.021

<https://doi.org/10.23947/2687-1653-2021-21-3-275-283>

Analysis of the speed and curvature of the trajectory in the problem of pursuing a set of targets

A. A. Dubanov  

Banzarov Buryat State University (Ulan-Ude, Russian Federation)

 alandubanov@mail.ru

Introduction. A kinematic model of group pursuit of a set of targets on a plane is considered. Pursuers use a technique similar to parallel approach method to achieve goals. Unlike the parallel approach method, the speed vectors of pursuers and targets are directed arbitrarily. In the parallel approach method, the instantaneous directions of movement of the pursuer and the target intersect at a point belonging to the circle of Apollonius. In the group model of pursuing multiple goals, the pursuers try to adhere to a network of predictable trajectories.

Materials and Methods. The model sets the task of achieving goals by pursuers at designated points in time. This problem is solved by the methods of multidimensional descriptive geometry using the Radishchev diagram. The predicted trajectory is a composite line that moves parallel to itself when the target moves. On the projection plane “Radius of curvature — speed value”, the permissible speed range of the pursuer is displayed in the form of level lines (these are straight lines parallel to one of the projection planes). Images of speed level lines are displayed on the projection plane “Radius of curvature — time to reach the goal”. The search for points of intersection of the speed line images and the appointed time level line is being conducted. Along the communication lines, the values of the intersection points are lowered to the plane “Radius of curvature — speed value”. Using the obtained points, we construct an approximating curve and look for the intersection point with the line of the assigned speed. As a result, we get values of the radius of the circle at the predicted line of the trajectory of the pursuer.

Results. Based on the results of the conducted research, test programs have been created, and animated images have been made in the computer mathematics system.

Discussion and Conclusions. This method of constructing trajectories of pursuers to achieve a variety of goals at a given time values can be in demand by developers of autonomous unmanned aerial vehicles.

Keywords: multidimensional analysis, Radishchev plot, target, pursuer, trajectory, radius of curvature.

For citation: A. A. Dubanov. Analysis of the speed and curvature of the trajectory in the problem of pursuing a set of targets. Advanced Engineering Research, 2021, vol. 21, no. 3, pp. 275–283. <https://doi.org/10.23947/2687-1653-2021-21-3-275-283>

Funding information: the research is done with the financial support from Buryat State University in 2021 (the innovation grant “Control of a four-link manipulator based on signals received from the neurointerface”).

© Dubanov A. A., 2021



Introduction. We consider a model for calculating the trajectory of the pursuer on a plane, where at each moment of time, a predicted trajectory from the pursuer to the target is built, and the pursuer will try to stick to it (Fig. 1).

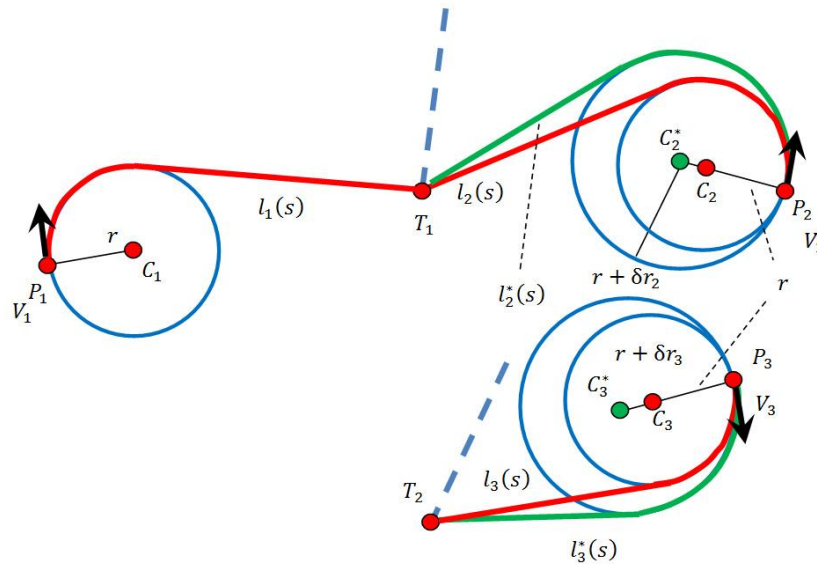


Fig. 1. Group pursuit of multiple goals

Curves $l_1(s)$, $l_2(s)$, $l_3(s)$ consist of a circular arc segment and a straight-line segment. In our model, the radius of the circles is the curvature constraint of the predicted trajectories of the pursuers^{1,2,3}.

The research task in this paper can be described as follows: pursuers, moving along a one-parameter network of predicted trajectories, must achieve their goals at designated times, including simultaneously. Methods of multidimensional descriptive geometry using the Radishchev diagram are selected for the solution. The one-parameter network (Fig. 2) consists of congruent lines of parallel transport. Each line is an analog of the line of sight (it is a straight line connecting the pursuer and the target).

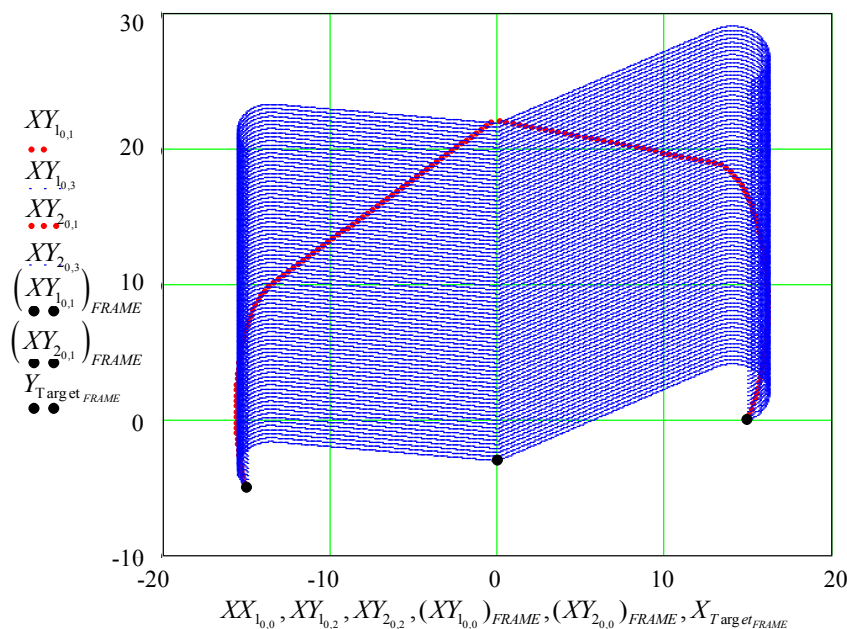


Fig. 2. One-parameter networks of predicted trajectory of pursuers

A combination of a circle and a straight line is selected for the model. There are many options for providing curvature constraints (Cornu spiral, a cubic parabola conjugating with a straight line, etc.). To achieve the goals, the pursuers use a method similar to the parallel approximation method [1–4]. However, in our case, the speed of the

¹Bannikov AS. A nonstationary group pursuit problem. Lobachevskie chteniya: Proc. 5th Youth Sci. School-Conf. Trudy matematicheskogo tsentra im. N. I. Lobachevskogo. Kazan: Izd-vo Kazanskogo matematicheskogo obshchestva; 2006. P. 26–28. (In Russ.)

²Izmestyev IV, Ukhobotov VI. Pursuit problem of low-maneuverable objects with a ring-shape terminal set. In: Proc. Int. Conf. Ryazan: Publ. House of RSU named for S. Yesenin; 2016. P. 17–18. (In Russ.)

³Borie R, Tovey C, Koenig S. Algorithms and Complexity Results for Pursuit-Evasion Problems. In: Proc. Int. Joint Conf. on Artificial Intelligence (IJCAI), 2009. P. 59–66.

pursuers is directed arbitrarily, and in the method of parallel approximation, the speed lines of the pursuer and the target intersect at a point on the Apollonian circle.

In the test program, written using the materials of the paper, objects move around a square $[-30:30] \times [-30:30]$. The calculation is made in meters. The studies were carried out for speeds of 20 m/s. The initial radius of the circles with the predicted trajectories was 2 m. If at the moment of the beginning of the pursuit, the pursuer was at point P_i with speed vector V_i , then the center of circle C_i of radius r_i will be at point:

$$C_i = P_i \pm r_i \cdot \frac{\begin{bmatrix} -V_{iy} \\ V_{ix} \end{bmatrix}}{|V_i|}.$$

Then, from the point of target position T_i , a tangent to circle (C_i, r_i) is constructed. The combination of the tangent and the circle is the baseline of the predicted trajectory of pursuer $l_i(s)$. Note that in the equation of the baseline from a one-parameter set of predicted trajectories, parameterization is performed from the arc length.

At the new position of target T_i , line $l_i(s)$ shifts while remaining parallel to itself (Fig. 3).

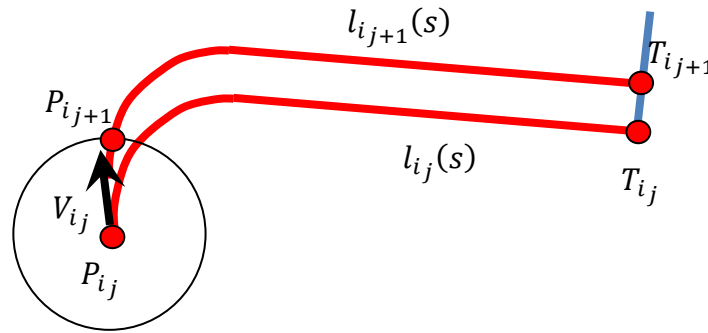


Fig. 3. Iterative process of calculating the trajectory of the pursuer

Assume that the i -th pursuer at the moment t_j is at point P_{ij} , while having a predictable trajectory $l_{ij}(s)$ between the current position of target T_{ij} . In this case, the next point of the pursuer trajectory will be P_{ij+1} .

P_{ij+1} — point of intersection of line $l_{ij+1}(s)$, which corresponds to the position of target T_{ij+1} at the next moment in time t_{j+1} and the circle with center P_{ij} and radius $|V_{ij}| \cdot \Delta t$, $\Delta t = t_{j+1} - t_j$. This is the model for constructing the trajectories of the pursuer^{4, 5}.

Consider the task of group pursuit, when a group of pursuers catches up with a group of targets. We assume that each pursuer P_i seeks to achieve its goal T_i , although some pursuers may have the same goals (Fig. 1, 2).

Moreover, pursuer P_i reaches goal T_i in a certain time t_i , moving at a certain speed V_i . To achieve the goals simultaneously, it is required that all t_i are equal to a certain value.

Figure 1 shows that to change the length of the baseline, you can change the radius of the tangent circle. The tangent is introduced so that the pursuer can smoothly switch to a straight trajectory. If this were the case, then the task would be reduced to the pursuit by the parallel approximation method.

The initial speed of the pursuer is directed arbitrarily, which provides using the parallel approximation method with respect to curvature constraints (Fig. 2). For this, a composite baseline is used, which, when the target moves, remains parallel to itself; there is a smooth transition to the parallel approximation method with respect to curvature constraints (Fig. 3). Figure 2 is supplemented with a link to an animated image where you can see a smooth transition to parallel approximation⁶.

The purpose of this paper is to describe the method by which the pursuer reaches the goal at the appointed time from the acceptable values. We can also consider the simultaneous achievement of goals by a group of pursuers [5–9].

⁴Dubanov AS, Seveen A-K. Kinematic model of the parallel approximation method: state registration certificate of computer software. Banzarov Buryat State University. RU 2020665641. No. 2020664886, 2020. (In Russ.)

⁵Dubanov AS, Seveen A-K. Modeling of trajectory of the pursuer on the surface using the parallel approximation method: state registration certificate of computer software. Banzarov Buryat State University. RU 2020666553. No. RU 2020666553, 2020. (In Russ.)

⁶Dubanov A. Dognat' odnovremennno. Ploskost' 1. URL: <https://www.youtube.com/watch?v=7VNHnwCbWrg> (accessed: 22.05.2021). (In Russ.)

Materials and Methods. Based on the research results, a test program for simultaneous achievement of goals by pursuers has been developed, which can be viewed at the author's resource. The proposed algorithm implements an iterative scheme for calculating the trajectory of the pursuer (Fig. 3).

The model assumes a dependence for pursuer P , who reaches goal T in time t :

$$t = F(P_s, T_s, n_p, n_T, V_p, V_T, R).$$

Here, P_s, T_s — coordinates of the position points of the pursuer and the target at the moment of the beginning of the pursuit; n_p, n_T — unit vectors of the direction of movement of the pursuer and the target at the time of the beginning of the pursuit; V_p, V_T — speed modules of the pursuer and the target during the pursuit; R — radius of the circle, whose meaning is shown in Fig. 1, 3.

In fact, the model calculates the number of steps for which the pursuer reaches the goal. With a known discrete time interval, the number of steps can be compared to real time.

If the target moves rectilinearly and uniformly, then the time-to-target dependence in the already started iterative process can be considered a function of two variables — the speed modulus of the pursuer and the radius of curvature of the circle:

$$t = F(V_p, R).$$

In the model, it is assumed that the pursuer moves at constant speed V_p , but nothing prevents us from changing the values of the speed modulus, as well as the radius of curvature. Let us assume that the speed module takes discrete values from the series $V_{p_i}, i \in [1: N]$, and the radii of the circles in Fig. 1, 3 take the values $R_j, j \in [1: M]$.

For further research, the Radishchev diagram is used, where coordinate planes (R, V) and (R, t) are used (Fig. 4).

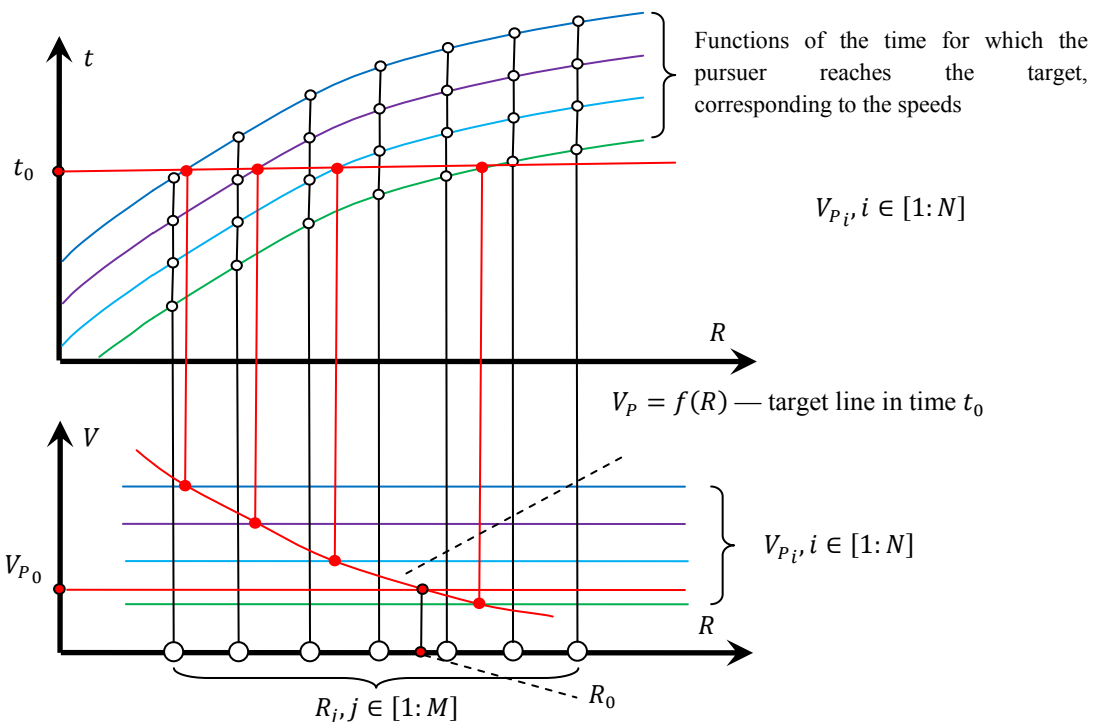


Fig. 4. Determination of the radius of the circle on the Radishchev diagram

Figure 4 shows the experimental construction of time dependences $t_{i,j} = F(V_{p_i}, R_j)$. Graphs on the plane (R, t) show how the time to reach the target depends on the radius of the circle R at fixed speed value V_p .

As one of the optimizing factors [10–11] on the plane (R, t) , equality $t = t_0$ is selected, where t_0 — the required time to achieve the target. Next, to solve our problem on plane (R, V) , equality $V_p = V_{p_0}$ is selected as the second optimizing factor, where V_{p_0} — the constant speed of the pursuer.

The problem statement says that the speed module of the pursuer is unchanged. Nevertheless, the constructed series of speed values is required for calculating the radius of the circle R_0 on the projection plane (R, V) .

Along the communication lines on the projection plane (R, V) , there are corresponding points of intersection with the lines of the speed level V_{P_i} (Fig. 4). According to the obtained points, a polynomial regression is performed in the test program, and as a result, we get a function of the dependence of the pursuer speed on the radius of the circle at which the target is achieved in time t_0 .

Then we seek the intersection point of function $V_p = f(R)$ with the line of the level $V_p = V_{P_0}$. Abscissa of the intersection point R_0 is the desired radius of the circle, at which pursuer P reaches target T during time t_0 at speed V_{P_0} .

The calculation is carried out under the condition that the target moves uniformly and rectilinearly. If the target changes direction or speed, then a new radius of the circle of the composite baseline is calculated (analogous to the line of sight of the parallel approximation method), a new time of reaching is set at the same speed of the pursuer.

With a uniform and rectilinear movement of the target, the lowest limit of the time of achievement is fixed when the speed of the pursuer is directed to point K on the Apollonius circle (Fig. 5). This position was considered in the works of R. Aizeks [12], L. S. Pontryagin [13], L. A. Petrosyan [14-16], N. N. Krasovsky and A. I. Subbotin [17].

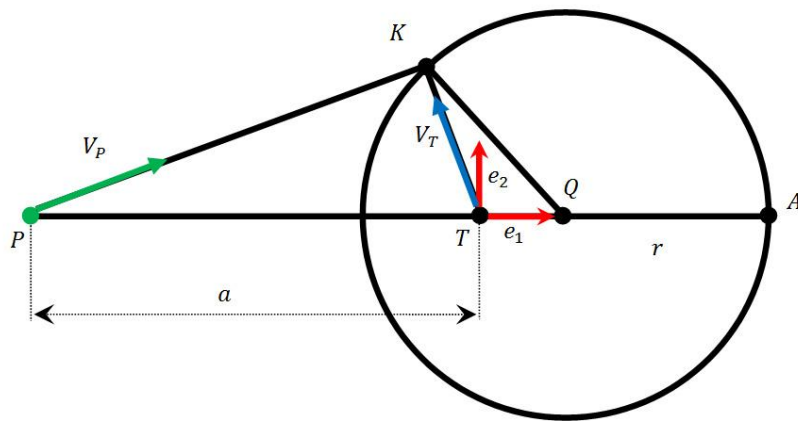


Fig. 5. The circle of Apollonius

The Apollonius circle is a geometric place of points, the ratio of the distances from which to two given points is a constant value, other than unity: $|PK|/|TK| = |V_p|/|V_T|$ (Fig. 5).

When considering the multiple pursuit of a group of targets in the test program, a preliminary calculation of the trajectories of the pursuers is made with the given initial parameters. From the times of achieving targets, the largest time is selected for calculating simultaneous achievement, and it will be the criterion for calculating the trajectories of the other pursuers^{7, 8}. This moment is illustrated in an animated image, where three pursuers achieve two targets simultaneously⁹.

Figure 6 shows how a shorter time was set for one of the pursuers to reach the target. Figure 6 is also supplemented with a link to an animated image where you can see the achievement of targets at different designated times^{10, 11, 12}.

⁷ Dubanov AS, Seveen A-K. Modeling of the method of parallel approximation on the surface: state registration certificate of computer software. RU 2021618896. No 2021617979, 2021. (In Russ.)

⁸ Dubanov AS, Seveen A-K. Parallel approach model on plane of group of pursuers with simultaneous achievement of the goal: state registration certificate of computer software. RU 2021618920. No. 2021614416, 2021. (In Russ.)

⁹ Dubanov A. NM 1. URL: <https://www.youtube.com/watch?v=tdbgoNoby3A> (accessed: 22.05.2021).

¹⁰ Dubanov A. NM 3. URL: <https://www.youtube.com/watch?app=desktop&v=F6MTsWZL2BY&feature=youtu.be> (accessed: 22.05.2021).

¹¹ Dubanov A. NM 2. URL: <https://www.youtube.com/watch?v=NNJDJOJT34I> (accessed: 17.08.2021).

¹² Dubanov A. NM 1. Ibid. (accessed: 17.08.2021).

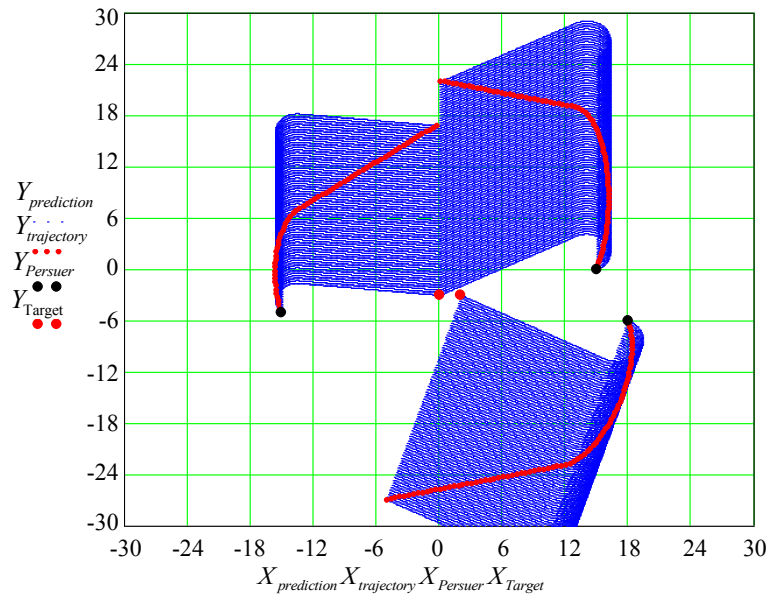


Fig. 6. Achieving targets at different designated times

Research Results. Figure 7 shows some results of multivariate analysis in the problem of simultaneous achievement of the target by two pursuers.

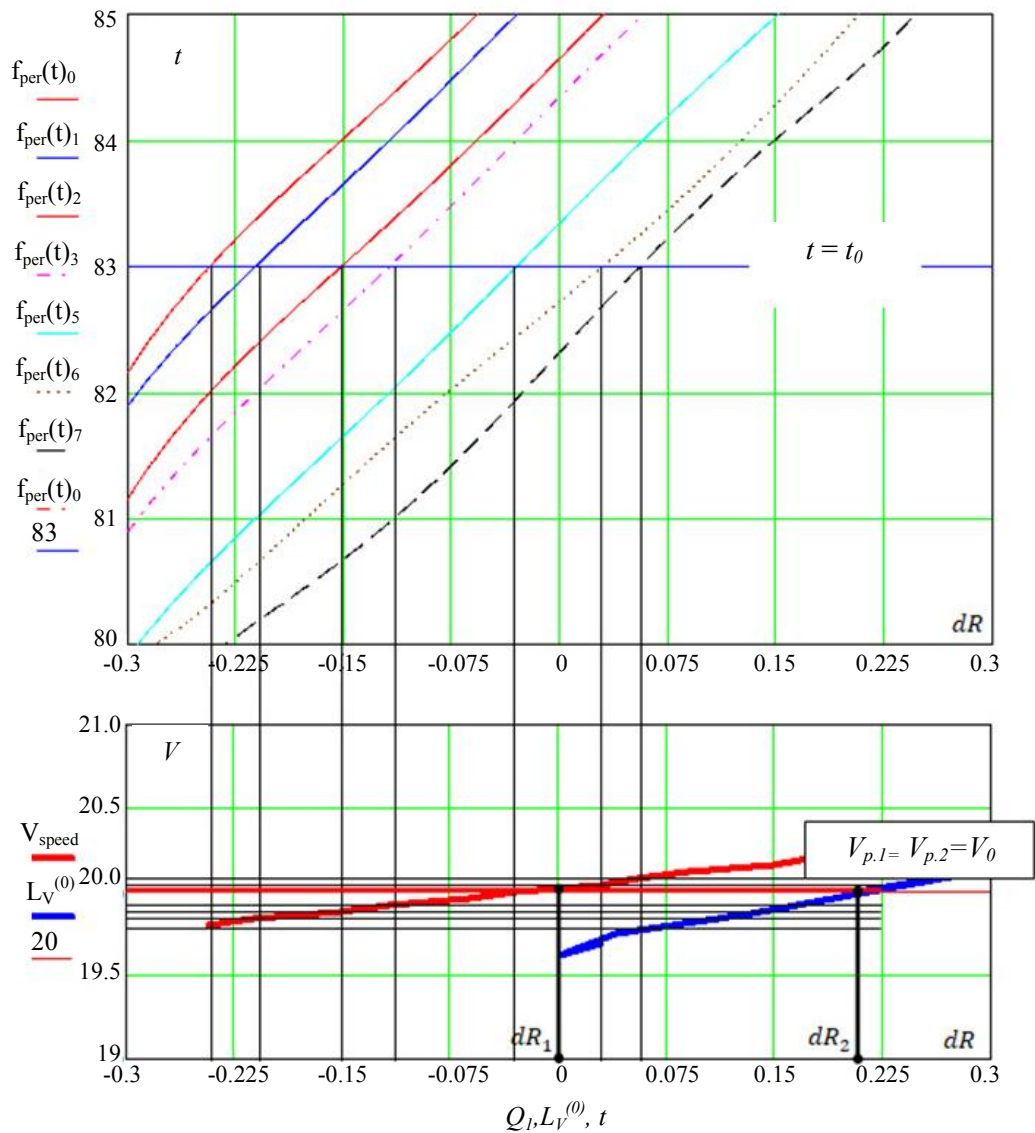


Fig. 7. Multivariate analysis results in the problem on simultaneous target achievement by two pursuers

The target moves rectilinearly and uniformly. A number of permissible speeds was built for each pursuer. The permissible values of the radius of the circle are varied using the discrete variable dR (scale in Fig. 7).

We construct a one-parameter network of lines on the projection plane (dR, t) . Each line corresponds to a certain speed value and expresses the dependence of the time-to-target on the increment of the radius of the circle. Figure 7 shows a one-parameter network of speed lines of one of the pursuers. A similar network was built for the second one in the test program of the multivariate analysis.

For each pursuer, the first optimizing factor is selected [10–11], which is responsible for simultaneous achievement:

$$t = t_0.$$

Here, t_0 — the longest of the times of reaching the target if the pursuers independently caught up with the target under the same initial conditions.

On the plane (dR, t) , we seek the intersection points of the lines of the level $t = t_0$ with the speed lines of the one-parameter network. The intersection points are found using the built-in procedures for solving equations. In the MathCAD computer mathematics system, this can be *root* procedure. Values dR and V on the projection plane (dR, V) correspond to the found intersection points.

The built-in polynomial regression procedure is applied to the obtained points on the projection plane, and the characteristic curve of the speed dependence on the radius of the circle of the composite baseline is found (Fig. 1).

On the projection plane (dR, V) , Figure 7 shows the same characteristic line of speed dependence for another pursuer. Then, the second optimizing factor $V_1 = V_2 = V_0$ is applied. In the test program, objects move at the same speeds. The built-in means of computer mathematics find the points of intersection with the line of the level $V = V_0$. Values dR_1 and dR_2 correspond to these points.

When starting the iterative process, the simultaneous achievement of the target by two pursuers was recorded (the animation to Fig. 2). At the same time, the values of the increments dR_1 and dR_2 to the initial radius of the circle were found and set:

- value of the time to reach the target t_0 ,
- speed modules V_0 , s.

The paper describes a method for achieving multiple goals by a group of pursuers with the ability to set the time to achieve them. Simultaneous achievement of goals is a particular result of this approach, which the method of parallel approximation develops. When implementing the method in space, it should be ensured that the vectors of the pursuer and the target are in the same plane¹³.

Let us consider the case of pursuit in three-dimensional space under the following conditions: we want to reduce the problem to the method of parallel approximation, but the speed of the pursuer is directed arbitrarily. In this case, the baseline of the predicted trajectories of the pursuer movement should be built in the plane formed by the line of sight and the speed of the pursuer.

The next step of the pursuer is the intersection point of a sphere with a radius equal to the step of the pursuer, and the baseline, moved in parallel so that one end of it is aligned with the point of the target position.

Let us turn to the question of finding the circle of Apollonius and point K in three-dimensional space. The circle itself will be in the plane formed by the line of sight and the speed of the target. We define such parameters of the Apollonian circle as the center of the circle (point Q), the radius of the circle r , the Apollonian point (A) and point K . This end, the target speed vector, the speed module of the pursuer, the positions of the pursuer, and the target, are taken into account. There is an analytical solution to this problem in a flat coordinate system (see Fig. 5). The coordinate center is located at the point of the target position. The abscissa vector will be a unit vector along the line of sight connecting the positions of the pursuer and the target. The ordinate vector will be perpendicular to the abscissa vector, but in the plane formed by the line of sight and the target speed vector.

¹³ Dubanov A. Simultaneous achievement of the goal on a plane. Geometrical modeling in MathCAD. URL: <http://dubanov.exponenta.ru> (accessed: 22.05.2021). (In Russ.)

Discussion and Conclusions. The multidimensional descriptive geometry methods used in this work are based on the variation of the speed modules and the radii of curvature of circles. At the same time, according to the conditions of the problem, the speed modules of the pursuers are unchanged.

The paper takes into account the results achieved in works [18, 19, 20].

The proposed approach makes it possible to analyze the modules of speeds and directions of the initial movement.

The model of four-dimensional space presented in the papers of V. P. Bolotov (Bolotov's hypergraph)¹⁴ should be used to analyze:

- speed modules,
- radii of circles adjacent to the pursuers,
- initial directions of movement of the pursuers.

The research results presented in the paper can be in demand by developers of unmanned aerial vehicles that perform group coordinated tasks. The role of the guidance operator can be reduced to specifying goals and monitoring the performance of tasks.

References

1. Bannikov AS. Some non-stationary problems of group pursuit. Proceedings of the Institute of Mathematics and Informatics at Udmurt State University. 2013;1(41):3–46. (In Russ.)
2. Petrov NN, Solov'eva NA. Group pursuit in the recurrent differential games. Proceedings of the Institute of Mathematics and Informatics at Udmurt State University. 2012;1(39):99–100. (In Russ.)
3. Blagodatskikh AI. Konfliktnoe vzaimodeistvie grupp upravlyaemykh ob"ektov. Izhevsk: USU Publ. House; 2009. 263 p. (In Russ.)
4. Blagodatskikh AI. Almost periodic processes with conflict control with many participants. Journal of Computer and Systems Sciences International. 2007;2:83–86. (In Russ.)
5. Ibragimov GI, Rikhsiev BB. On some sufficient conditions for optimality of the pursuit time in the differential game with multiple pursuers. Automation and Remote Control. 2006;4:16–24. (In Russ.)
6. Pashko SV. Garantirovannoe vremya presledovaniya dlya strategii parallel'nogo sblizheniya v sluchae ravenstva skorostei igrokov. Komp'yuternaya matematika. 2014;1:140–149. (In Russ.)
7. Pashko SV. Guaranteed time of pursuit for the strategy of parallel approach. Dopovidi Natsional'noi akademii nauk Ukraini. 2014;4:43–48. (In Russ.) <https://doi.org/10.15407/dopovidi2014.04.043>
8. Pashko SV, Yalovets AL. Maksimal'noe vremya presledovaniya dlya strategii parallel'nogo sblizheniya. Problemi programuvannya. 2014;4:78–93. (In Russ.)
9. Volkov VYa, Chizhik MA. Graficheskie optimizatsionnye modeli mnogofaktornykh protsessov. Omsk: OGIS; 2009. 101 p. (In Russ.)
10. Pashko SV. Complexity of pursuit optimization problems on a plane. Journal of Automation and Information Sciences. 2013;45(5):25–37. (In Russ.) 10.1615/JAutomatInfScien.v45.i5.30
11. Pashko SV, Yalovets AL. Numerical Methods for Solving the Pursuit Optimization Problems. Problemi programuvannya. 2013;4:74–85. (In Russ.)
12. Aizeks R. Differentsial'nye igry. Moscow: Mir; 1967. 480 p. (In Russ.)
13. Pontryagin LS. A linear differential evasion game. Proceedings of the Steklov Institute of Mathematics. 1971;112:30–63. (In Russ.)
14. Petrosyan LA. Differentsial'nye igry presledovaniya. Leningrad: LSU Publ. House; 1977. 222 p. (In Russ.)
15. Petrosyan LA, Rikhsiev BB. Presledovanie na ploskosti. Moscow: Nauka; 1991. 94 p. (In Russ.)
16. Petrosyan LA, Zenkevich NA, Shevkoplyas EV. Teoriya igr. St. Petersburg: BKhV-Peterburg; 2012. 424 p. (In Russ.)
17. Krasovsky NN, Subbotin AI. Pozitsionnye differentsial'nye igry. Moscow: Fizmatlit; 1974. 456 p. (In Russ.)

¹⁴ Bolotov VP. Nachertatel'naya geometriya mnogomernogo prostranstva. URL: http://vm.msun.ru/Autor/Dis_dokt/Ngeo_mng.htm (accessed: 22.05.2021). (In Russ.)

18. Samatov BT. The pursuit-evasion problem under integral-geometric constraints on pursuer controls. Automation and Remote Control. 2013;74(7):1072–1081.
19. Gafurjan Ibragimov, Atamurat Sh. Kuchkarov, Fudziah Ismail, et al. Multi pursuer differential game of optimal approach with integral constraints on controls of players. Journal of Mathematics. 2015;19(3):963–976. [10.11650/tjm.19.2015.2288](https://doi.org/10.11650/tjm.19.2015.2288)
20. Petrov NN, Solov'eva NA. Group pursuit with phase constraints in recurrent Pontryagin's example. International Journal of Pure and Applied Mathematics. 2015;100(2):263–278. [10.12732/ijpam.v100i2.8](https://doi.org/10.12732/ijpam.v100i2.8)

Received 05.07.2021

Revised 26.07.2021

Accepted 02.08.2021

About the Author:

Dubanov, Alexander A., associate professor of the Geometry and Methods of Teaching Mathematics Department, Banzarov Buryat State University (24a, Smolin St., Ulan-Ude, 670000, RF), Cand.Sci. (Eng.), ResearcherID: [AAG-6697-2021](https://orcid.org/0000-0002-1855-2562), ORCID: <https://orcid.org/0000-0002-1855-2562>, alandubanov@mail.ru

The author has read and approved the final manuscript.

INFORMATION TECHNOLOGY, COMPUTER SCIENCE, AND MANAGEMENT



UDC 004.722:519.172

<https://doi.org/10.23947/2687-1653-2021-21-3-284-289>

A method for generating a local network graph based on the analysis of address sets



V. V. Galushka ¹, D. V. Fatkhi ¹, E. R. Gazizov ²

¹ Don State Technical University (Rostov-on-Don, Russian Federation)

² Kazan Agricultural State University (Kazan, Russian Federation)

✉ galushkavv@yandex.ru

Introduction. The paper deals with the problem of automated construction of a local area network using tools and methods for traffic analysis at the link layer of OSI model. The problem is caused by two factors. These are difficulties of the manual determination of the communication between equipment and the lack of physical access to communication lines of an already functioning network. The purpose of the work is to reduce the time spent on building a local network diagram through automating the process of determining the communication between the equipment.

Materials and Methods. To solve the set tasks, a method for determining the relative location of devices is proposed. The network adapters of a specialized software and hardware complex, which are connected to a communication line break at different points of the network, are used in opposite directions. The method used is based on calculations of intersections of address sets received from these adapters. The structural schemes of the construction of such a software and hardware complex and the requirements for it are given. The methods of obtaining MAC addresses from transit packets are described. Examples of libraries of software components for performing this operation are given. The structure of a relational database is proposed for storing the received data. The format and content of the fields of its table are described.

Results. Using the developed methods, a typical example of an Ethernet network shows a way to determine the relative location of end devices specified by their MAC addresses, as well as at least two switches located between them. The signs by which it is possible to judge the presence of switching equipment in a particular segment are determined. A method is proposed that enables through using a set of relational operations, to sequentially refine the network topology until the required accuracy is achieved.

Discussion and Conclusions. The results obtained can be used under the administration of large local networks with an extensive structure. The proposed approach allows you to reduce the time required for building a scheme. This is possible due to the automation of the process of obtaining information about devices operating on the network and their mutual location.

Keywords: network topology, graph, tree, local network, traffic analysis, sets, relational operations.

For citation: V. V. Galushka, D. V. Fatkhi, E. R. Gazizov. A method for generating a local network graph based on the analysis of address sets. Advanced Engineering Research, 2021, vol. 21, no. 3, pp. 284–289. <https://doi.org/10.23947/2687-1653-2021-21-3-284-289>

© Galushka V. V., Fatkhi D. V., Gazizov E. R., 2021



Introduction. Large local area networks are characterized by a complex configuration of physical connections, which to a great extent determines the efficiency of their work [1, 2]. In practice, the organization does not always have a detailed scheme or other documentation describing the network equipment and its interconnections. This significantly complicates the administration procedures and conditions the urgency of the problem of determining the structure of connections in the operated network for further construction of the layout and connection of nodes.

Communication lines are most often hidden behind the elements of the structure or decoration of the building, only switchgear is available. In this case, it is impossible to understand to which of the network nodes each connected

cable leads. Therefore, the task arises on constructing a network diagram based on the analysis of data obtained from the traffic captured at certain points. We are talking about places that are potentially available for connecting additional software and hardware that analyze traffic. The objective is to reduce the time spent on building a local network scheme.

The described task is complicated by the fact that all the information related to the functioning of the local network belongs to the second (data link) layer of the OSI model, and a significant part of the important data in the packet belongs to a higher level — the network [3, 4].

Most methods of traffic analysis are designed for processing network-level information [5]. In this regard, there is a need to develop methods that allow you to get all the necessary data for building a network diagram from the packet headers of the data link layer of the OSI model. On the other hand, network topologies at the data link layer are simpler than at the network layer, and they are always strictly regulated by the relevant standards¹.

Materials and Methods. The Ethernet standard, which is widely used for building local computer networks, provides for the use of the “tree” topology for organizing connections between nodes [5]. In graph theory, a “tree” is defined as a connected circuit-free graph [6]. An important consequence of this definition is that there is one and only one path between any pairs of vertices in the tree [7]. This allows you to abandon the search for routes within such a network and greatly simplify the operation of the equipment.

When constructing a graph, the set of its vertices and the connections between them is determined [8]. In relation to the network graph, vertices are network hardware. To address it within the local network, the MAC addresses assigned by the manufacturer are used. They are unique for each device and have 6 bytes in size [9]. The header of each network packet contains two MAC addresses: the sender and the recipient. They do not change during the transmission of a packet within the local network, and therefore in the problem under consideration, they can be used to identify network nodes.

When building a network graph, the major difficulty is determining the connections. Each connection links two vertices, whose relative location, as noted above, is unknown due to their great distance or hidden telecommunications routing. Connections can link devices of different types: switch-computer or switch-switch. The latter constitute the data transmission infrastructure and are of the greatest interest in terms of analyzing the network topology. In contrast, the connections of switchgear with computers describe the final vertices of the graph. At the same time, computers connected to the same switch can be conditionally combined into a group, since their mutual location relative to other computers will be the same. As a group, we can also consider larger sets of nodes, including computers connected to two or more nearby switches (i.e., those responsible for communication within one floor of a building or several offices of one department). In general, nodes that are part of a set should be located closer to each other than to nodes that are not part of the set or are part of another set [10]. At the first approximation, the entire local network can be considered as such a set, because its nodes are closely interconnected and separated from other networks [11].

The research idea is to consistently refine the network topology. For this, we will divide the set of MAC addresses of the devices included in it into smaller subsets, up to the definition of groups of computers connected to separate switches.

The division into subsets is performed relative to the points at which a hardware device capable of analyzing network packets and extracting address and other information from them is connected to the network. Such a device can be a laptop or a single-board computer that can work simultaneously with two network adapters. This will allow them to be connected to break the connection. As a result, a part of the network will be connected to each of the two network adapters.

It is important to note the difference between the terms “vertex” and “point”. A vertex is a part of the network graph that denotes some equipment: a switch or an end device. A point is the connection point of the specified hardware complex, which is always located between two vertices.

Taking into account the linking of the analyzing device to the connection break, it is required to provide the operability of the communication line in which this break occurs. To that end, the network adapters must be connected through the operating system. A “bridge” type connection is used, when packets arriving at one of the interfaces are transmitted to the other one using the OSI model data link layer mechanisms, that is, without taking into account IP

¹ IEEE 802.3-2018 — IEEE Standard for Ethernet. IEEE Standard Association. standards.ieee.org. URL: https://standards.ieee.org/standard/802_3-2018.html (accessed: 11.04.2021).

addresses, routing, NAT, etc. This method of organizing the connection is completely transparent to other devices on the network, it does not change packets and does not manifest itself in any other way.

The main task of the device under consideration is to extract MAC addresses from transit packets. At this (first) stage of building a local network graph, traffic capture utilities (to write it into a file and analyze) or specialized libraries of software components (to analyze traffic in real time) are used [12, 13]. Depending on the operating system, the libraries may differ; however, as a rule, they are all based on Pcap (Packet Capture).

Regardless of the method of obtaining MAC addresses, information on them must be stored in the database. Taking into account the previously described features of the building a network diagram, we note the following requirements. For each MAC address, additional information is recorded:

- about the point to which the device that received the MAC address is connected;
- about the network interface from which the MAC address was received as the sender's address [14].

As a result, the database table will be described by relation A with the following scheme:

$A(\underline{id}, address, point, side)$.

Here, id — primary key used only for identifying records in the table; $address$ — MAC address of the device in the network extracted from the passing packet; $point$ — network connection point (physical location); $side$ — symbol of the network interface that transmitted the packet from which the MAC address was extracted.

After the formation of the MAC address database for a certain number of traffic capture points, the next stage begins — building a network diagram. It is based on information about the distribution of MAC addresses obtained for different connection points. Let us denote two arbitrary of them as p_1 and p_2 . For each point, two sets of addresses should be received, each — from a separate network adapter. Let us denote X and Y — sets of addresses for point p_1 , Z and V — sets of addresses for point p_2 (Fig. 1).

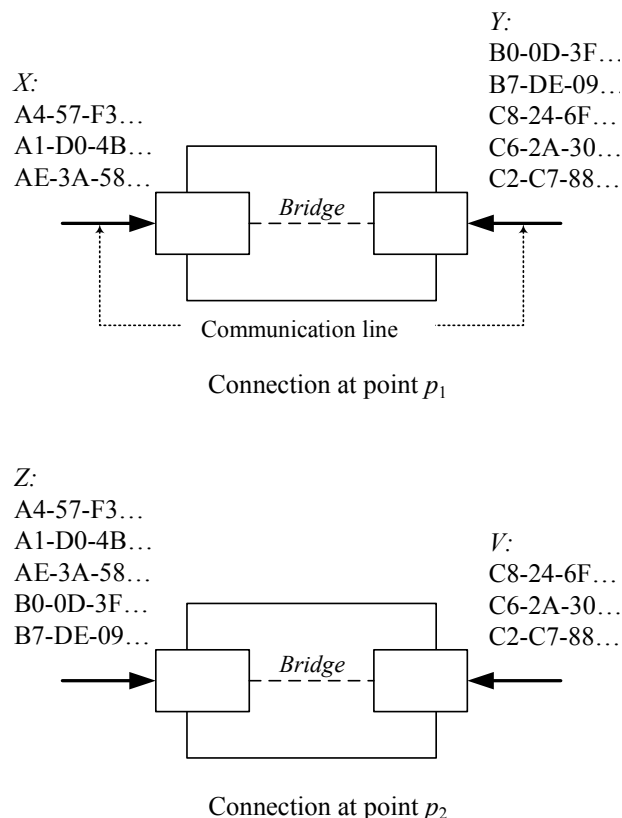


Fig. 1. Distribution of addresses across sets when connecting to different points of the network

From now on, only the first part is specified for the MAC addresses to shorten the record. Within the framework of the example under consideration, it is unique, and this is enough to reflect the work of the method.

Based on the obtained distribution of addresses across sets corresponding to different network interfaces, it is possible to draw initial conclusions about the mutual location of devices. To do this, you need to calculate all possible intersections for two points, that is, $X \cap Z$, $X \cap V$, $Y \cap Z$, $Y \cap V$.

It is advisable to calculate intersections by means of a database management system. This is because:

- information on the address belonging to a set is stored in the database,
- operations on sets are supported in relational algebra [15].

You need to execute queries equivalent to the following set of expressions:

$$X \cap Z = \Pi_{\text{address}} (\sigma_{\text{point}=1 \wedge \text{side}=1} (A)) \cap (\sigma_{\text{point}=2 \wedge \text{side}=1} (A)),$$

$$X \cap V = \Pi_{\text{address}} (\sigma_{\text{point}=1 \wedge \text{side}=1} (A)) \cap (\sigma_{\text{point}=2 \wedge \text{side}=2} (A)),$$

$$Y \cap Z = \Pi_{\text{address}} (\sigma_{\text{point}=2 \wedge \text{side}=1} (A)) \cap (\sigma_{\text{point}=1 \wedge \text{side}=1} (A)),$$

$$Y \cap V = \Pi_{\text{address}} (\sigma_{\text{point}=2 \wedge \text{side}=2} (A)) \cap (\sigma_{\text{point}=1 \wedge \text{side}=2} (A)).$$

Research Results. Let us consider an example of the application of the proposed methodology for constructing a network topology based on the distribution of sets of MAC addresses shown in Fig. 1. Determine the required intersections of the sets:

$$X \cap Z = \{A4-57-F3, A1-D0-4B, AE-3A-58\},$$

$$X \cap V = \emptyset,$$

$$Y \cap Z = \{B0-0D-3F, B7-DE-09\},$$

$$Y \cap V = \{C8-24-6F, C6-2A-30, C2-C7-88\}.$$

You can notice that one of the intersections (X and V) — is an empty set. This result is obtained for oppositely directed sides. Accordingly, the other sets (Y and Z), on the contrary, represent the sides directed at each other, and the result of their intersection is the addresses located between the measurement points, that is, between p_2 and p_1 .

The remaining intersections represent the addresses located on opposite sides of the measurement points. X and V represent oppositely directed sides. Therefore, the remaining intersection, in which X (that is, $X \cap Z$) participates, includes addresses located on the side of point p_1 , $Y \cap V$ — on the side of point p_1 . Thus, it is possible to make an initial conclusion on the relative location of all the addresses obtained under the analysis, as well as on their location relative to the measurement points (Fig. 2).



Fig. 2. Mutual arrangement of devices and points

It should be remembered that the points on this diagram are not network nodes (in particular, switches). However, the results obtained allow us to make the following assumption: if a set includes several addresses, it means that there is at least one switch inside it. We will substantiate the statement as follows: several computers cannot be connected directly; this requires appropriate network equipment (Fig. 3).

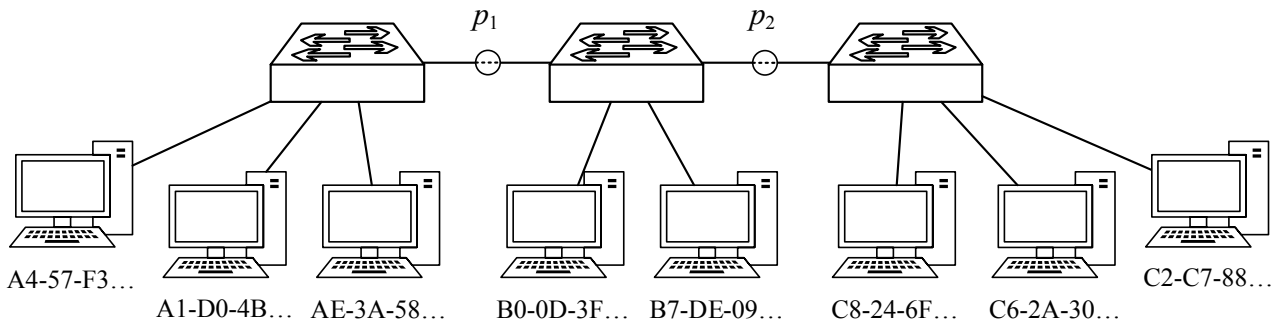


Fig. 3. Network scheme

The scheme shown in Fig. 3 is not final since there may be not one, but several switches inside each of the sets. At the next stages of the method, you should perform similar operations for each of the obtained sets, receiving MAC addresses at other points in the network. Each new measurement will provide refining the scheme and supplementing it with new switching nodes.

Discussion and Conclusions. A method for efficiently constructing a network scheme is proposed. The approach is based on an automated analysis of open information extracted from packets transmitted over the network. This technique is an alternative to the physical search for communication lines and the determination of the devices

connected by them. The application of the proposed solutions can significantly reduce the time spent by system administrators on determining the location of all devices and drawing them on the network diagram. The advantage of the method is the possibility of sequential refinement of the topology of network connections to obtain the required accuracy.

References

1. Kuz'menko NG. Komp'yuternye seti i setevye tekhnologii. St. Petersburg: Nauka i tekhnika; 2013. 368 p. (In Russ.)
2. Galushka VV. Seti i sistemy peredachi informatsii. Rostov-on-Don: DSTU Publ. House; 2016. 105 p. (In Russ.)
3. Stefano-Niko Orzen. Interaction understanding in the OSI model functionality of networks with case studies. IEEE 9th Int. SACI, 2014. P. 327–330. URL: www.researchgate.net/publication/269301474_Interaction_understanding_in_the_OSI_model_functionality_of_networks_with_case_studies (accessed: 18.08.2021). [10.1109/SACI.2014.6840086](https://doi.org/10.1109/SACI.2014.6840086)
4. Piyush Saxena. OSI Reference Model — A Seven Layered Architecture of OSI Model. International Journal of Research. 2014;1(10):1145–1156.
5. Lagutin IA. Opredelenie topologii s pomoshch'yu protokola LLDP v setyakh Juniper. Perspektivy razvitiya informatsionnykh tekhnologii. 2013;16:66–70. URL: <https://cyberleninka.ru/article/n/opredelenie-topologii-s-pomoschyu-protokola-lddp-v-setyah-juniper/viewer> (accessed: 10.04.2021). (In Russ.)
6. Alekseev VE, Talanov VA. Grafy i algoritmy. Struktury dannykh. Modeli vychislenii. Moscow: Binom. Laboratoriya znaniy; 2012. 320 p. (In Russ.)
7. Ifenthaler D, Gibson D, Dobozy E. Informing learning design through analytics: Applying network graph analysis. Australasian Journal of Educational Technology. 2018;34(2):117–132. <https://doi.org/10.14742/ajet.3767>
8. Asel'derov ZM, Donets GA. Predstavlenie i vosstanovlenie grafov. Kiev: Naukova dumka; 2001. 96 p. (In Russ.)
9. Mao Yan, Kam-Yiu Lam, Song Han, et al. Hypergraph-based data link layer scheduling for reliable packet delivery in wireless sensing and control networks with end-to-end delay constraints. Information Sciences. 2014;278:34–55. [10.1016/j.ins.2014.02.006](https://doi.org/10.1016/j.ins.2014.02.006)
10. Grigor'yan A. Introduction to Analysis on Graphs. Providence, Rhode Island: American Mathematical Society; 2018. 150 p.
11. Anduo Wang, Xueyuan Mei, Jason Croft, et al. Ravel: A Database-Defined Network. In: Proc. Symposium on SDN Research. 2016;5:1–7. URL: www.researchgate.net/publication/304918854_Ravel_A_Database-Defined_Network (accessed: 21.08.2021). <https://doi.org/10.1145/2890955.2890970>
12. Jiaqian Li, Chengrong Wu, Jiawei Ye, et al. The Comparison and Verification of Some Efficient Packet Capture and Processing Technologies. 2019 IEEE International Symposium on DASK, 2019. P. 967–973. URL: www.ieeexplore.ieee.org/abstract/document/8890423 (accessed: 18.08.2021). [10.1109/DASC/PiCom/CBDCCom/CyberSciTech.2019.00177](https://doi.org/10.1109/DASC/PiCom/CBDCCom/CyberSciTech.2019.00177)
13. Saavedra MZNL, Yu W. Towards Large Scale Packet Capture and Network Flow Analysis on Hadoop. In: Proc. 6th Int. Workshop on Computer Systems and Architectures; 2018. P. 186–189. URL: www.researchgate.net/publication/329905189_Towards_Large_Scale_Packet_Capture_and_Network_Flow_Analysis_on_Hadoop (accessed: 18.08.2021). [10.1109/CANDARW.2018.00043](https://doi.org/10.1109/CANDARW.2018.00043)
14. József Marton, Gábor Szárnyas, Dániel Varró. Formalising openCypher Graph Queries in Relational Algebra. In: Proc. 21st European Conf. on Advances in Databases and Information Systems. 2015;10509:53–68. [10.1007/978-3-319-66917-5_13](https://doi.org/10.1007/978-3-319-66917-5_13)
15. Alekh Jindal, Samuel Madden, Malu Castellanos, et al. Graph Analytics using Vertica Relational Database. IEEE Xplore, 2015. P. 1191–1200. URL: www.ieeexplore.ieee.org/document/7363873 (accessed: 18.08.2021).

Received 26.07.2021

Revised 09.08.2021

Accepted 24.08.2021

About the Authors:

Galushka, Vasily V., associate professor of the Computer Systems and Information Security Department, Don State Technical University (1, Gagarin sq., Rostov-on-Don, 344003, RF), Cand.Sci. (Eng.), ORCID: <http://orcid.org/0000-0003-2369-065X>, galushkavv@yandex.ru

Fatkhi, Denis V., associate professor of the Information Technology Department, Don State Technical University (1, Gagarin sq., Rostov-on-Don, 344003, RF), Cand.Sci. (Eng.), ORCID: <https://orcid.org/0000-0003-1538-1363>, Zmey2257@mail.ru

Gaziziov, Evgeniy R., associate professor of the Physics and Mathematics Department, Kazan State Agrarian University (65, K. Marx St., Kazan, 420015, Republic of Tatarstan, RF), Cand.Sci. (Eng.), ORCID: <http://orcid.org/0000-0002-9837-9850>, pim.kazgau@mail.ru

Claimed contributorship

V. V. Galushka: basic concept formulation; research objective and tasks setting; developing a multi-address separation method. D. V. Fatkhi: development of a hardware complex for traffic capture; practical implementation of the proposed methods. E. R. Gaziziov: definition of the database structure and generation of relational set intersection operations.

All authors have read and approved the final manuscript.

INFORMATION TECHNOLOGY, COMPUTER SCIENCE, AND MANAGEMENT



UDC 519.688

<https://doi.org/10.23947/2687-1653-2021-21-3-290-296>

To the problem of using an automated workplace by people with disabilities



A. A. Baskakov , A. G. Tarasov 

Moscow State University of Technology “STANKIN” (MSTU “STANKIN”) (Moscow, Russian Federation)

✉ aleks.baskakov@mail.ru

Introduction. Employees of the banking sector with health restrictions have negative experience of using internal software to interact with customers and perform their official duties. Many employees, for example, with hearing problems, would like to work in call centers, but do not have this opportunity due to the outdated software. The research objective is to analyze the priority tasks for the further development of software products, taking into account the existing health problems of employees.

Materials and Methods. One of the subsystems of the automated workplace (hereinafter referred to as the AWP) was selected the software, which allows the employee to interact directly with the clients of the given organization. The analysis used the method of expert evaluation by T. L. Saati with the assistance of one of the experts in the development of software for people with disabilities.

Results. Using the fundamental preference scale and expert opinion in the field of software development for people with disabilities, a priority matrix was built for each of the criteria (subtitles, simplified fonts, voice guidance, simplified and remote management) and platforms (IOS, Android, Windows OS), as well as a global priority matrix for all criteria and platforms.

Discussions and Conclusions. An expert assessment of several characteristics of the software of a commercial banking organization of the Russian Federation was carried out to identify the disadvantages of using the software by employees with disabilities. During the analysis, intermediate conclusions were made: the most demanded criterion for people with hearing problems is “Subtitle”; for people without the ability to leave the house — “Remote control”; for people with amputations or irreversible limb injuries — “Simplified control”. The other parameters are not recommended for implementation.

Keywords: expert assessment, automated workplace, disability, commercial software, analytic hierarchy process.

For citation: A. A. Baskakov, A. G. Tarasov. To the problem of using an automated workplace by people with disabilities. Advanced Engineering Research, 2021, vol. 21, no. 3, P. 290–296. <https://doi.org/10.23947/2687-1653-2021-21-3-290-296>

© Baskakov A. A. Tarasov A. G., 2021



Introduction. The interaction of a client and an employee of a corporate organization is implemented through the complex software, which is designed to control access to the company's products and accelerate the processing of client requests. This is, for example, the customer relationship management system (CRM system) [1], which has proven itself well in the call center. There is also software for the cybersecurity department, where logging and listening of client or employee events takes place. All of the above, in contrast to the products used directly by customers, is poorly adapted for employees with physical disabilities (disability).

The analysis of some software characteristics is carried out to identify weaknesses in this problem. The assessment was carried out by the method of analyzing hierarchy of T. L. Saaty with the involvement of an expert on software for people with disabilities.

Materials and Methods. Expert evaluation by the Analytic Hierarchy Process (AHP) is the decomposition of the problem and the identification of the importance of criteria with the help of experts in this field. This method is well suited under the conditions of complete certainty and when there are many criteria [1].

According to expert opinion, the solution to the most acute problems with software for people with disabilities can be:

- simplified fonts for people with trouble seeing;
- voice guidance for visually impaired people;
- simplified management for people with amputations or irreversible limb injuries;
- subtitles for people with hearing problems;
- remote control for people without the ability to leave the house.

These problems can be implemented on the three most popular platforms for employee interaction with the application (channels): Android, iOS, Web browser. Initially, the problem is decomposed into criteria, and the decomposition is complete if each platform interacts with each criterion (Fig. 1).

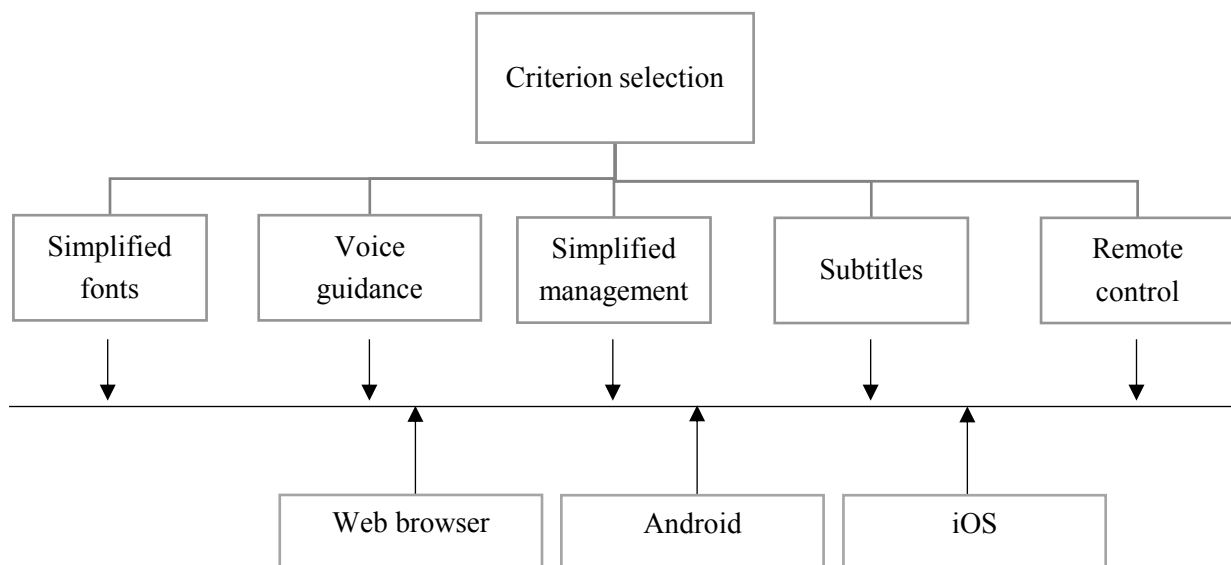


Fig. 1. Hierarchy of selection criteria for people with disabilities

To determine preferences for each platform and each problem, a pairwise comparison matrix is built. To do this, it is required to specify the evaluation scale (fundamental scale) [2–4], which has the form of an associative table (Table 1).

Table 1

Fundamental scale of preferences

Degree of preference	Definition
1	Both alternatives are the same in preference
2	Intermediate position between the same and average preference
3	One of the alternatives, according to the expert, is more preferable than the second
4	Intermediate position between average and moderately strong preference
5	One of the alternatives, according to the expert, is clearly preferable than the second
6	Intermediate position between moderately strong and very strong preference
7	One of the alternatives, according to the expert,

Degree of preference	Definition
	is much more preferable than the second
8	Intermediate position between a very strong and absolutely strong preference
9	One of the alternatives, according to the expert, is absolutely preferable than the second

Research Results. Priority¹ is calculated for each criterion [5]. To that end, a matrix is built (Table 2). Each criterion is compared to all the others on a scale from 1 to 9. Next, the product and sum for each criterion are found to analyze the local priority vector. The sum of local priorities, if calculated correctly, should be equal to one [6].

From the calculations, it can be concluded that the most preferred criterion is “Subtitles”. The next preferred criteria are “Simplified management” and “Remote control”.

Local priority vector V_B is found from the formula:

$$V_B = \frac{\sqrt[n]{\prod_{i=1}^n K_i}}{\sum_{i=1}^n K_i}, \quad (1)$$

where n — number of criteria; K — criterion.

Table 2

Assessment of the criteria importance

Criterion	Matrix by criteria					Calculation parameters from formula (1)		
	Simplified fonts	Voice guidance	Simplified management	Subtitles	Remote control	Product	$\sqrt[n]{\text{product}}$	Local priority vector
Simplified fonts	1	5	1/4	1/2	1/3	0.20	0.72	0.12
Voice guidance	1/5	1	1/5	1/4	1/4	0.002	0.28	0.04
Simplified management	4	5	1	1/2	1/3	3.33	1.27	0.21
Subtitles	2	3	5	1	1	30	1.97	0.32
Remote control	3	2	3	1	1	18	1.78	0.29
Total	10.2	16	9.45	3.25	2.91	—	6.02	~ 1.000

Consistency index I shows the degree of consistency of the expert's estimates [7] and is calculated from the formulas:

$$I = \frac{|\alpha - n|}{n-1}, \quad (2)$$

$$\alpha = \sum_{i=1}^n V_i \cdot S_i, \quad (3)$$

where V — priority vector; S — sum of criteria; n — i -th criterion.

Consistency ratio R is determined from the formula:

$$R = \frac{I}{L} \cdot 100\%, \quad (4)$$

where L — random consistency.

¹ Krugova, I. V. Analiz kriteriev innovatsionnykh proektov PAO «Megafon» na osnove metoda analiza ierarkhii Saaty. In: Proc. III Sci.-Pract. All-Russian Conf. Tolyatti: Izd-vo Kachalin Aleksandr Vasil'evich; 2017. P. 297–302. (In Russ.)

Random consistency is imperative values, which are given in Table 3 for matrices of different dimensions [8, 9]. In this case, the value is taken for a matrix of 5 criteria.

Table 3

Random consistency values for matrices of different orders

Matrix size	1	2	3	4	5	6	7	8	9	10
Random consistency	0	0	0.58	0.9	1.12	1.24	1.32	1.41	1.45	1.49

We calculate from formulas (2)–(4):

$$\alpha = 10.2 \cdot 0.12 + 16 \cdot 0.04 + 9.45 \cdot 0.21 + 3.25 \cdot 0.32 + 2.91 \cdot 0.29 = 5.7324;$$

$$I = |5.7324 - 5| / (5 - 1) = 0.1831;$$

$$R = 0.1831 / 1.12 \cdot 100 = \sim 16 \ %.$$

Parameter R has a valid value (no more than 20 %).

At this stage, priority is determined for each of the criteria, and consistency of expert opinions is checked [10, 11]. The calculations are given in Tables 4–8.

Table 4

Priority matrix for the “Simplified fonts” criterion

Platform	Matrix for platforms			Calculation parameters		
	Web	Android	iOS	Product	$\sqrt[3]{}$ of product	Priority vector
Web	1	2	6	12	2.28	0.59
Android	1/2	1	4	2	1.25	0.32
iOS	1/6	1/4	1	0.04	0.34	0.08
Total	1.66	3.25	11	–	3.87	–

Using formulas (2)–(4) and Table 4, we calculate the consistency estimate [12]:

$$\alpha = 1.66 \cdot 0.59 + 3.25 \cdot 0.32 + 11 \cdot 0.08 = 2.8994;$$

$$I = |2.8994 - 3| / (3 - 1) = 0.0503;$$

$$R = 0.0503 / 0.58 \cdot 100 = 8.67 \ %.$$

The value of parameter R is valid

Table 5

Priority matrix for the “Voiced guidance” criterion

Platform	Matrix for platforms			Calculation parameters		
	Web	Android	iOS	Product	$\sqrt[3]{}$ of product	Priority vector
Web	1	1/3	2	0.66	0.87	0.23
Android	3	1	5	15	2.46	0.64
iOS	1/2	1/5	1	0.1	0.46	0.12
Total	4.5	1.53	8	–	3.79	–

Using the previous methodology and the data from Table 5, we calculate the consistency score:

$$\alpha = 4.5 \cdot 0.23 + 1.53 \cdot 0.64 + 8 \cdot 0.12 = 2.97;$$

$$I = |2.97 - 3| / (3 - 1) = 0.015;$$

$$R = 0.015 / 0.58 \cdot 100 = 2.58 \ %.$$

The value of parameter R is valid.

Table 6

Priority matrix for the “Simplified management” criterion

Platform	Matrix for platforms			Calculation parameters		
	Web	Android	iOS	Product	$\sqrt[3]{}$ of product	Priority vector
Web	1	1	2	2	1.259	0.4
Android	1	1	2	2	1.259	0.4
iOS	1/2	1/2	1	0.25	0.629	0.19
Total	2.5	2.5	5	–	3.147	–

We calculate the consistency score for simplified management according to the data from Table 6:

$$\alpha = 2.5 \cdot 0.4 + 2.5 \cdot 0.4 + 5.0 \cdot 0.2 = 3.0;$$

$$I = |2.95 - 3| / (3 - 1) = 0.025;$$

$$R = 0.025 / 0.58 \cdot 100 = 4.3 \, \%.$$

And in this case, the value of parameter R is valid.

Table 7

Priority matrix for the “Subtitles” criterion

Platform	Matrix for platforms			Calculation parameters		
	Web	Android	iOS	Product	$\sqrt[3]{}$ of product	Priority vector
Web	1	1/5	1/2	0.1	0.46	0.13
Android	5	1	1	5	1.70	0.49
iOS	2	1	1	2	1.26	0.36
Total	8	2.2	2.5	–	3.42	–

Let us calculate the consistency score using the data from Table 7:

$$\alpha = 8 \cdot 0.13 + 2.2 \cdot 0.49 + 2.5 \cdot 0.36 = 3.018;$$

$$I = |3.018 - 3| / (3 - 1) = 0.009;$$

$$R = 0.009 / 0.58 \cdot 100 = 1.5 \, \%.$$

The value of parameter R is valid.

Table 8

Priority matrix for the “Remote control” criterion

Platform	Matrix for platforms			Calculation parameters		
	Web	Android	iOS	Product	$\sqrt[3]{}$ of product	Priority vector
Web	1	1/2	1/6	0.083	0.436	0.101
Android	2	1	1/5	0.4	0.736	0.172
iOS	6	5	1	30	3.107	0.726
Total	9	6.5	1.36	–	4.279	–

We calculate the consistency score based on the data from Table 8:

$$\alpha = 9 \cdot 0.101 + 6.5 \cdot 0.172 + 1.36 \cdot 0.726 = 3.01436;$$

$$I = |3.01436 - 3| / (3 - 1) = 0.025;$$

$$R = 0.007 / 0.58 \cdot 100 = 1.2 \, \%.$$

The value of parameter R is valid.

The initial data and the results of the calculation of global priorities are shown in Table 9.

Table 9

Initial data and results of the calculation of global priorities

Platform	Matrix of global priorities by criteria					Global priority vector
	Simplified fonts	Voiced guidance	Simplified management	Subtitled	Remote control	
	0.12	0.04	0.21	0.32	0.29	
Web	0.59	0.23	0.4	0.13	0.101	0.23489
Android	0.32	0.64	0.4	0.49	0.172	0.35468
iOS	0.08	0.12	0.19	0.36	0.726	0.38004
Sum	–	–	–	–	–	~1

The calculation of global priority C of each platform relative to the criteria is performed from the formula [13]:

$$C = \sum_{ni}^n P_g \cdot P_l,$$

where n — i -th criterion; P_g — global priority of i -th criterion; P_l — relative priority of each platform for i -th criterion.

Calculate the global priority of all alternatives:

- for Web: $(0.12 \cdot 0.59) + (0.04 \cdot 0.23) + (0.21 \cdot 0.4) + (0.32 \cdot 0.13) + (0.29 \cdot 0.101) = 0.23489$;
- for Android: $(0.12 \cdot 0.32) + (0.04 \cdot 0.64) + (0.21 \cdot 0.4) + (0.32 \cdot 0.49) + (0.29 \cdot 0.172) = 0.35468$;
- for IOS: $(0.12 \cdot 0.08) + (0.04 \cdot 0.12) + (0.21 \cdot 0.19) + (0.32 \cdot 0.36) + (0.29 \cdot 0.726) = 0.38004$.

Based on the calculation results, the priority is the iOS platform aimed at the development of functionality for people with disabilities, the Android platform is the closest to the priority [14].

Discussion and Conclusions. The conducted research using the hierarchy analysis method, considering the expert opinion, has shown that the most required criterion for people with hearing problems is “Subtitles” (index 0.32); for people without the ability to leave home — “Remote control” (index 0.29); for people with amputations or irreversible limb injuries — “Simplified management” (index 0.21). Other parameters are not recommended for implementation.

For the implementation of the “Subtitles” criterion, the required platform is Android OS (index 0.49). The iOS operating system has also turned out to be necessary enough (index 0.36). “Remote control” is most needed on the iOS platform (index 0.726). The “Simplified management” criterion equally requires Android and the Web version of the service (both indexes are 0.4). The global platform index for all criteria has shown the highest priority of iOS development.

References

1. Grinberg P. CRM so skorost'yu sveta. St. Petersburg: Simvol Plyus; 2007. 528 p. (In Russ.)
2. Rubtsov NV. Usage of analytic hierarchy process in vulnerability scoring process for IP-telephony systems. Izvestiya SFedU. Engineering Sciences. 2010;106(5):52–55. (In Russ.)
3. Erick F, Pandapota S. Proposal to use the Analytic Hierarchy Process Method Evaluate Bank Credit Submissions. Procedia Computer Science. 2021;179:232–241. <https://doi.org/10.1016/j.procs.2021.01.002>
4. Abimbola H, Afolayan, Bolanle Ojokoh, Adebayo O Adetunmbi. Performance analysis of fuzzy analytic hierarchy process multi-criteria decision support models for contractor selection. Scientific African. 2020;9:1–12.
5. Vdovchenko DG, Yushkova OI. Primenenie metoda analiza ierarkhii Toma Saati pri sovershenii transfera igroka. Sovremennaya matematika i kontseptsii innovatsionnogo matematicheskogo obrazovaniya. 2018;5(1):482–485. (In Russ.)
6. Kuznetsov MA. The choice of the programming language by the analytic hierarchy process of Thomas Saaty. NAUKA-RASTUDENT.RU. 2016;5:8. (In Russ.)
7. Bokhovko AG. The choice of the biometrical way of authentication by the analytic hierarchy process of Thomas Saaty. NAUKA-RASTUDENT.RU. 2016;2:18. (In Russ.)
8. Slavnov KV, Kupin IV, Sidorin MV. O vozmozhnosti modifikatsii metoda analiza ierarkhii T. Saati dlya otsenki sistem kontrolya konfidentsial'noi informatsii. Nauchnye issledovaniya i razrabotki molodykh uchenykh. 2016;15:73–78. (In Russ.)
9. Saliha Ünver, Ibrahim Ergenc. Safety risk identification and prioritize of forest logging activities using analytic hierarchy process (AHP). Alexandria Engineering Journal. 2020;60(1):1591–1599. [10.1016/j.aej.2020.11.012](https://doi.org/10.1016/j.aej.2020.11.012)

10. Abhijit Madjumbara, Manoj Kumar Tiwarib, Aastha Agarwala, et al. A new case of rank reversal in analytic hierarchy process due to aggregation of cost and benefit criteria. *Operations Research Perspectives*. 2021;8:100185. <https://doi.org/10.1016/j.orp.2021.100185>
11. Battsengel Enkhbayar, Justin S. Chang. Identifying priority attributes for improving Ulaanbaatar bus services using the analytic hierarchy process. *Transportation Research Procedia*. 2020;48(2):2990-2998. [10.1016/j.trpro.2020.08.186](https://doi.org/10.1016/j.trpro.2020.08.186)
12. Panagis Foteinopoulos, Alexios Papacharalampopoulos, Panagiotis Stavropoulos. Block-based Analytical Hierarchy Process applied for the evaluation of Construction Sector Additive Manufacturing. *Procedia CIRP*. 2019;81:950-955. [10.1016/j.procir.2019.03.233](https://doi.org/10.1016/j.procir.2019.03.233)
13. Francis L. Mayo, Evelyn B. Taboada. Ranking factors affecting public transport mode choice of commuters in an urban city of a developing country using analytic hierarchy process: The case of Metro Cebu, Philippines. *Transportation Research Interdisciplinary Perspectives*. 2020;4:100078.
14. Shivi Garg, Niyati Baliyan. Comparative analysis of Android and iOS from security viewpoint. *Computer Science Review*. 2021;40:100372. <https://doi.org/10.1016/j.cosrev.2021.100372>

Received 26.07.2021

Revised 09.08.2021

Accepted 24.08.2021

About the Authors:

Baskakov, Alexey A., postgraduate student of the Information Technology and Computer Systems Department, Moscow State University of Technology “STANKIN” (1, Vladkovsky Lane, Moscow, 127055, RF), ORCID: <https://orcid.org/0000-0001-9931-6520>, aleks.baskakov@mail.ru

Tarasov, Alexey G., associate professor of the Information Technology and Computer Systems Department, Moscow State University of Technology “STANKIN” (1, Vladkovsky Lane, Moscow, 127055, RF), Cand.Sci. (Eng.), ORCID: <https://orcid.org/0000-0002-5284-7073>, tarasov.ag@mail.ru

Claimed contributorship

A. A. Baskakov: computational analysis; text preparation; search for scientific literature; formulation of conclusions. A. G. Tarasov: academic advising; research objectives and tasks setting; the text revision.

All authors have read and approved the final manuscript.